電 子 426

Fabrication and magneto-optical properties of semiconductor / magnetic hybrid structures and their application to magneto-optical devices

(半導体・磁性体複合構造の作製、磁気光学特性、及び磁気光学デバイスへの応用)

by

Hiromasa SHIMIZU

Department of Electronic Engineering,
The University of Tokyo.

December 14, 2001

Dissertation Supervisor

Professor Masaaki TANAKA

Contents

1.Introduction 3

1.1 Background of this research 3

1.1.1 Semiconductor spin electronics 3

1.1.2 Materials in semiconductor spin electronics 3

1.2 The problems in spin electronics ~ What can spin electronics bring about? ... 6

1.3 Purpose of this research 7

1.4 Outline of this thesis 9

References 10

2.Epitaxial growth, magnetic and magneto-optical properties of (GaMn)As and its quantum heterostructures 12

2.1 Epitaxial growth of (GaMn)As thin films and (GaMn)As / AlAs superlattices. 13

2.2 Magnetic and transport properties of (GaMn)As 14

2.3 Magneto-optical properties of (GaMn)As 14

2.3.1 Magneto-optical effects 14

2.3.2 Previous discussions on the MCD spectra of DMSs 17

2.3.3 Transmission MCD spectra of (GaMn)As 18

2.3.4 Investigations on quantum size effect and ferromagnetic ordering of (GaMn)As / AlAs superlattices by magneto-optical measurements 18

2.4. Summary 22

References 23

3.Fabrication, structural, optical and magneto-optical properties of MnAs nanoclusters embedded in a GaAs matrix 36

3.1 Fabrication of MnAs nanoclusters embedded in GaAs (GaAs:MnAs) 36

3.2 Structural characterizations of GaAs:MnAs 37

3.3 Magnetic properties of GaAs:MnAs 38

3.4 Optical transmission and magneto-optical properties of GaAs:MnAs 40

3.4.1 GaAs:MnAs 40

3.4.2 Improvement of optical transmission in [GaAs:MnAs] / AlAs superlattices ... 41

3.4.3 Optical transmission and magneto-optical properties of GaAs:MnAs in a longer wavelength region of 1-1.6 μm and the effect of Si doping 42

3.5 The origin of the optical loss and magneto-optical effect in GaAs:MnAs 43

3.6 Comparison of optical transmission and magneto-optical properties between (GaMn)As and GaAs:MnAs at room temperature 44

3.7 Summary 46
References 47

4.Enhancement of magneto-optical effect in multilayer structures composed of the semiconductor / magnetic hybrid structure GaAs:MnAs and GaAs / AlAs DBR 60
4.1 Fabrication of a one-dimensional semiconductor-based magneto-photonic crystal 61
4.2 Magneto-optical properties of the multilayer structure 62
4.3 Theoretical analysis of the magneto-optical effect of the multilayer structures 62
4.4 Supression of the optical absorption loss in GaAs:MnAs 63
4.4.1 Introduction of [GaAs:MnAs] / AlAs superlattice structures 64
4.4.2 Longer wavelength operation and the effect of Si doping 65
4.5 Advantages of these multilayer structures 66
4.6 Summary 67
References 67

5.Design of semiconductor-waveguide-type optical isolators using the non-reciprocal refractive index change in the magneto-optical waveguides having MnAs clusters 76
5.1 Design of a waveguide-type optical isolator using the non-reciprocal loss/gain shift in the magneto-optical waveguide having MnAs clusters ~TM mode operation~ .. 77
5.1.1 Device structure 77
5.1.2 Calculation procedure 78
5.1.3 Calculation results 79
5.2 Design of a waveguide-type optical isolator using the non-reciprocal loss/gain shift in the magneto-optical waveguide having MnAs clusters ~TE mode operation~ 80
5.2.1 Device structure 80
5.2.2 Calculation procedure 80
5.2.3 Calculation results 82
5.3 Summary 82
References 83

6.Concluding remarks 92
Acknowledgements 94
Appendix Theoretical calculation of the multilayer structure 95
Publications and presentations 99

~Chapter 1~
Introduction

1.1 Background of this research

1.1.1 Semiconductor spin electronics

Semiconductors and magnetic materials are two major fundamental materials in solid state physics and both have a huge market in industry. The electronic and optoelectronic properties of group IV semiconductors (Si, Ge etc.) and III-V compound semiconductors (GaAs, InP etc. and related compounds.) have been extensively studied. These properties have been applied to processors, dynamic random access memories (DRAMs), laser diodes (LDs), and so on. On the other hand, the magnetic and transport properties of ferromagnetic metals, such as Fe, Co etc. and related alloys, have been extensively investigated for application to non-volatile memory and magnetic field sensor devices. Also, the magneto-optical properties of ferrimagnetic garnets, such as Bi substituted rare-earth Fe garnets, have been examined and applied to optically non-reciprocal devices like optical isolators and circulators. Both semiconductors and magnetic materials greatly contribute to today's information technology. However, research and development activities on these two materials have been carried out quite independently. This is because semiconductors and magnetic materials are very dissimilar in crystal structures, chemical bonding, and thermodynamic properties, so that integration of semiconductors and magnetic materials had been considered to be difficult.

In spite of many difficulties, semiconductor (III-V or Si) / magnetic hybrid materials have been successfully fabricated owing to the progress in fabrication technology in a recent decade [1.1]. In this new class of materials, researchers attempt to use spin-related functions or the spin degree of freedom, which may open a new paradigm in future electronics. And today, an interdisciplinary research field so called "*semiconductor spin electronics*" covering both semiconductors and magnetic materials and their applications, is a very hot topic both inside and outside of Japan. In the next section, we will describe the historical background of the research in semiconductor / magnetic hybrid materials related to this thesis.

1.1.2 Materials in semiconductor spin electronics

In this section, representative materials in semiconductor spin electonics are overviewed. Here we describe the properties of II-VI based diluted magnetic semiconductors (DMSs), III-V based ferromagnetic semiconductors, ferromagnetic thin

films on semiconductor substrates, magnetic nanoclusters embedded in semiconductor matrix, and some of the attractive new materials.

- *II-VI based diluted magnetic semiconductors*

II-VI based diluted magnetic semiconductors (DMSs) are II-VI alloy compound semiconductors, where a fraction of cations are replaced by transition metals such as Mn, Cr, Fe, etc, and expressed as $(A^{II}_{1-x}TM_x)B^{VI}$ (TM: transition metal). Representatives of DMSs are (CdMn)Te and (ZnMn)Se. Since the number of valence electrons in transition metals is two $((3d)^n(4s)^2$ (n=1,2...9)), transition metals are relatively easy to be incorporated into II-VI semiconductors with high TM concentrations both as bulks and epitaxially grown thin films. Therefore, II-VI based DMSs have been extensively studied since the 1970's [1.2]. II-VI based DMSs show paramagnetic properties at room temperature and antiferromagnetic properties or spin glass behaviors at low temperature, if the carrier (hole) concentrations are not sufficient. They show a giant magneto-optical effect due to the large *sp-d* exchange interaction between *sp* electrons in the host semiconductors and localized *d* electrons of the transition metals. The magneto-optical characteristic of (CdHgMn)Te and (CdMn)Te bulk crystals is applied to Faraday rotators in optical isolators in a wavelength region of 650-980nm, where ferrimagnetic garnets, most frequently used magneto-optical materials, are not transparent and difficult to be used for optical isolators [1.3].

- *III-V based ferromagnetic semiconductors*

· (InMn)As

The solubility limit of magnetic ions such as Mn in III-V semiconductors (GaAs, InAs) is quite low ($\sim10^{18}$cm^{-3}) in the thermodynamic equilibrium state, compared with that of II-VI semiconductors. Therefore, it is difficult to dope sizable amount of magnetic ions in III-V semiconductors by crystal growth methods using the thermodynamic equilibrium state. To overcome the solubility limit, Munekata and Ohno et al. applied low-temperature molecular-beam epitaxy (LT-MBE), where the growth temperature is 200-300℃, and successfully fabricated III-V based diluted magnetic semiconductor $(In_{1-x}Mn_x)$As for the first time in 1989 [1.4]. The maximum Mn concentration x in (InMn)As is 0.17 and they observed ferromagnetic ordering in *p*-type (InMn)As with its transition temperature ~10K [1.5]. This is the first observation of ferromagnetic ordering in III-V based DMSs. Mn ions in (InMn)As work as acceptors as well as magnetic ions, thus most (InMn)As films show *p*-type conduction. It was found that there is positive correlation between the ferromagnetic transition temperature and the hole concentration. This phenomenon is called carrier (hole) induced ferromagnetism. After those findings,

photo-carrier induced [1.6] and electric field induced [1.7] ferromagnetic ordering were observed in (InMn)As / GaSb heterostructures, which are unique phenomena in semiconductor based systems.

・(GaMn)As

In 1996-1997, some researcher groups succeeded in fabricating GaAs based DMS, $(Ga_{1-x}Mn_x)As$, independently [1.8-1.10] by LT-MBE at the growth temperature of 250℃ with the highest Mn concentration $x \sim 0.08$. (GaMn)As showed higher ferromagnetic transition temperatures (maximum ~110K) than those of (InMn)As and it was found that its ferromagnetic ordering was induced by carriers (holes) as was the case in (InMn)As [1.11]. Also it was reported that the ferromagnetic transition temperature strongly depends on its growth conditions such as growth temperature and As overpressure during the growth [1.12, 1.13]. Since (GaMn)As shows excellent compatibility with GaAs / AlAs (quantum) heterostructures, researches on (GaMn)As based heterostructures have been extensively done, such as (GaMn)As / AlAs superlattices [1.14], resonant tunneling diodes with a (GaMn)As electrode [1.15], injection of spin polarized holes to InGaAs / GaAs quantum well light emitting diodes using a (GaMn)As electrode [1.16], fabrication of (GaMn)As / AlAs / (GaMn)As magnetic tunnel junctions and their large tunneling magneto-resistance ratios (max 75%) [1.17, 1.18]. These phenomena realized in (GaMn)As based heterostructures can give new functionalities to semiconductor based systems.

● *Ferromagnetic intermetallic compound (TM-Ga, Al TM-As) thin films on GaAs / Si substrates and their multilayers*

Ferromagnetic metal / semiconductor heterostructures are another approach for spin electronics. Tanaka et al. successfully grew MnGa and MnAl thin films on GaAs substrate by MBE. Also they fabricated MnGa / NiGa multilayers and observed multisteps in magnetization curves [1.1]. After that, W. Roy et al. successfully fabricated ferromagnet (MnGa) / semiconductor (GaAs) / ferromagnet (MnGa) trilayer structures and extensively investigated the interlayer coupling through the semiconducting GaAs layer [1.19].

Tanaka and Akeura et al. successfully fabricated MnAs single crystal thin films on GaAs and Si substrates. MnAs is a ferromagnetic metal having the hexagonal crystal structure of NiAs type with the Curie temperature of 313K (= 40℃). It was reported that epitaxial relationship between MnAs and GaAs and the magnetic anistropy depend on whether Mn atoms or As atoms are supplied first on the GaAs surface [1.1]. Although growth of semiconductors on metal surfaces is considered to be quite difficult, Tanaka,

Saito, Takahashi et al. successfully overgrew GaAs on MnAs / (111)B GaAs by controlling the As template on the MnAs surface. Double steps were observed in magnetization curves of MnAs / GaAs / MnAs trilayers. At present, tunneling magneto-resistance properties were extensively studied in MnAs / (GaAs, AlAs) / MnAs trilayer structures [1.20, 1.21].

- *Ferromagnetic granular system: MnAs nanoclusters embedded in a III-V semiconductor matrix*

(GaMn)As described earlier is a metastable material grown by LT-MBE. When (GaMn)As is annealed at far above the growth temperature, typically 500-700℃, hexagonal MnAs clusters are formed with their average size ~10nm due to phase separation [1.22]. Although MnAs is a ferromagnet with its Curie temperature of 313K, the overall structure shows superparamagnetic properties, because there is no coupling among the MnAs nanoclusters embedded in a GaAs matrix. In this thesis, we denote this granular system (MnAs nanoclusters in GaAs) as GaAs:MnAs.

- *Searching for new materials*

III-V based ferromagnetic semiconductors attract much attention as mentioned above. However, its maximum ferromagnetic transition temperature is limited to 110K, which is much below room temperature. Room temperature ferromagnetism is desirable for device applications. For that purpose, theoretical predictions have been done using the Zener model [1.23] and the first principle calculation of electronic structures [1.24]. Also experimental approaches are being carried out. Representatives of these new materials are II-VI based wide gap DMS, Mn doped ZnO [1.25], Cr doped GaAs, (GaCr)As [1.26], II-IV-V_2 type chalcopyrite semiconductor based DMS, ($CdMnGeP_2$) [1.27], zinc-blende type artificial compound CrAs [1.28], and so on. However, in these recently reported materials, it is not clear whether the semiconductor matrix is really ferromagnetic or some ferromagnetic precipitates are responsible for the observed magnetization. Detailed structural and mageneto-optical characterizations will be required.

1.2 The problems in spin electronics ~ What can spin electronics bring about?

What kind of applications can we consider using the materials mentioned in section 1.1.2 ? One of the advantages of semiconductor / magnetic hybrid materials over conventional magnetic materials is their excellent compatibility with nonmagnetic Si,

GaAs substrates and/or semiconductor (quantum) heterostructures. At present, there are several aspects of research activities from fundamental physics to device applications, as follows.

- Fundamental physics
  Towards full understanding of the origin of ferromagnetic ordering in ferromagnetic semiconductors.
- Material science
  Towards sysnthesis of ferromagnetic semiconductors with room temperature ferromagnetism (both theoretical predictions and experiments).
- Magneto-electronic devices
  Towards magneto-tunnel junctions using ferromagnetic semiconductor based quantum heterostructures. Magnetic random access memories (MRAMs).
  Injection of spin polarized carriers from ferromagnetic electrodes (semiconductors or metals) into semiconductors and/or heterostructures.
- Magneto-optical devices
  Towards magneto-optical devices using semiconductor / magnetic hybrid materials and their integration with III-V optoelectronic devices.

1.3 Purpose of this research

One of the goals in semiconductor spin electronics is to realize functions which can not be obtained only either by semiconductors or magnetic materials as follows (see Fig. 1.1); for instance, optical isolators using semiconductor / magnetic hybrid materials and their integration with semiconductor laser diodes, magnetic tunnel junctions with resonant tunneling structure, and so on.

In this thesis, we focus on the magneto-optical effect of semiconductor / magnetic hybrid structures. The magneto-optical effect has two important meanings. First, the magneto-optical measurement is a powerful tool for investigating the fundamental properties such as band structures and dielectric responses of the materials. This is indispensable for material design and device applications. Second, the magneto-optical effect is an important phenomenon from technological viewpoints. Optical isolators and circulators use the non-reciprocal property of the magneto-optical effect and are indispensable devices in the optical telecommunication system. So far, ferrimagnetic garnets and II-VI based diluted magnetic semiconductors (bulk crystals in both) are used in these magneto-optical devices and it has been considered to be impossible to realize

magneto-optical devices using III-V semiconductors.

To design and realize magneto-optical devices using III-V semiconductor / magnetic hybrid structures like (GaMn)As and GaAs:MnAs, it is essential to fabricate required structures, and grasp their fundamental properties, such as structural, magnetic, optical and magneto-optical properties. For these purposes, we have fabricated (GaMn)As and its quantum heterostructures, and GaAs:MnAs, MnAs nanoclusters embedded in a GaAs.

In the study of (GaMn)As and its quantum heterostructures, we focuse on their magnetic circular dichroism (MCD), in order to elucidate their band structures, especially the quantum size effect in (GaMn)As / AlAs heterostructures. Since the band structure of (GaMn)As and the quantum size effect in (GaMn)As / AlAs heterostructures have not been fully understood yet, magneto-optical characterizations of (GaMn)As and its quantum heterostructures are important for realizing (GaMn)As based magneto-electronic devices, such as magnetic tunnel junctions with resonant tunneling structures for novel MRAM applications and magneto-optical devices.

In the study of GaAs:MnAs, we investigate its structural, magnetic, optical and

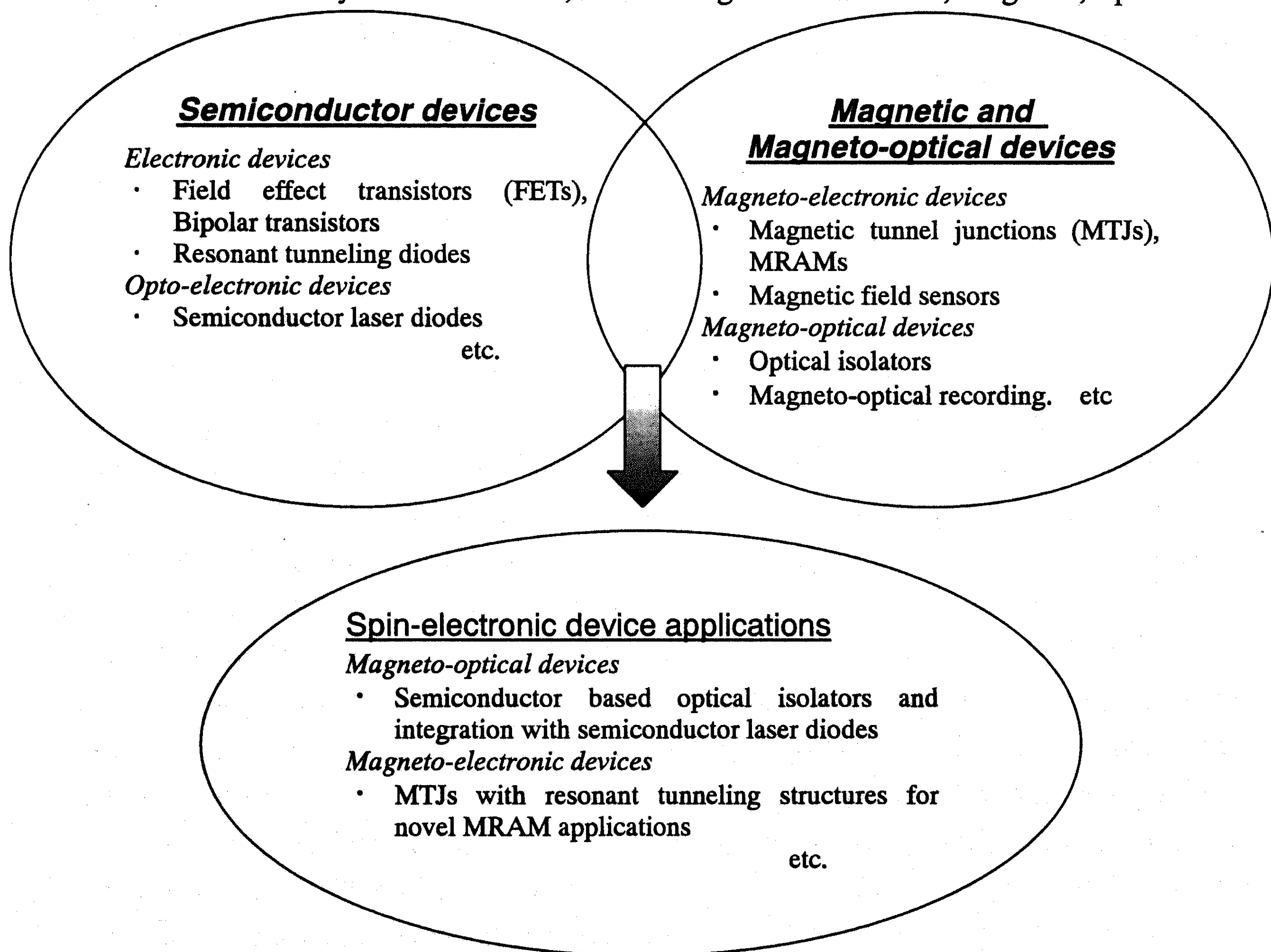

Fig.1.1 New directions of semiconductor spin electronics

magneto-optical properties. This magnetic granular system is a novel material and their optical transmission and magneto-optical properties and their physical origin have not been clarified yet, so that it is important to investigate these fundamental characteristics thoroughly, towards magneto-optical device applications.

Since (GaMn)As and GaAs:MnAs are obtained only by epitaxial growth, we have to consider thin-film-type magneto-optical devices. In this thesis, we propose and examine two kinds of approaches for thin-film-type magneto-optical devices and their integration with III-V optoelectronic devices. The first approach is "one-dimensional semiconductor-based magneto-photonic crystal (SMPC)". In SMPC, we aimed to enhance the magneto-optical effect of GaAs:MnAs utilizing multiple reflection of light within the film by combination with GaAs / AlAs distributed Bragg reflectors. The other approach is semiconductor-waveguide-type optical isolators with MnAs nanoclusters utilizing the non-reciprocal refractive index change of the magneto-optical waveguide. For integration of optical isolators with semiconductor laser diodes, waveguide-type optical isolators are strongly desired. Since the MnAs nanocluster system is fully compatible with semiconductor heterostructures, waveguide-type optical isolators are considered to be one of the most promising approaches for novel integrated optical devices, for example, semiconductor laser diodes integrated with optical isolators.

1.4 Outline of this thesis

This thesis is composed of 6 chapters.

In Chapters 2 and Chapter 3, fundamental properties of semiconductor / magnetic hybrid structures are described. In Chapter 2, epitaxial growth of III-V ferromagnetic semiconductor (GaMn)As and (GaMn)As / AlAs superlattices are described and their magneto-optical properties and the quantum size effect are investigated. In Chapter 3, fabrication of MnAs nanoclusters embedded in a GaAs matrix (hereafter we denote as GaAs:MnAs) are described and their magnetic, structural, and magneto-optical properties are presented.

In Chapters 4 and Chapter 5, two types of optical isolators using GaAs:MnAs are studied. In Chapter 4, enhancement of the magneto-optical effect in the multilayer structures composed of GaAs:MnAs and GaAs / AlAs distributed Bragg reflectors are investigated. In Chapter 5, semiconductor-waveguide-type optical isolators using the non-reciprocal refractive index change in the magneto-optical waveguide having MnAs clusters are proposed and theoretically analyzed.

Finally, concluding remarks of this thesis are described in Chapter 6.

References

[1.1] M. Tanaka, J. Mater. Sci. & Eng. **B31**, 117 (1995)., Physica **E2**, 372 (1998).

[1.2] J. K. Furdyna, J. Appl. Phys. **64**, R29 (1988)., "Diluted Magnetic Semiconductors" in Semiconductor and Semimetals, edited by J. K. Furdyna and J. Kossut (Academic press, 1988), Vol. 25.

[1.3] K. Onodera, T. Matsumoto and M. Kimura, Electron. Lett., **30**, 1954 (1994).

[1.4] H. Munekata, H. Ohno, S. von Molnar, Armin Segmuller, L. L. Chang, and L. Esaki, Phys. Rev. Lett., **63**, 1849 (1989).

[1.5] H. Ohno, H. Munekata, S. von Molnar, and L. L. Chang, J. Appl. Phys., **69**, 6103, (1991).

[1.6] H. Munekata, T. Abe, S. Koshihara, A. Oiwa, M. Hirasawa, S. Katsumoto, Y. Iye, C. Urano, and H. Takagi, J. Appl. Phys., **81**, 4862, (1997)., S. Koshihara, A. Oiwa, M. Hirasawa, S. Katsumoto, Y. Iye, C. Urano, and H. Takagi, H. Munekata, Phys. Rev. Lett., **78** 4617, (1997).

[1.7] H. Ohno, D. Chiba, F. Matsukura, T. Omiya, E. Abe, T. Dietl, Y. Ohno, and K. Ohtani, Nature **408**, 944, (2000).

[1.8] H. Ohno, A. Shen, F. Matsukura, A. Oiwa, A. Endo, S. Katsumoto, and Y. Iye, Appl. Phys. Lett., **69**, 363, (1996)., H. Ohno, Science **281**,951 (1998).

[1.9] T. Hayashi, M. Tanaka, T. Nishinaga, H. Shimada, and Y. Otuka, J. Cryst. Growth, **175/176**, 1063, (1997).

[1.10] A. Van Esch, L. Van Bockstal, J. De Boeck, G. Verbanck, A. S. van Steenbergen, P. J. Wellmann, B. Grientens, R. Bogaerts, F. Herlach, and G. Borghs, Phys. Rev. B **56** 13103 (1997).

[1.11] F. Matsukura, H. Ohno, A. Shen, and Y. Sugawara, Phys. Rev. B, **57**, R2037, (1998).

[1.12] H. Shimizu, T. Hayashi, T. Nishinaga, M. Tanaka, Appl. Phys. Lett., **74** 398 (1999).

[1.13] A. Shen, F. Matsukura, S. P. Guo, Y. Sugawara, H. Ohno, M. Tani, H. Abe, H. C. Liu, J. Cryst. Growth, **201/202**, 679 (1999).

[1.14] T. Hayashi, M. Tanaka, K. Seto, T. Nishinaga, and K. Ando, Appl. Phys. Lett. **71**, 1825 (1997).

[1.15] H. Ohno. N. Akiba, F. Matsukura, A. Shen, K. Ohtani, and Y. Ohno, Appl. Phys. Lett., **73,** 363 (1998).

[1.16] Y. Ohno, D. K. Young, B. Beschoten, F. Matsukura, H. Ohno, and D. D. Awschalom, Nature **402**, 790, (1999).

[1.17] T. Hayashi, H. Shimada, H. Shimizu, and M. Tanaka, J. Cryst. Growth, **201/202**, 689 (1999).

[1.18] M. Tanaka and Y. Higo, Phys. Rev. Lett., **87**, 026602 (2001).
[1.19] W. Van Roy, H. Akinaga, S. Miyanishi, K. Tanaka and L. H. Luo, Appl. Phys. Lett., **69**, 711 (1996).
[1.20] M. Tanaka, K. Saito, and T. Nishinaga, Appl. Phys. Lett., **74**, 64 (1999)
[1.21] K. Takahashi, and M. Tanaka, J. Appl. Phys., **87**, 6695, (2000).
[1.22] J. De Boeck, R. Oesterholt, A. Van Esch, H. Bender, C. Bruynseraede, C. Van Hoof, and G. Borghs, Appl. Phys. Lett., **68**, 2744, (1996).
[1.23] T. Dietl, H. Ohno, F. Matsukura, J. Cibert, and D. Ferrand, Science, **287**, 1019, (2000)
[1.24] K. Sato, and H. Katayama-Yoshida, Physica **E 10**, 251, (2001)
[1.25] T. Fukumura, Zhengwu Jin, A. Ohtomo, H. Koinuma, and M. Kawasaki, Appl. Phys. Lett., **75**, 3366, (1999).
[1.26] H. Saito, W. Zaets, R. Akimoto, K. Ando, Y. Mishima, and M. Tanaka, J. Appl. Phys., **89**, 7392, (2001).
[1.27] G. A. Medvedkin, T. Ishibashi, T. Nishi, K. Hayata, Y. Hasegawa, and K. Sato, Jpn. J. Appl. Phys. **39**, L949, (2000).
[1.28] H. Akinaga, T. Manago, and M. Shirai, Jpn. J. Appl. Phys., **39**, L1118, (2000).

~Chapter 2~

Epitaxial growth, magnetic and magneto-optical properties of (GaMn)As and its quantum heterostructures

The band structure of ferromagnetic semiconductor (GaMn)As has not been fully understood yet and the origin of ferromagnetic ordering is still controversial. In order to elucidate the band structure of (GaMn)As, Ando et al. measured reflection magnetic circular dichroism (MCD) spectra on (GaMn)As thin films and investigated the *sp-d* exchange interaction between the *sp* band electrons and local *d* electrons [2.1]. They observed strong enhancement of MCD, which indicates a strong *sp-d* hybridization and concluded the *sp-d* exchange interaction is antiferromagnetic judging from the sign of the MCD spectra. Shirai et al. investigated the band structure of hypothetical zinc-blende type $Ga_{0.5}Mn_{0.5}As$ by first-principle calculations and showed that the dominant component near the Fermi level was As 4p orbitals and strong hybridization between the Mn 3*d* and As 4*p* states caused the ferromagnetism in (GaMn)As [2.2]. Okabayashi et al. investigated the valence band dispersions in (GaMn)As by angle-resolved photoemission spectroscopy [2.3]. They compared the band dispersion of (GaMn)As with that of GaAs, and observed a small energy shift caused by Mn doping for one of the valence band. In addition, they observed new states near the Fermi level. Hayashi et al. measured reflection MCD spectra on (GaMn)As / AlAs superlattices to investigate the quantum size effect in (GaMn)As / AlAs superlattices. They indicated the existence of quantized energy levels in (GaMn)As / AlAs superlattices (SLs) with 30 periods, although the interpretation of R-MCD spectra includes some difficulties due to the multiple reflection of light within the films [2.4]. Also, they reported that the SLs having relatively thick (GaMn)As layers ($\geq$7nm) are ferromagnetic at low temperature, while the SLs having thin (GaMn)As layers ($\leq$5nm) are paramagnetic even at 2K [2.4].

Although optical measurements are powerful tool to investigate the band structures and the quantum size effect of the magnetic materials, experimental investigations are limited [2.1, 2.4]. Magneto-optical measurements, especially, MCD measurement, are one of the most effective probing methods to investigate the band structures. Previous MCD measurements are carried out in reflection geometries and the interpretation of reflection MCD (R-MCD) spectra includes some ambiguities due to the multiple reflection of light within the films. Transmission MCD (T-MCD) spectra correspond to the band structures of the materials more directly than R-MCD spectra, therefore T-MCD measurements are strongly desired.

In this chapter, epitaxial growth of III-V based ferromagnetic semiconductor (GaMn)As thin films and (GaMn)As / AlAs superlattices is briefly described and their magnetic and transport properties are shown. Then, magneto-optical properties, especially transmission magnetic circular dichroism (T-MCD), of (GaMn)As and (GaMn)As / AlAs superlattices are presented, focusing on their band structures and quantum size effect.

2.1 *Epitaxial growth of (GaMn)As thin films and (GaMn)As / AlAs superlattices*

The epitaxial growth of (GaMn)As thin films and related heterostructures was done by molecular-beam epitaxy (MBE) using ULVAC MBC 508 system having standard solid sources of Ga (purity 7N), Al (5N), In (7N), As (valved cracker cell, EPI), Si, Be, and Mn (4N), and a reflection high-energy electron diffraction (RHEED) system with a 20keV electron gun.

The growth procedure of (GaMn)As is as follows. First we grew an undoped GaAs buffer layer with typical thickness of 50 nm at 580℃ on a semi-insulating (001) GaAs substrate. For the samples for optical transmission measurements, a 200nm-thick $Al_{1-x}Ga_xAs$ layer with x = 0.8~0.9, was grown after growing the GaAs buffer layer. This $Al_{1-x}Ga_xAs$ layer works as a sacrifice etch-stop layer when we remove the GaAs substrate by chemical selective etching. Then the substrate temperature was lowed to 250℃ under the As flux. The substrate temperature was changed and the As flux was also lowered to tune the growth conditions for (GaMn)As. Then the growth of a $(Ga_{1-x}Mn_x)As$ thin film was started by opening the Ga and Mn shutters simultaneously with a fixed growth rate of 0.5μm/hr. The surface reconstruction of (GaMn)As was (1×2), and with increasing the substrate temperature or decreasing the As overpressure, the two-fold streaks became stronger. At the initial stage of the growth of (GaMn)As, RHEED intensity oscillations can be observed, which means that layer-by-layer growth occurs. The Mn concentration x was determined by the lattice constant of the (GaMn)As film measured by X-ray diffraction using the Vegard's law [2.5]. The initial data of the Mn concentration in (GaMn)As was calibrated by electron probe micro-analysis (EPMA) measurements [2.5]. When the Mn concentration x is higher than 0.08, or the growth temperature is too high, the growth results in the formation of hexagonal MnAs clusters or Mn surface segregation, as shown in the phase diagram of Fig. 2.1 [2.6].

The epitaxial growth of (GaMn)As / AlAs superlattices was carried out by supplying the Ga, Mn fluxes and the Al flux alternatively with growth interruptions of 10-20 sec at each interface.

2.2 *Magnetic and transport properties of (GaMn)As*

($Ga_{1-x}Mn_x$)As films show strong *p*-type conduction and their magnetic and transport properties strongly depend on the Mn concentration and growth conditions. Fig. 2.2 shows the temperature dependence of the resistivity of the ($Ga_{0.957}Mn_{0.043}$)As samples grown under different substrate temperatures T_s (Fig. 2.2 (a)) and As/Ga ratios (Fig. 2.2(b)). The carrier (hole) concentration and resistivity of a typical ferromagnetic (GaMn)As film are $1\times10^{20}cm^{-3}$ and 0.01Ωcm at room temperature, respectively. These properties are also strongly dependent on the growth conditions during the growth of (GaMn)As [2.7, 2.8]. With decreasing the growth temperature and increasing the As overpressure during the growth, the hole concentration and the ferromagnetic transition temperature become lower, as shown in Fig. 2.3 [2.7]. This is because the excess As atoms incorporated during the LT-MBE, which works as deep donors, compensate holes supplied by Mn acceptors, and the density of excess As strongly depends on the growth conditions. These experimental results show that the ferromagnetism in (GaMn)As is induced by carriers (holes).

2.3 *Magneto-optical properties of (GaMn)As*

In this section, we describe the optical and magneto-optical properties of (GaMn)As. Before showing experimental results, the physics and the measurement setup of the magneto-optical effect (Faraday effect) is briefly introduced.

2.3.1 *Magneto-optical effects*

Magneto-optical effects arise from the interaction between light and a matter when the matter is subjected to a magnetic field or the matter is magnetized [2.9]. Magneto-optical effects can be classified into three categories; the Faraday effect, the Cotton-Mouton or Voigt effect, and the magneto-optical Kerr effect (MOKE). Among them, the Faraday effect and the magneto-optical Kerr effect are important from technological viewpoints and briefly explained as follows. The Faraday effect is a phenomenon that when linear polarized light passes through a matter in a direction parallel to the magnetization of the matter, the plane of polarization is rotated and its polarization changed from linear to elliptical. These phenomena arise from the fact that in a magnetized medium, the refractive indices for right- and left-handed circularly polarized

light are different. The reason for this difference can be explained as follows. Let us derive the main formula for the Faraday effect for the magnetized medium. The dielectric-permeability tensor of the magnetized medium is expressed as equation (2-1), taking into account the uniaxial optical anisotropy driven by magnetization.

$$\tilde{\varepsilon} = \begin{pmatrix} \varepsilon_{xx} & \varepsilon_{xy} & 0 \\ -\varepsilon_{xy} & \varepsilon_{xx} & 0 \\ 0 & 0 & \varepsilon_{zz} \end{pmatrix} \qquad (2-1)$$

Here, the z-axis of the coordinate system is set along the direction of both the magnetization and the light propagation direction.

$$\begin{cases} \nabla \times E = -\mu_0 \dfrac{\partial H}{\partial t} & (2-2) \\ \nabla \times H = \varepsilon_0 \tilde{\varepsilon} \dfrac{\partial E}{\partial t} & (2-3) \end{cases}$$

Let us solve Maxwell's equations (2-2) and (2-3).

Here, we assume the light is the plane wave, and ***E*** and ***H*** have a harmonic dependence on the time and the coordinates,

$$\exp(i\omega(t - \frac{n}{c}z))$$

where ω is the angle frequency, c is the light velocity, n is the refractive index of the matter. From (2-2) and (2-3), we obtain the main wave equation (2-4).

$$\nabla^2 E = \frac{1}{c^2} \varepsilon_0 \tilde{\varepsilon} \frac{\partial^2 E}{\partial t^2} \qquad (2-4)$$

Substituting (2-1) into (2-4), we get the following formula (2-5),

$$\begin{cases} (n^2 - \varepsilon_{xx})E_x - \varepsilon_{xy}E_y = 0 \\ \varepsilon_{xy}E_x + (n^2 - \varepsilon_{xx})E_y = 0 \end{cases} \qquad (2-5)$$

where E_x and E_y are x and y components of $\boldsymbol{E}$.

A non-trivial solution of (2-5) exists if

$$n_{\pm}^2 = \varepsilon_{xx} \pm i\varepsilon_{xy} \qquad (2-6)$$

Substituting (2-6) into (2-5), we obtain two modes with right and left circular polarizations (2-7).

$$E_y = \pm iE_x \qquad (2-7)$$

The Faraday rotation θ_F is a difference in phase between the transmitted right and left circular polarized light and can be expressed as (2-8),

$$\theta_F = -\omega(n_+ - n_-)\frac{l}{2c} \qquad (2-8)$$

where l is the sample thickness.

The Faraday ellipticity η_F is an arctangent of the ratio between the long axis and the short axis of the transmitted light, and can be expressed as (2-9),

$$\eta_F = -\omega(k_+ - k_-)\frac{l}{2c} \qquad (2-9)$$

where k_+ and k_- are the extinction coefficients for right and left circular polarized light. Since the relationship between the absorption coefficient α and the extinction coefficient κ is express as (2-10),

$$\alpha = \frac{2\omega\kappa}{c} \qquad (2-10)$$

the magnetic circular dichroism(MCD), which is the difference in the absorption coefficient between the right and left circular polarized light (2-11), is equal to the Faraday ellipticity η_F.

$$MCD = \Delta\alpha = -\frac{1}{4}(\alpha_+ - \alpha_-)l \qquad (2-11)$$

The non-diagonal term ε_{xy} is the odd function of magnetization, therefore the rotation of the polarization is optically non-reciprocal. This phenomenon is applied to Faraday rotators in optical isolators; the optical devices in which the light can pass through in only one direction.

The optical anisotropy of a magnetized medium manifests itself also in the reflection of light from its surface. This phenomenon is the magneto-optical Kerr effect. It consists in an influence of the magnetization of the medium on the reflected light. The magneto-optical Kerr effect is applied to the magneto-optical recording, such as magneto-optic (MO) disks.

The dielectric-permeability tensor is unique to its material and has strong relationship with its electronic structure. Therefore, a magneto-optical measurement, which can estimate the parameters mentioned above, is a powerful tool for investigating the electronic structure of the materials.

Using the Zeeman splitting energy ΔE and the energy derivative of the absorption coefficient $d\alpha/dE$, equation (2-11) is expressed as follows [2.10, 2.11].

$$MCD \quad [\text{deg.}/thickness] = -\frac{45}{\pi}\Delta E\frac{d\alpha(E)}{dE} \qquad (2-12)$$

From eq. (2-12), the MCD signal should be sharply pronounced at critical point

energies where $d\alpha/dE$ is large, and therefore it gives much information about the band structure and the degree of the *sp-d* exchange interaction ($\propto \Delta E$), especially in II-VI based diluted magnetic semiconductors [2.10]. The relation between *s-d* and *p-d* exchange integral $N_0\alpha$ and $N_0\beta$ and Zeeman splitting energy ΔE can be expressed as follow,

$$\Delta E = N_0(\alpha - \beta)x < S_z > \qquad (2-13)$$

where $N_0\alpha$ and $N_0\beta$ are *s-d* and *p-d* exchange integral, $<S_z>$ is the thermal average spin per Mn ion.

Here, Faraday effect measurements were carried out using the circular polarization modulation technique in two measurement systems [2.12]. One is an MCD measurement system (JASCO J-700) with the wavelength range of 200-1100nm, the measurement temperature range of 7-300K, and the maximum magnetic field of 1.2T. The other one is a hand-made Faraday effect (both rotation and ellipticity) measurement system for room temperature measurements with the wavelength range of 800-1700nm, and the maximum magnetic field of 1.2T. Fig. 2.4 shows the Faraday effect measurement set-up of the latter system.

2.3.2 Previous discussions on the MCD spectra of DMSs

Ando et al. measured reflection MCD (hereafter R-MCD) spectra on (GaMn)As thin films and investigated the *sp-d* exchange interaction between the *sp* band electrons and local *d* electrons [2.1]. Fig. 2.5 (b) and (c) show the R-MCD spectra of $(Ga_{1-x}Mn_x)As$ with x_{Mn} = 0.005 and 0.074. As a reference, the R-MCD spectrum of a semi-insulating GaAs substrate is shown in Fig. 2.5 (a). The MCD signal near the E_0 and E_1 critical points of GaAs are significantly enhanced. The sign of R-MCD is negative at the E_0 and E_1 critical points. From the polarity of MCD, the character of *p-d* exchange can be estimated by Equation (2-13). The Mn ions in GaAs replace the Ga sites thus the *d* orbitals mix with the *p* valence band, not the *s* conduction band. Therefore, the absolute value of $N_0\beta$ should be larger than that of $N_0\alpha$. Accordingly, they concluded that the *p-d* exchange interaction in (GaMn)As is antiferromagnetic. However, R-MCD measurements include some difficulties due to the multiple reflection of light within the film, as shown in Fig. 2.5. Therefore, transmission MCD measurements are desired for better understanding the *p-d* exchange interaction in (GaMn)As.

Fig. 2.6 show transmission MCD spectra of $(Cd_{0.67}Mn_{0.33})Te$, whose *p-d* exchange interaction is well understood. In transmission MCD spectra of (CdMn)Te, negative peak are observed at E_0 critical point, which shows antiferromagnetic *p-d* exchange interaction.

2.3.3 *Transmission MCD spectra of (GaMn)As*

Before the MCD measurement, the samples were mounted on sapphire substrates, and GaAs substrates and $Al_{0.9}Ga_{0.1}As$ stop-etching layers were selectively removed by chemical etching. Then, MCD spectra were measured with both the incident light and the magnetic field perpendicular to the film plane (Faraday configuration).

Fig. 2.7(b) shows a transmission MCD spectrum of an 80nm-thick (GaMn)As film with x_{Mn} = 0.043 at 7K under the magnetic field of 1T. The ferromagnetic transition temperature of this (GaMn)As film is 70K. An MCD spectrum of an 80nm-thick GaAs film is shown as a reference in Fig. 2.7(a). It was found that the MCD signal was enhanced near the Γ critical points (E_0, $E_0+\Delta_0$) and the Λ critical points (E_1, $E_1+\Delta_1$) in (GaMn)As, compared with the MCD spectrum of GaAs. This shows strong hybridization between the *sp* itinerant electrons and localized *d* electrons in (GaMn)As. By using equation (2-12), the Zeeman splitting energy was estimated to be 50meV at 1.8eV (near the Γ point) and 8meV at 3eV (near the Λ point). However, the MCD peak energy (1.89eV) of (GaMn)As is much higher than the bandgap energy of GaAs (1.52eV), as shown in Fig. 2.7(a), and the interpretation of the MCD spectra is more complicated than that in (CdMn)Te. Because the Mn ions in (GaMn)As work as acceptors as well as local magnetic moments, it was suggested experimentally [2.13] and theoretically [2.14] that the MCD signal at 1.8-1.9eV was caused by the Moss-Burstein shift due to the large hole concentration (~$10^{20}cm^{-3}$) in (GaMn)As. The effect of the Mn intra-atomic (*d-d**) transition is also discussed [2.15]. To investigate this issue, we changed the bandgap energy of the host semiconductor, by changing it from GaAs to $Al_{0.3}Ga_{0.7}As$. Fig. 2.7(c) show an MCD spectrum of $((Al_{0.3}Ga_{0.7})_{0.96}Mn_{0.04})As$. The MCD peak of (AlGaMn)As shifted toward higher energy by the change of the bandgap energy in the host semiconductor. By comparing the MCD spectra between (GaMn)As and (AlGaMn)As, it is clear that the Mn intra-atomic transition is not the origin of the broad positive MCD peak of (GaMn)As, because the MCD signal from the Mn intra-atomic transition is unique to Mn ions and independent of the type of host semiconductors. From these results, the origin of MCD signal around 1.5-2.5eV is the optical transitions between the valence band, which is hybridized with the Mn *d* bands and splitted due to the *p-d* exchange interaction, and the conduction band of the host semiconductor.

2.3.4 *Investigations on quantum size effect and ferromagnetic ordering of (GaMn)As / AlAs superlattices by magneto-optical measurements*

(1) Previous studies

Although bandgap engineering and wavefunction engineering are well established and widely used in nonmagnetic semiconductor heterostructures [2.16], they are far from

mature in magnetic semiconductor heterostructures (MSHs). One of the most interesting and promising MSHs for bandgap engineering is (GaMn)As / III-V (GaAs, AlAs) heterostructures [2.17,18], because atomically abrupt interfaces can be formed [2.17] and (GaMn)As can be ferromagnetic with the maximum Curie temperature of ~ 110K [2.18].

While the studies on (GaMn)As based ultrathin MSHs are limited so far [2.4], recently, large tunneling magnetoresistance (TMR) ratios (maximum 75%) were observed at 8K in (GaMn)As / AlAs / (GaMn)As single-barrier magnetic tunnel junctions (MTJs) [2.19]. It was theoretically predicted that by introducing resonant tunneling diode (RTD) structures, the TMR ratio could be enlarged further at higher bias voltages corresponding to resonant quantized levels [2.20], thus the problem of the strong bias dependence of TMR in single barrier MTJs is predicted to be solved.

Existence of quantized energy levels in (GaMn)As / AlAs superlattices (SLs) was indicated by reflection magnetic circular dichroism (R-MCD) measurements of (GaMn)As / AlAs SLs with 30 periods [2.4], although the interpretation of R-MCD spectra includes some difficulties due to multiple reflection of light within the films. Also, it was reported that the SLs having relatively thick (GaMn)As layers (≥7nm) are ferromagnetic at low temperature, while the SLs having thin (GaMn)As layers (≤5nm) are paramagnetic even at 2K [2.4]. In this section, *transmission* MCD (T-MCD) spectra of carefully fabricated (GaMn)As / AlAs ultrathin heterostructures is described. A clear blue shift in the T-MCD spectra due to the quantum size effect and ferromagnetic ordering were observed even when the (GaMn)As thickness is only 2nm.

(2) Quantum size effect in MCD spectra

For this study, four (GaMn)As / AlAs heterostructure samples were prepared by low temperature molecular-beam epitaxy (LT-MBE) at growth temperature T_s = 250℃ as shown in Fig. 2.8. The thickness d of $(Ga_{1-x}Mn_x)As$ layers are 12, 5, 2 and 1nm and the thickness of AlAs layers was fixed at 2.8nm. The Mn concentration x of one sample with d = 12nm was 0.045, and x of other samples with d = 5, 2, and 1nm was 0.071. Here, the sample structure was carefully designed: (1) The stacking number of (GaMn)As layers was only 3 so that high crystalline quality was maintained without degradation throughout LT-MBE growth. (2) The total film thickness was kept almost constant in the range of 84-116nm, which is much smaller than the wavelength used in the MCD measurements, thus the influence of multiple interference of light on the MCD spectra was eliminated.

Fig. 2.9(b)-(e) show T-MCD spectra of these heterostructure samples with d = 12, 5, 2 and 1nm at 9K under the magnetic field of 1T. An MCD spectrum of an 80nm-thick (GaMn)As single film is shown as a reference in Fig. 2.9(a). Although a negative sharp peak appeared at 1.52eV corresponding to the bandgap energy of GaAs, which comes from

the remaining part of the GaAs substrate in some samples (for example, Fig. 2.9(e)), this does not have important meanings in the present results.

The spectral features of the heterostrcture sample whose (GaMn)As layer is relatively thick (d = 12nm, Fig. 2.9(b)) is almost identical with that of the 80nm-thick (GaMn)As sample (Fig. 2.9(a)). However, it was found that the MCD peak systematically shifted toward higher energy with decreasing the (GaMn)As layer thickness from 5nm to 1nm, compared with that (1.89eV) of the 80nm-thick (GaMn)As sample. The peak energy was 1.95, 2.02, and 2.33eV for d = 5, 2, and 1nm, respectively. In addition, a broad shoulder was observed at around 2.2eV in Fig. 2.9(c) (d = 5nm) and a new peak was observed at 2.53eV in Fig. 2.9(d) (d = 2nm), which are not observed in the bulk (GaMn)As sample (Fig. 2.7(a)). Furthermore, we calculated the quantized energy levels in these heterostructures by the Kronig-Penny model, assuming that (GaMn)As has the same band parameters as those of GaAs, and the calculated lowest transition energy between the 1st electron subband and the 1st heavy hole subband at the Γ point was marked by arrows in Fig. 2.9(b)-(e).

Here we discuss the reason why this clear blue shift was observed in ultrathin (≤5nm) (GaMn)As samples. The hole concentration of (GaMn)As is as large as 10^{20}cm^{-3}, so that the Fermi level is ~100meV below the top of the valence band at the Γ point, as schematically shown in Fig. 2.10 (a). This large Fermi energy leads to the MCD peak shift toward higher energy in bulk (GaMn)As [2.13, 2.14]. In thicker (>5nm) (GaMn)As samples, the 1st subband energy level in the valence band (23meV for heavy holes and 81meV for light holes in case of d = 5nm by our calculation above) is probably smaller than the Fermi energy, therefore occupied with holes. In this case, the initial state in the optical transition is not the lowest hole subband in the valance band, as depicted in Fig. 2.10 (b). Also the calculated lowest transition energy (1.65eV) for d = 5nm is smaller than that of the MCD peak energy (1.89eV) of the bulk (GaMn)As. These situations can make it difficult to probe the quantized levels clearly in MCD spectra of thicker (GaMn)As samples. On the other hand, in thinner (GaMn)As samples, the 1st subband energy in the valence band becomes larger (91meV for heavy holes and 220meV for light holes in case of d = 2nm by our calculation above) and the lowest transition energy (1.95eV between the 1st electron subband and the 1st heavy hole subband for d = 2nm) exceeds the MCD peak energy of the bulk (GaMn)As, so that the initial state in the optical transition is probably the 1st subband level in the valence band and therefore the MCD shifted toward higher energy. Also, with decreasing the quantum well thickness, the energy separation between the 1st and 2nd transition energies becomes larger, so that the newly observed MCD peak at 2.53eV in Fig. 2.9(d) (d = 2nm) possibly corresponds to the transition energy between the 2nd electron and 2nd heavy hole subband. These situations are depicted in Fig. 2.10

(c) and (d).

Next, we discuss the formation of quantized levels from another point of view. The mean free path of carriers (holes) has to be longer than the (GaMn)As layer thickness for quantized levels to be formed. Since the Hall mobility of (GaMn)As is quite low (the order of $1cm^2/Vs$), the mean free path of carriers is expected to be small. The mean free path of carriers was calculated to be 4.3nm assuming that hole mobility is $5cm^2/Vs$ and

$$l = v_{th}\tau$$

$$v_{th} = \sqrt{\frac{3k_B T}{m_h^*}}$$

$$\tau = \frac{m_h^* \mu_h}{e}$$

using the following formula,

where l is mean free path, v_{th} is thermal velocity of carrier, τ is scattering time, μ_h is mobility of hole, k_B is Bolzmann constant, T is temperature, and m_h* is effective mass of hole.

This calculated mean free path is comparable to the (GaMn)As layer thickness where the blue shift was observed in the MCD spectra, although estimation of the mobility in (GaMn)As has some error because the contribution of the anomalous Hall effect was neglected in estimating the Hall mobility of (GaMn)As. This small mean free path is probably an important factor to determine whether or not quantized states are formed in (GaMn)As / AlAs heterostructures.

(3) Ferromagnetic ordering

In order to study the ferromagnetic ordering in ultrathin ($\leq$5nm) (GaMn)As films, we measured magnetic field B dependence of T-MCD of all the samples from 9K to 80K. Fig. 2.11(a) shows the result of the (GaMn)As sample with d = 2nm. Since the easy magnetization direction of (GaMn)As is in-plane, there was no residual magnetization at zero field under the present T-MCD measurement condition where the magnetic field was applied perpendicular to the sample. To estimate the ferromagnetic transition temperature, we made the Arrott plot (M^2-B/M plot) of the same sample (d = 2nm) and calculated the spontaneous magnetizations assuming that T-MCD is proportional to the magnetization M of the sample, as shown in Fig. 2.11(b). Similar results were obtained for the (GaMn)As sample with d = 5nm, indicating that ferromagnetic ordering was observed even in the ultrathin (GaMn)As samples of d = 5nm and 2nm with their T_c ~ 70K. This is the first observation of ferromagnetism in such very thin (2nm) (GaMn)As layers. Previously it was reported that SLs composed of thinner (GaMn)As (<7nm) layers were paramagnetic

and highly resistive [2.4]. The difference between the present and previous results is the number of stacking (GaMn)As and AlAs layers (30 in the previous and 3 in the present case). Since this material system is grown by LT-MBE and low temperature growth of AlAs is generally rather difficult, interface roughness is amplified and the interface quality deteriorates with increasing the SL stacking period, as schematically shown in Fig. 2.12. In the present ultrathin heterostructures, the interfaces were kept smooth, therefore holes are not localized but mobile and can mediate the ferromagnetic ordering in the (GaMn)As layers even at d = 2nm.

To clarify whether the carriers (holes) are delocalized in the thin (GaMn)As layer, we measured temperature dependence of the sheet resistance of ultrathin (GaMn)As samples with d = 2 and 1nm, as shown in Fig. 2.11. The sample with d = 2nm showed small temperature dependence of resistance, which shows that holes are mobile, whereas the sample with d = 1nm showed an insulating behavior which indicates that holes are localized. In the thinnest sample with d = 1nm, the MCD intensity at 1T per (GaMn)As thickness is almost the same as that of the sample with d = 2nm, although clear ferromagnetic ordering was not observed at 9K. Therefore, it can be said that the threshold thickness of ferromagnetic ordering in (GaMn)As is between 1nm and 2nm. This threshold thickness is comparable to the average distance between Mn ions (0.8nm) in (GaMn)As with x_{Mn} = 0.071.

2.4. Summary

In chapter 2, we described the epitaxial growth, transport, magnetic and magneto-optical properties of (GaMn)As thin films and related heterostructures. The origin of T-MCD spectra of these materials was investigated. It was found that the origin of T-MCD signal of (GaMn)As thin films around the photon energy of 1.5-2.5eV is the optical transitions between the valence band, which is hybridized with the Mn d bands and splitted due to the p-d exchange interaction, and the conduction band of the host semiconductor. Furthermore, we clearly observed a systematic blue shift in the T-MCD spectra of ultrathin (GaMn)As / AlAs heterostructures whose (GaMn)As layer thickness d is thinner than 5nm. The mechanism of the blue shift was discussed in term of the quantum size effect. Also, ferromagnetic ordering was found even in the (GaMn)As / AlAs heterostructures with d = 2nm. This systematic blue shift and ferromagnetic ordering in ultrathin (GaMn)As / AlAs heterostructures can lead to interesting applications such as (GaMn)As based magnetic tunnel junctions with resonant tunneling structures which was proposed in ref [2.16].

References

[2.1] K. Ando, T. Hayashi, M. Tanaka, and A. Twardowski, J. Appl. Phys., **83**, 6548, (1998).

[2.2] M. Shirai, T. Ogawa, I. Kitagawa, and N. Suzuki, J. Magn. Magn. Mater., **177-181**, 1383, (1998).

[2.3] J. Okabayashi, A. Kimura, O. Rader, T. Mizokawa, A. Fujimori, T. Hayashi, and M. Tanaka, Phys. Rev. **B64**, 125304, (1999).

[2.4] T. Hayashi, M. Tanaka, K. Seto, T. Nishinaga, and K. Ando, Appl. Phys. Lett. **71**, 1825 (1997).

[2.5] T. Hayashi, M. Tanaka, T. Nishinaga, H. Shimada, and Y. Otuka, J. Cryst. Growth, **175/176**, 1063, (1997).

[2.6] M. Tanaka, J. Vac. Sci. Technol. **B16**, 2267 (1998).

[2.7] H. Shimizu, T. Hayashi, T. Nishinaga, M. Tanaka, Appl. Phys. Lett., **74** 398 (1999).

[2.8] A. Shen, F. Matsukura, S. P. Guo, Y. Sugawara, H. Ohno, M. Tani, H. Abe, H. C. Liu, J. Cryst. Growth, **201/202**, 679 (1999).

[2.9] Modern Magneto Optics And Magneto Optical Materials, edited by A. K. Zvezdin and V. A. Kotov (Institute of Physics Publishing, 1997) Studies in Condensed Matter Physics.

[2.10] J. K. Furdyna, J. Appl. Phys. **64**, R29 (1988); "Diluted Magnetic Semiconductors" in Semiconductor and Semimetals, edited by J. K. Furdyna and J. Kossut (Academic press, 1988), Vol. 25.

[2.11] K. Ando, K. Takahashi, and T. Okuda, Phys. Rev. **B46**, 12289 (1992).

[2.12] K. Sato, Jpn. J. Appl. Phys. **20**, 2403, (1981).

[2.13] J. Szczytko, W. Mac, A. Twardowski, F. Matsukura, and H. Ohno, Phys. Rev. **B59**, 12935 (1999).

[2.14] T. Dietl, H. Ohno, and F. Matsukura, Phys. Rev. **B63**, 195205 (2001).

[2.15] B. Beschoten, P. A. Crowell, I. Malajovich, D. D. Awschalom, F. Matsukura, A. Shen, and H. Ohno, Phys. Rev. Lett., **83**, 3073 (1999).

[2.16] L. Esaki and R. Tsu, IBM J. Res. Rev. **14**, 61 (1970); H. Sakaki, Proc. in Symp. on Foundations of Quantum Mechanics (Physical Society of Japan, Tokyo, 1984), p94.

[2.17] M. Tanaka, J. Vac. Sci & Technol. **B16**, 2267 (1998); M. Tanaka, H. Shimizu, T. Hayashi, H. Shimada, and K. Ando, J. Vac. Sci & Technol. **A18**, 1247 (2000).

[2.18] H. Ohno, Science **281**, 951 (1998); H. Ohno, J. Magn. Magn. Mat. **200**, 110 (1999).

[2.19] M. Tanaka and Y. Higo, Phys. Rev. Lett., **87**, 026602 (2001).

[2.20] T. Hayashi, M. Tanaka, and A. Asamitsu, J. Appl. Phys., **87**, 4673 (2000).

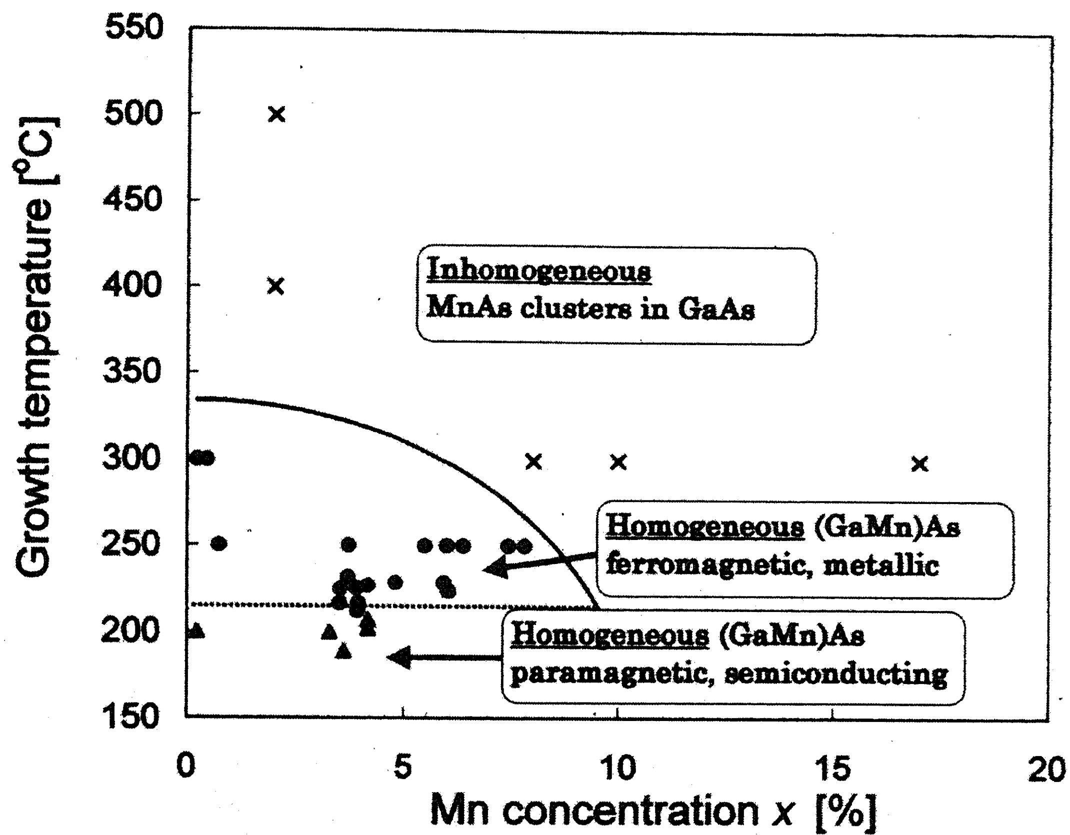

Fig. 2.1 Diagram of the film properties of (Ga, Mn, As) in relation to two growth parameters, Mn concentration x and growth temperature [2.6].

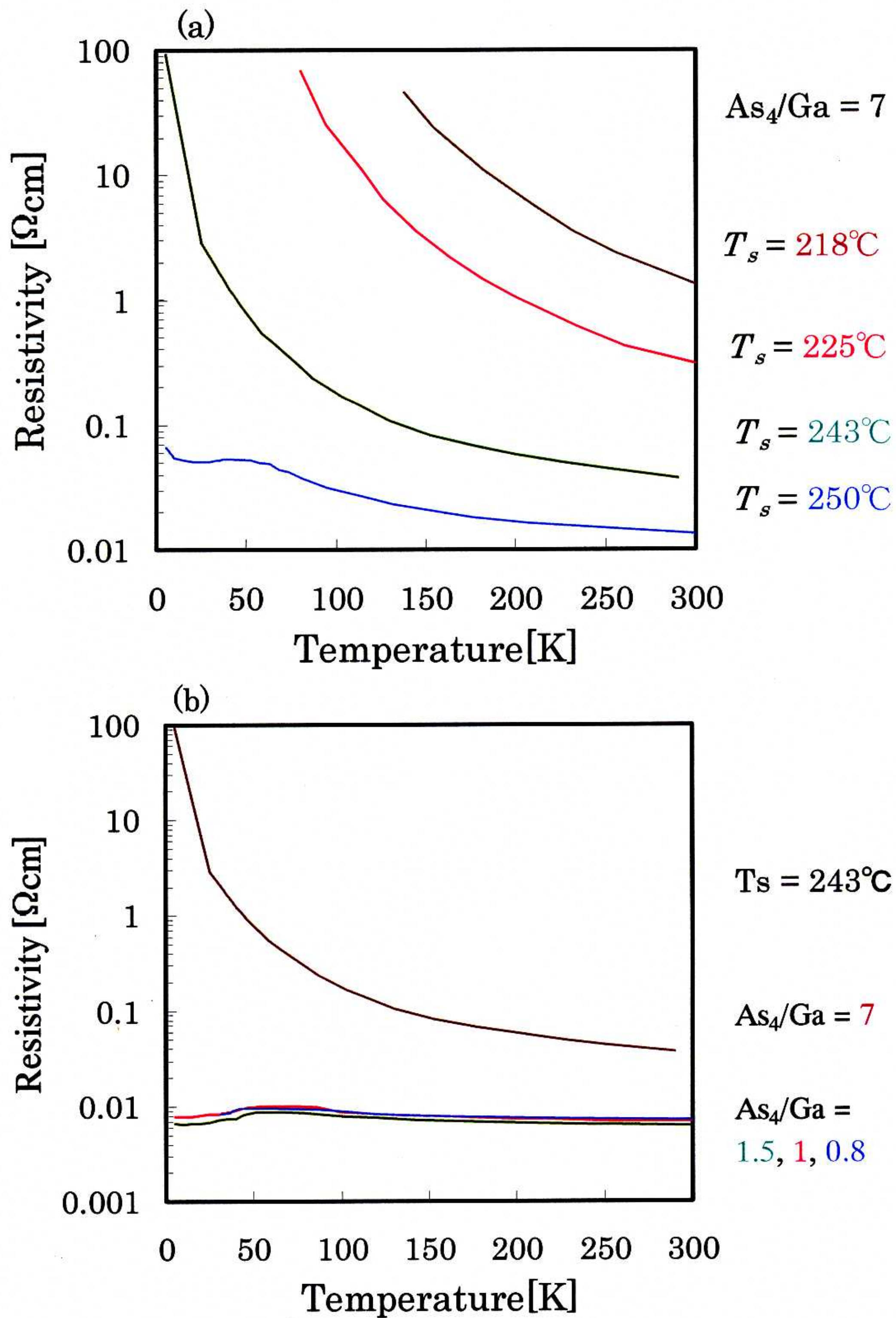

Fig. 2.2 Temperature dependence of resistivity of $(Ga_{0.957}Mn_{0.043})As$ samples, (a) grown under different substrate temperatures T_s with the As_4/Ga ratio fixed at 7, and (b) grown under different As_4/Ga ratios with the substrate temperature T_s fixed at 243℃. Difference among samples with As_4/Ga = 1.5, 1, and 0.8 is too small to distinguish, so the curves are overlapped in the whole temperature range.

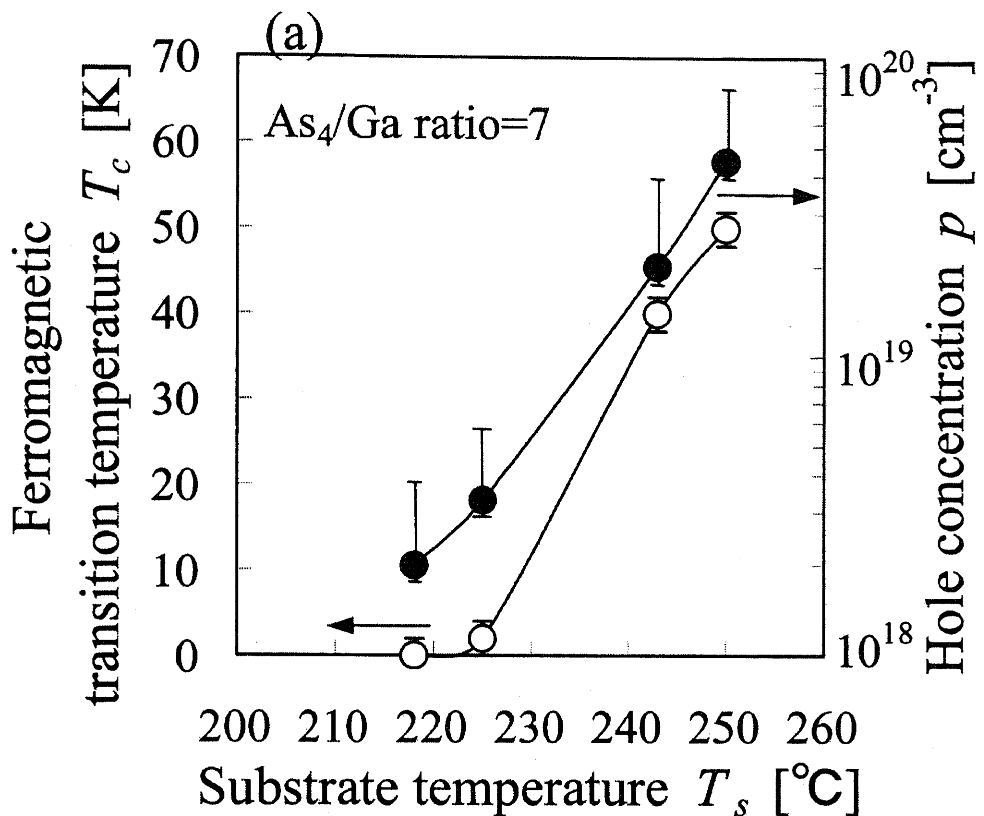

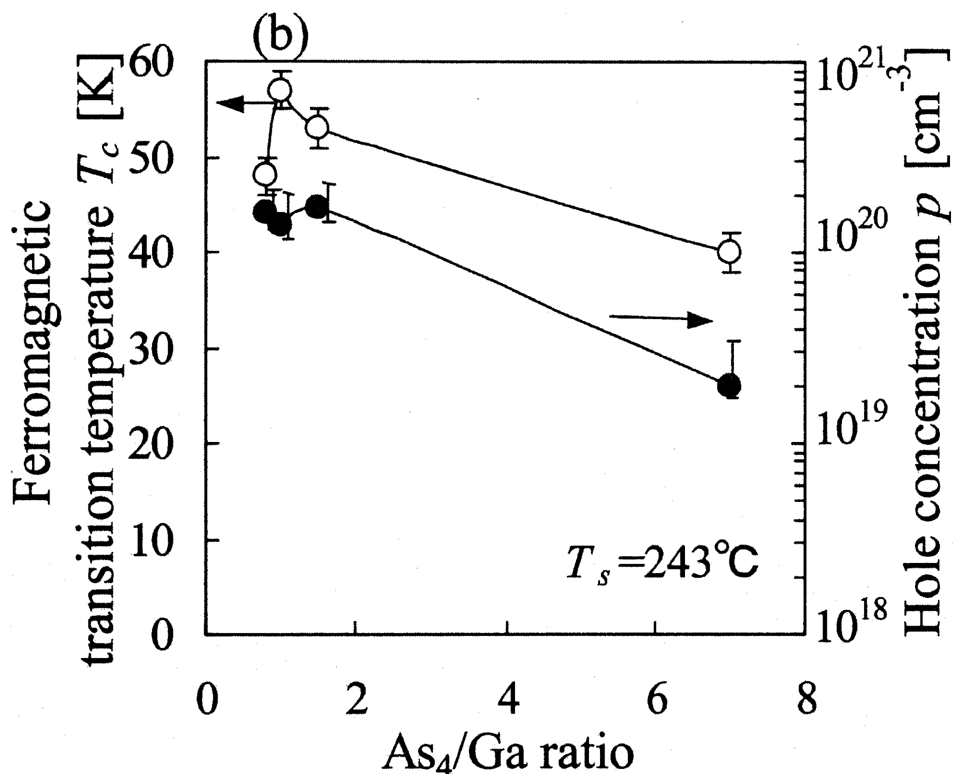

Fig. 2.3 Hole concentration p and ferromagnetic transition temperature T_c of (GaMn)As samples, (a) grown under different substrate temperatures T_s with the As_4/Ga ratio fixed at 7, and (b) grown under different As_4/Ga ratios with the substrate temperature T_s fixed at 243℃.

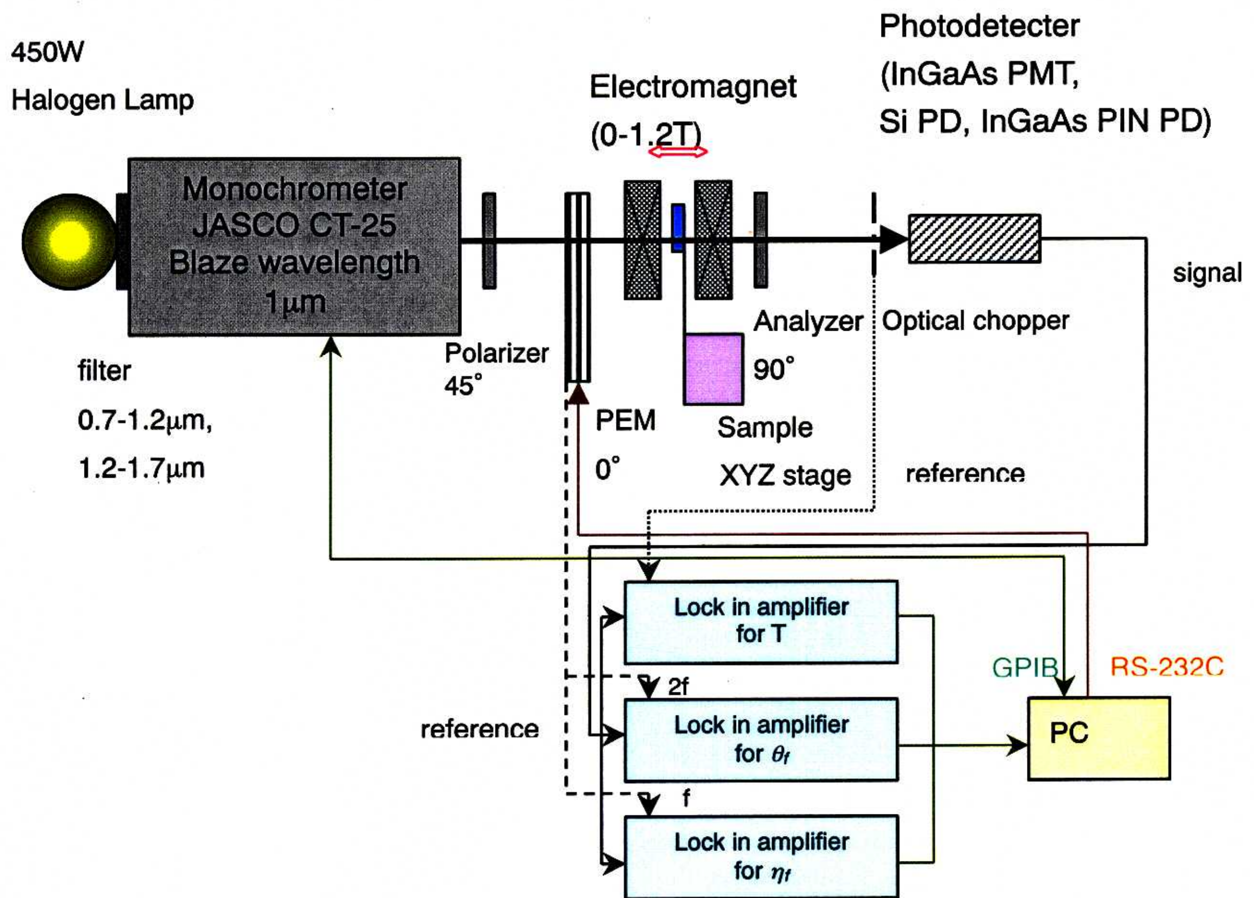

Fig. 2.4 Measurement setup for Faraday effect (Faraday rotation and ellipticity) using the circular polarization modulation technique.

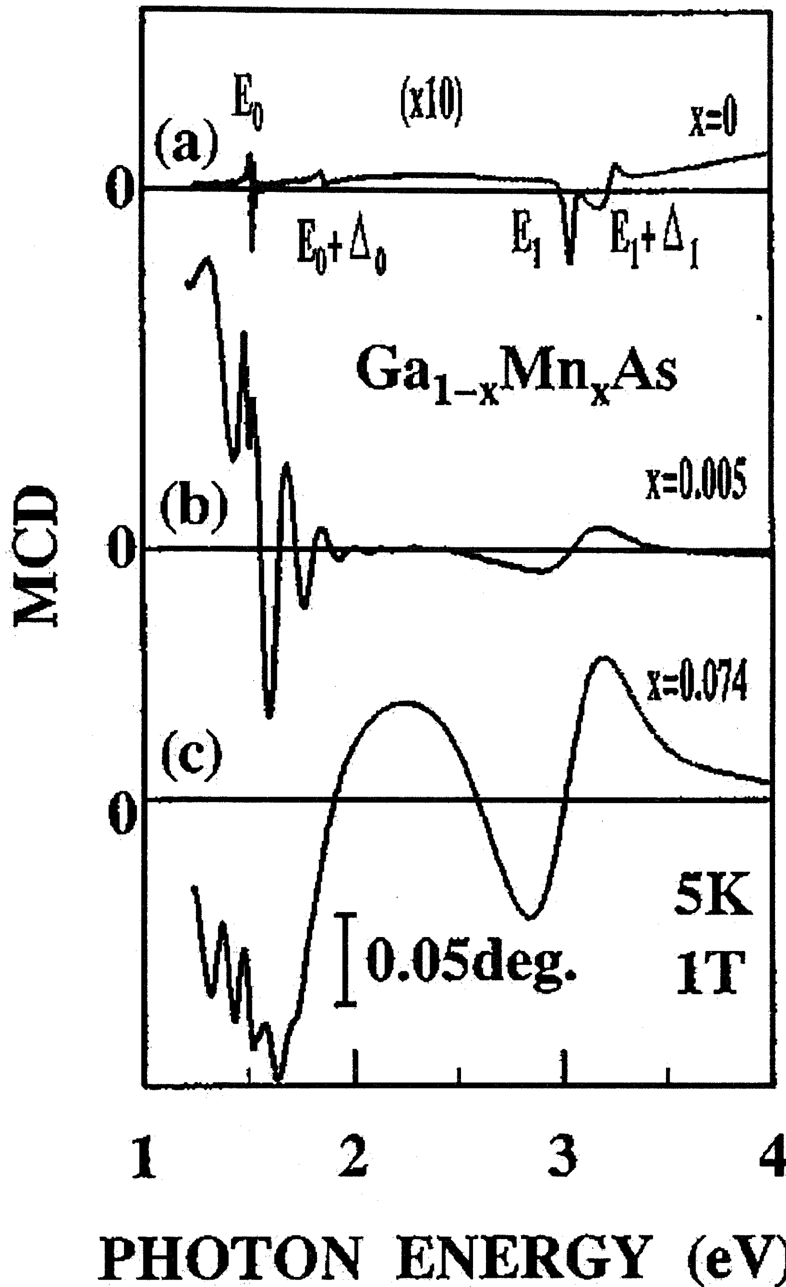

Fig. 2.5 Reflection MCD spectra of (a) a semi-insulating GaAs substrate and (b), (c) (GaMn)As films at 5K under the magnetic field of 1T applied perpendicular to the film plane. The spectrum of GaAs substrate is magnified 10 times because the signal is weaker than that of (GaMn)As [2.1].

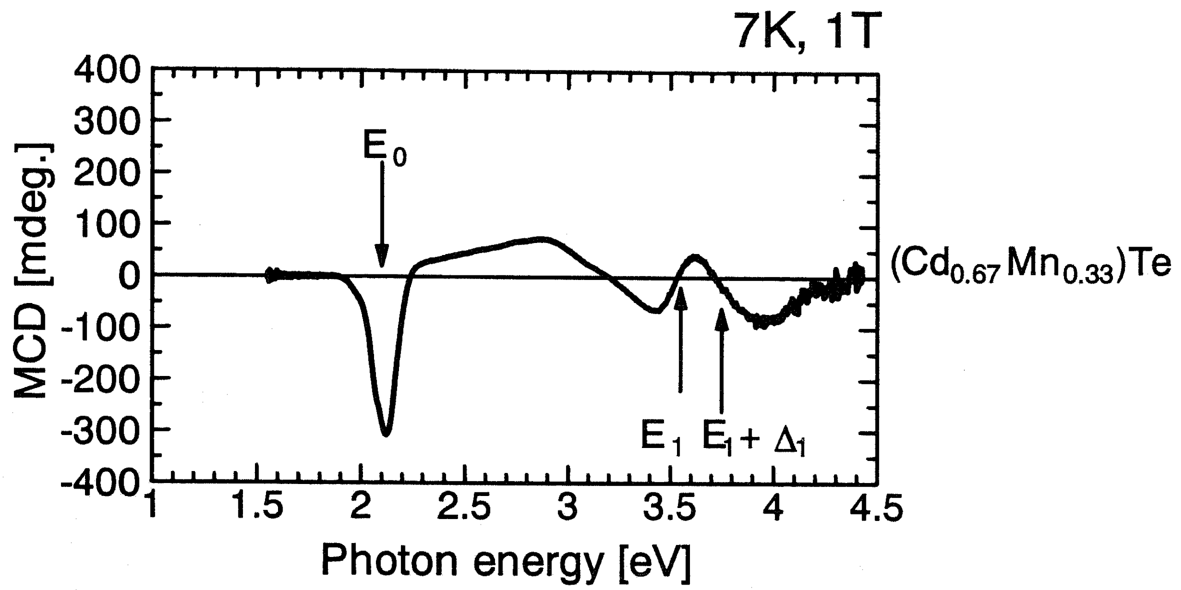

Fig. 2.6 Transmission MCD spectrum of $(Cd_{0.67}Mn_{0.33})Te$ thin film grown on sapphire substrate at 7K under the magnetic field of 1T applied perpendicular to the film plane.

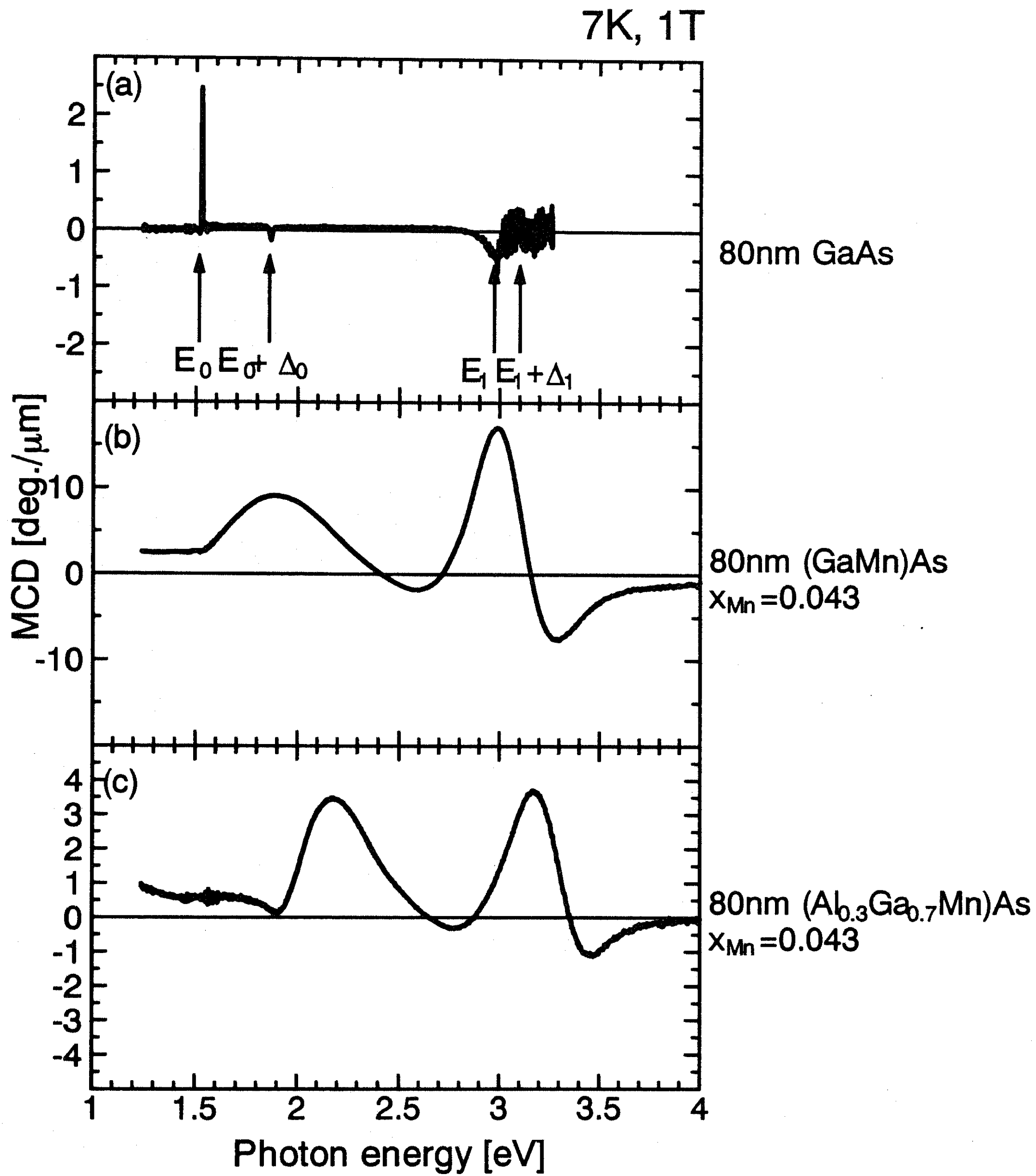

Fig.2.7 Transmission MCD spectra of (b) ($Ga_{1-x}Mn_x$)As and (c) (($Al_{0.3}Ga_{0.7})_{1-x}Mn_x$)As with x_{Mn}=0.043, measured at 9K under the magnetic field of 1T applied perpendicular to the film plane. An MCD spectrum of a 80nm thick GaAs single film is also shown as a reference in (a).

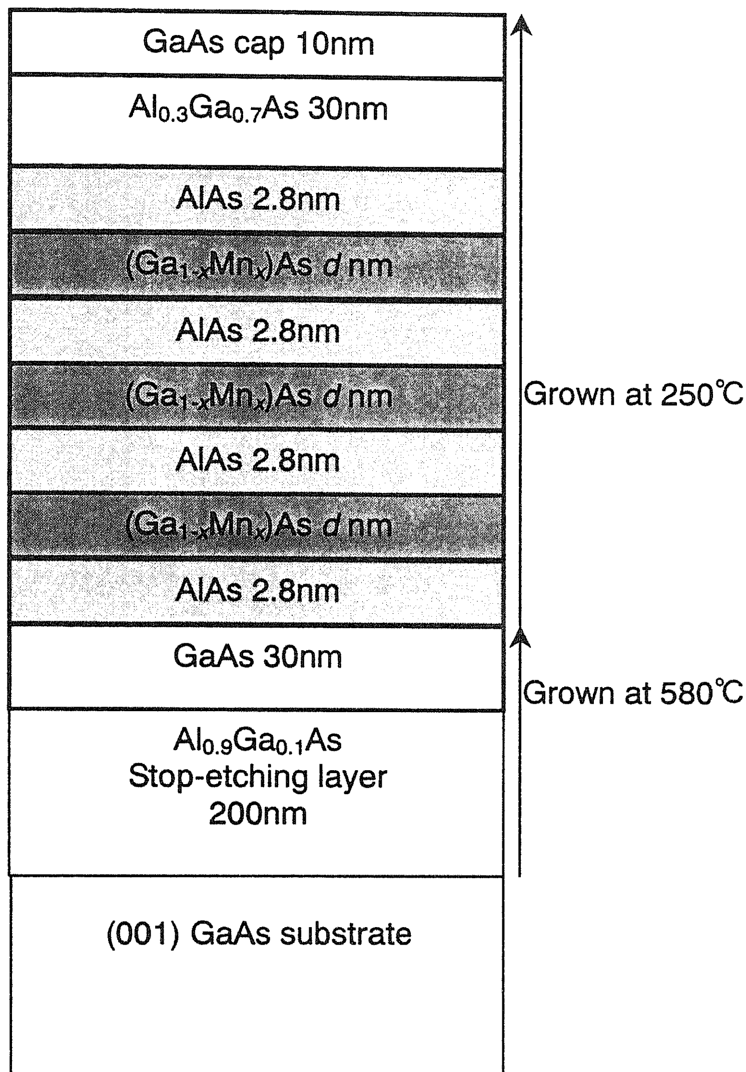

Fig. 2.8 Sample structure of the ultrathin (GaMn)As / AlAs heterostructures for T-MCD measurements. Four samples with d = 12, 5, 2, and 1nm were fabricated. The Mn concentration x of the sample with d = 12nm is 0.045, and x of the samples with d = 5, 2, and 1nm is 0.071.

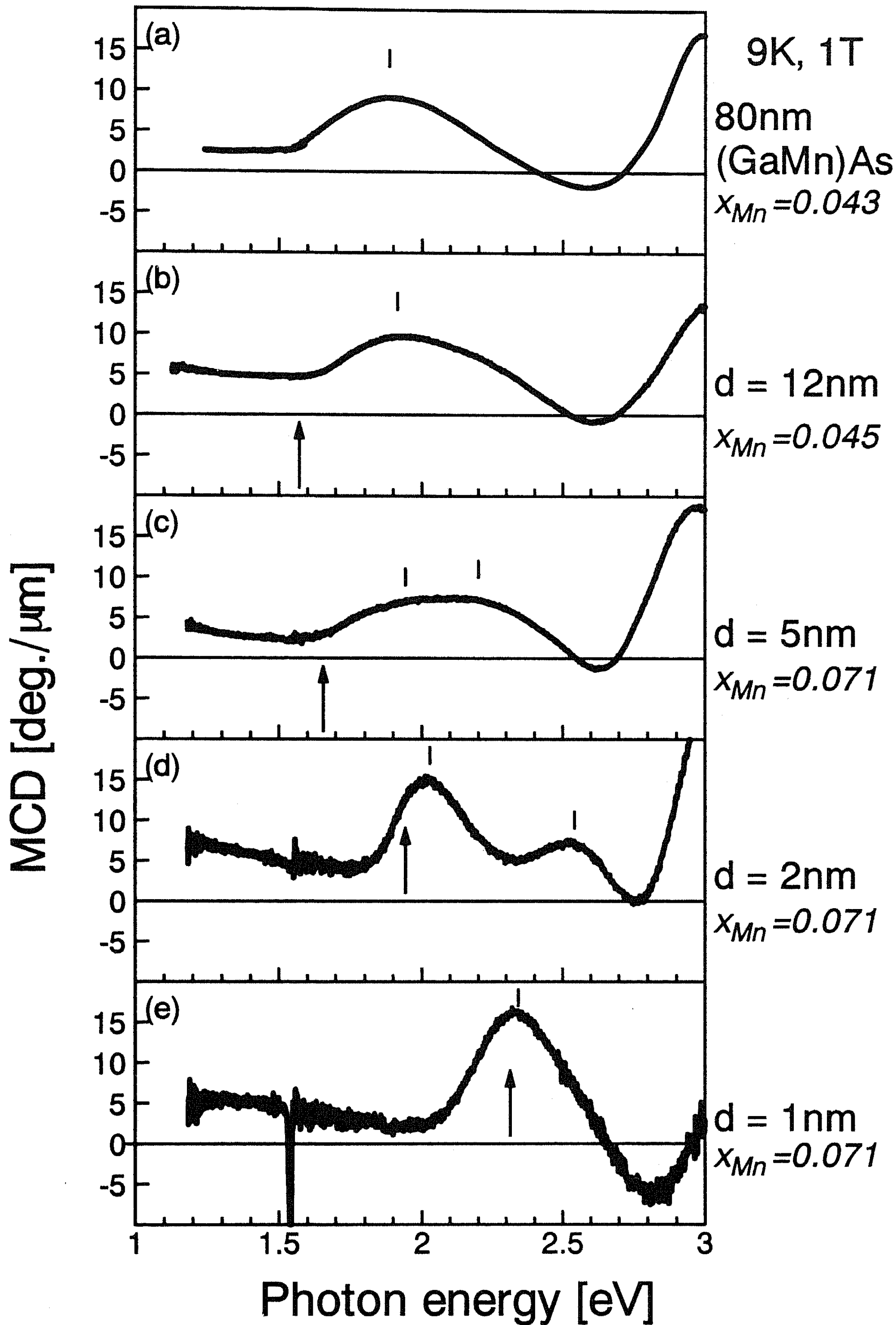

Fig. 2.9 MCD spectra of ultrathin $(Ga_{1-x}Mn_x)As$ / AlAs heterostructures with (b) d = 12nm, (c) d = 5nm, (d) d = 2nm, and (e) d = 1nm, measured at 9K under the magnetic field of 1T applied perpendicular to the film plane. An MCD spectrum of a 80nm thick $(Ga_{0.957}Mn_{0.043})As$ single film is also shown as a reference in (a). MCD peaks of these spectra are marked by lines for the eyes. Calculated transition energy positions using the Kronig-Penny model are marked by arrows in (b)-(e).

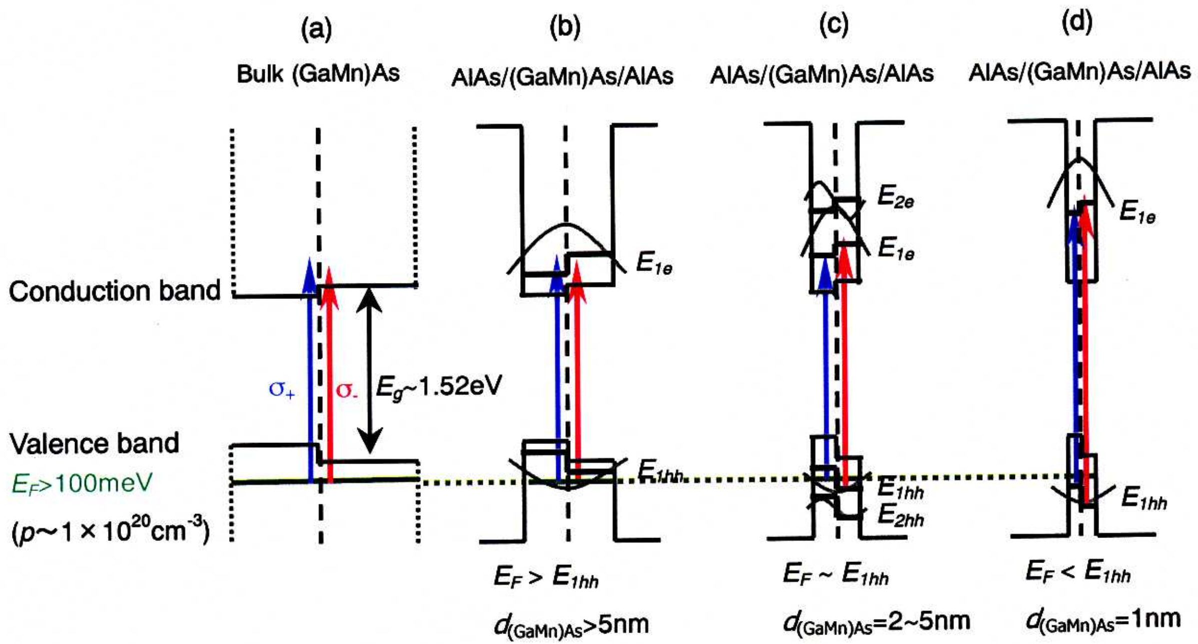

Fig. 2.10 Schematic pictures of the band alignment in bulk (GaMn)As and AlAs / (GaMn)As / AlAs heterostructures. E_F and $d_{(GaMn)As}$ denote the Fermi energy and the thickness of (GaMn)As layer respectively. Blue and red arrows correspond to σ_+ and σ_- optical transition respectively.

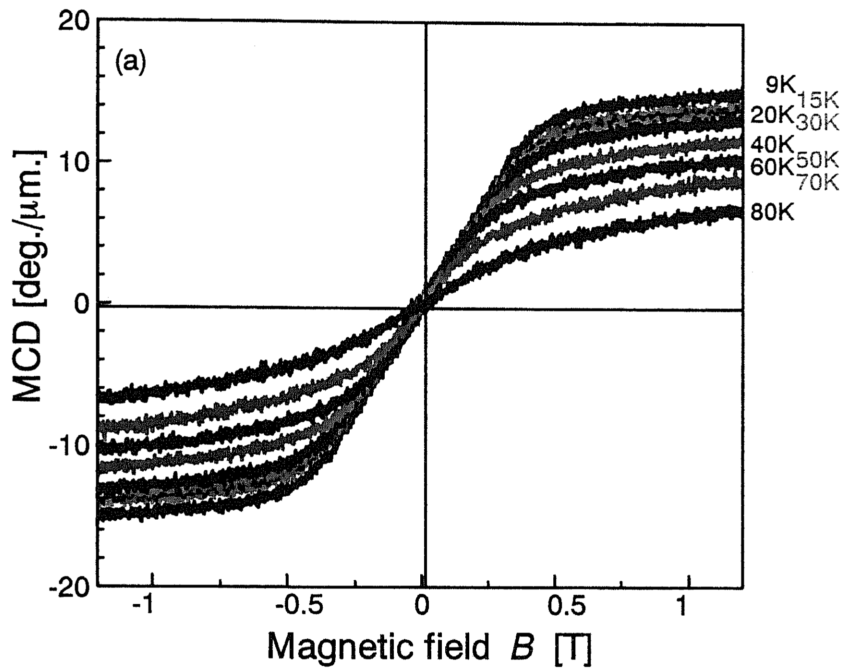

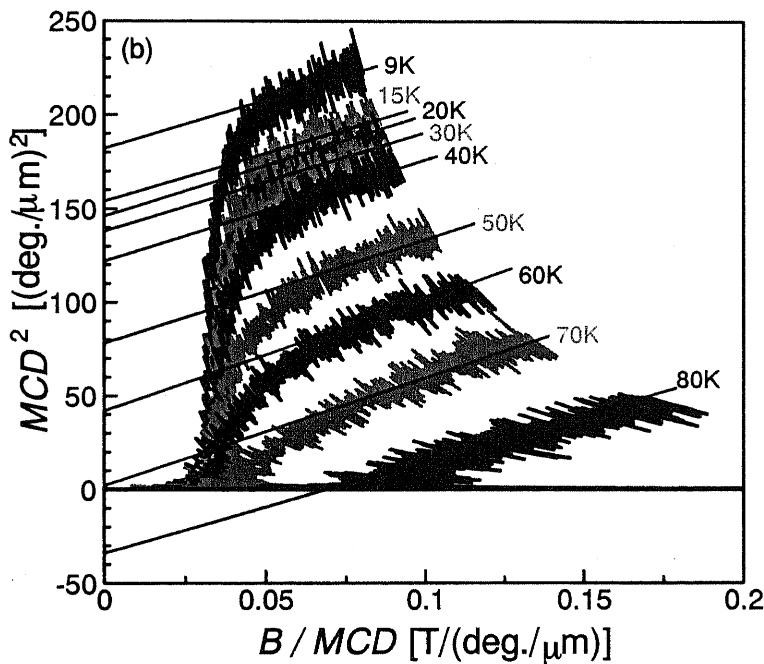

Fig. 2.11(a) Magnetic field (B) dependence of the MCD intensity of the sample with d = 2nm measured at 9K – 80K. The measurement wavelength was fixed at 615nm, corresponding to 2.02eV, which is the peak energy of the MCD spectrum (Fig. 2(d)).
(b) Arrott plot (M^2-B/M) of the sample with d = 2nm assuming that T-MCD is proportional to the magnetization M of the sample. By extrapolating these curves from high magnetic field to zero field as shown by lines, the spontaneous magnetizations can be calculated, and the ferromagnetic transition temperature of the sample with d = 2nm was estimated to be 70K.

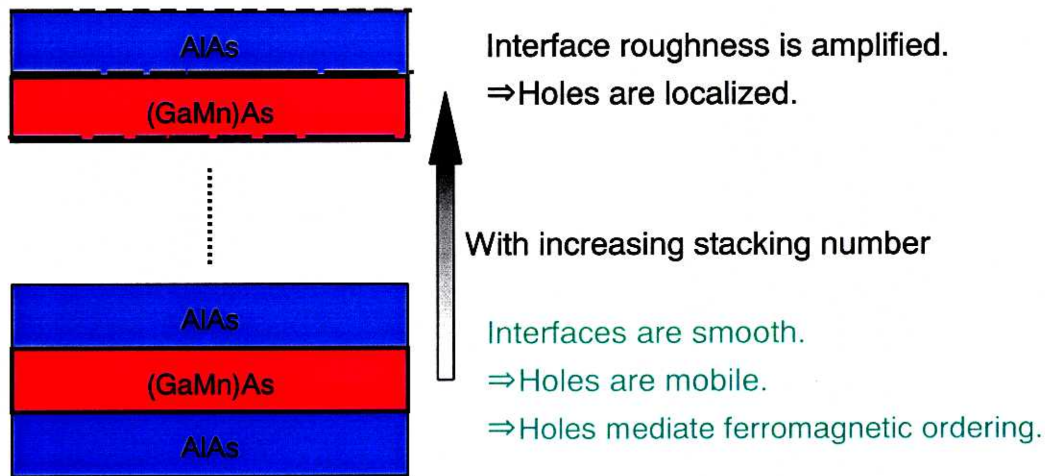

Fig. 2.12 Schematic picture of the interface roughness in the (GaMn)As / AlAs superlattice grown by low-temperature molecular-beam epitaxy.

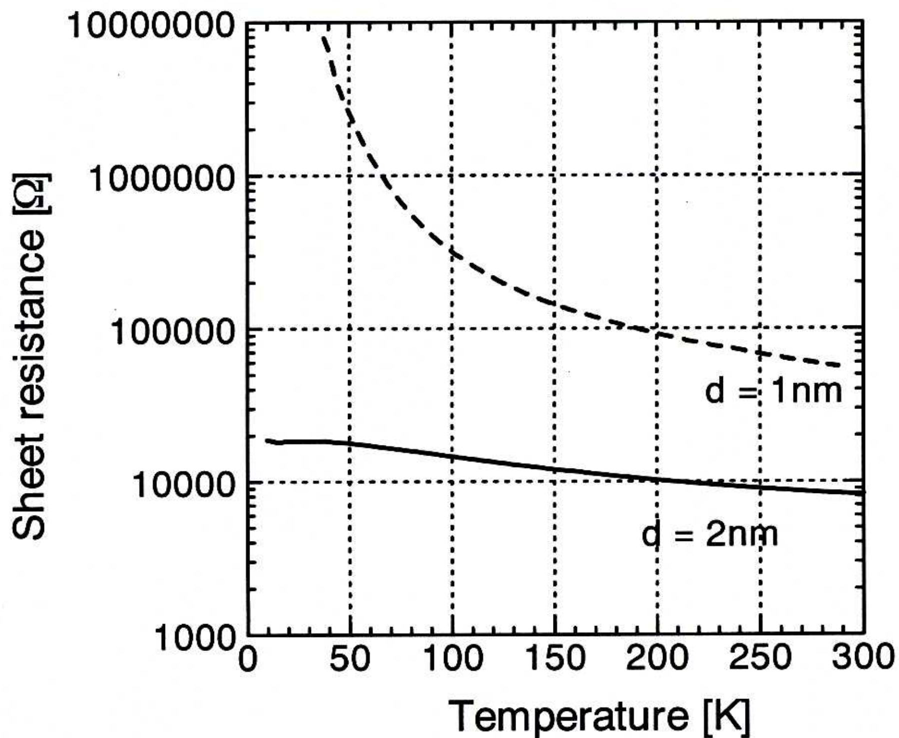

Fig. 2.13 Temperature dependence of sheet resistance of (GaMn)As / AlAs heterostructure samples with d = 2nm (solid curve) and d = 1nm (dashed surve).

~Chapter 3~

Fabrication, structural, optical and magneto-optical properties of MnAs nanoclusters embedded in a GaAs matrix

The granular material, MnAs nano-scale clusters embedded in a GaAs matrix (hereafter GaAs:MnAs), is also attractive for spin electronics, because GaAs:MnAs shows magnetization *at room temperature* [3.1]. So far, magneto-transport measurements were carried out on GaAs:MnAs thin films and negative magneto-resistance of 1.5% at 30K in 1T was reported [3.2]. Magneto-optical characterizations were also carried out on GaAs:MnAs thin films and Faraday rotation of 0.2 deg./μm was reported [3.3]. However, detail characterizations, with focus on the relations among the structural, magnetic, optical and magneto-optical properties have not been carried out, and the origin of the optical loss and magneto-optical effects of GaAs:MnAs has not been clarified yet.

In order to apply GaAs:MnAs to the magneto-optical devices, as will be described in Chapter 4 and Chapter 5, it is necessary to grasp its structural, magnetic, optical and magneto-optical properties. In this chapter, a fabrication method of the granular material, GaAs:MnAs, is introduced. Then, structural characterizations of GaAs:MnAs are presented. Lastly, magnetic, optical transmission and magneto-optical properties of GaAs:MnAs are investigated. Furthermore, the origin of the optical loss in GaAs:MnAs and the comparison of the magneto-optical properties between (GaMn)As and GaAs:MnAs are discussed.

3.1 Fabrication of MnAs nanoclusters embedded in GaAs (GaAs:MnAs)

When (GaMn)As is annealed at temperature higher than its growth temperature, typically 500-700℃, MnAs nanoclusters are formed in a GaAs matrix, with their average diameter around 10nm, due to phase separation [3.1]. This is because (GaMn)As is a metastable material grown by low-temperature molecular-beam epitaxy and contains excess As atoms whose concentration is slightly larger (by ~1%) than the stoichiometric composition. When (GaMn)As is annealed, the excess As atoms react with Mn atoms and MnAs nanoclusters, which is thermodynamically more stable, are formed in a GaAs matrix.

In this study, we fabricated this GaAs:MnAs material by annealing in the MBE growth chamber with As flux of $\sim 1\times 10^{-5}$Torr. This annealing method is compatible with

the overgrowth of GaAs / AlAs heterostructures on GaAs:MnAs as described later. The evolution of the RHEED reconstruction pattern during the heating of (GaMn)As from 250℃ to 620℃ was (1×2) → c(4×4) → (2×4) → (3×1), and no indication of surface segregation of Mn atoms was observed. After the annealing of (GaMn)As and the formation of GaAs:MnAs, the surface was so smooth that RHEED intensity oscillations were observed at the initial stage of the regrowth of GaAs / AlAs at the growth temperature T_s of 580℃. Therefore it was confirmed that there were no problems in the overgrowth of GaAs / AlAs heterostructures on the GaAs:MnAs surface.

3.2 *Structural characterizations of GaAs:MnAs*

To characterize the structural properties, we fabricated GaAs:MnAs multilayers separated by 3nm-thick AlAs spacers, as shown in Fig. 3.1. The multilayer structures consisting of GaAs:MnAs and AlAs were obtained by annealing (GaMn)As / AlAs multilayers grown by MBE at 250℃. For structural characterizations, cross sectional images by transmission electron microscopy (TEM) were taken on these samples. These samples were obtained by annealing ($Ga_{1-x}Mn_x$)As / AlAs multilayer structures at 580℃ under the As flux for 1 hour in our MBE growth chamber. Fig. 3.1(a) shows a TEM image of 50nm-thick GaAs:MnAs layers with different Mn concentrations x_{Mn} = 0.011, 0.023, and 0.048, and Fig. 1(b) shows a TEM image of GaAs:MnAs layers with different thicknesses of 50, 20, 10, 5, and 2nm at a constant Mn concentration x_{Mn} = 0.048. From Fig. 3.1(a), it was found that with increasing the Mn concentration, the average size of the MnAs nanoclusters decreases and the density increases. The average D_{MnAs} and standard deviation ΔD_{MnAs} of the MnAs nanocluster diameter were estimated from 586 MnAs clusters in a 450nm-wide TEM image. The estimated values of D_{MnAs} and ΔD_{MnAs} are 9.7nm and 3nm in the x_{Mn} = 0.011 region, 6.9nm and 1.4nm in the x_{Mn} = 0.023 region, and 6.1nm and 1.2nm in the x_{Mn} = 0.048 region, respectively (see also Table 3.1(a)). From Fig. 3.1(b), it was found that with decreasing the GaAs:MnAs nanocluster layer thickness at a constant Mn concentration, ΔD_{MnAs} decreased. The values of D_{MnAs} and ΔD_{MnAs} estimated from a 450nm-wide scope of TEM are 6.1nm and 1.2nm in the 50nm-thick layer, 6.1nm and 1.1nm in the 20nm-thick layer, 6.1nm and 0.8nm in the 10nm-thick layer, and 5.7nm and 0.9nm in the 5nm-thick layer, respectively (see also Table 3.1(b)). No MnAs cluster was observed in the 2nm-thick layer. Note that in the 5nm and 10nm-thick GaAs:MnAs layers, there were no large MnAs clusters whose size much exceeds the GaAs:MnAs layer thickness, whereas some large MnAs clusters exceeding 10nm in diameter were observed in the thicker (20nm and 50nm-thick) GaAs:MnAs layers.

(a)

x_{Mn}	D_{MnAs} [nm]	ΔD_{MnAs} [nm]
0.048	6.1	1.2
0.023	6.9	1.4
0.011	9.7	3

(b)

$d_{GaAs:MnAs}$ [nm]	D_{MnAs} [nm]	ΔD_{MnAs} [nm]
50	6.1	1.2
20	6.1	1.1
10	6.1	0.8
5	5.7	0.9

Table 3.1 The average D_{MnAs} and standard deviation ΔD_{MnAs} of the MnAs nanocluster diameter. (a) Mn concentration x_{Mn} dependence, (b) GaAs:MnAs layer thickness $d_{GaAs:MnAs}$ dependence.

From these structural characterizations, it can be said that we can suppress the formation of large MnAs clusters and reduce the fluctuation in the MnAs nanocluster size by introducing superlattice structures composed of a few nanometer-thick GaAs:MnAs and AlAs layers.

With increasing the annealing temperature, the MnAs cluster size and density of each layer became larger and smaller respectively. Fig. 3.1(c) shows a TEM image of MnAs clusters, which is the same structure as that of Fig. 3.1(a), but annealed at different temperature of 650℃ for 1hour under the As flux.

Fig. 3.1(d) shows a high resolution lattice image of MnAs nanoclusters taken from the same sample of Fig. 3.1(b). No dislocations can be observed either in the MnAs nanoclusters or in the GaAs / AlAs layers, indicating excellent crystalline quality of the GaAs:MnAs nanocluster system and excellent compatibility with GaAs / AlAs heterostructures. The relationship of crystal orientation between the hexagonal MnAs and zinc-blende GaAs is [0001]MnAs // [-110]GaAs, [-1-120]MnAs // [110]GaAs and (-1100)MnAs // (001)GaAs, which is the same relationship as in typeA MnAs films grown on (001) GaAs substrates [3.2].

3.3 *Magnetic properties of GaAs:MnAs*

We have done magnetization measurements on GaAs:MnAs samples by a superconducting quantum interference device (SQUID). Fig. 3.2 (a) shows magnetization curves of GaAs:MnAs (x_{Mn} = 0.06) at room temperature (300K) and 2K. The GaAs:MnAs sample was fabricated by annealing ($(Ga_{0.94}Mn_{0.06})As$) at 580℃ under the As flux for 1 hour and the sample thickness was 200nm. Although MnAs is a ferromagnet with its Curie temperature of 40℃, in case that MnAs is dispersed as nanoscale clusters in

a nonmagnetic GaAs matrix, the sample shows a superparamagnetic property, where the magnetization saturates at low magnetic field with no residual magnetization. The magnetization curves can be expressed by the Brillouin function of J = ∞ (Langevin function) as follows [3.5], assuming that no magnetic couplings exist among the MnAs nanoclusters.

$$\frac{M}{M_s} = \coth(\alpha) - \frac{1}{\alpha} \qquad (3-1)$$

$$\alpha = \frac{\mu_0 M_s V H}{k_B T}$$

Here, $\mu_0 M_s$ is the saturation magnetization of the ferromagnet, V is the volume of the cluster, H is the applied magnetic field, k_B is the Bolzmann constant, and T is temperature. Fig. 3.2 (b) shows the calculated magnetization curve of GaAs:MnAs assuming that the saturation magnetization of MnAs is 880 emu/cc [3.5], and the MnAs clusters are spherical with the diameter of d. By comparing Fig. 3.2 (a) with Fig. 3.2 (b), the average diameter of the MnAs clusters in this sample was estimated to be 6nm.

Interestingly, it was found that the magnetization of GaAs:MnAs was enlarged with Si doping during the growth of (GaMn)As. Fig. 3.3 show magnetization curves of Si-doped (solid curve) and undoped (dashed curve) GaAs:MnAs samples (x_{Mn} = 0.06) at 300K measured by SQUID. The magnetization under a magnetic field of 1T at 300K and 2K of the undoped GaAs:MnAs sample were 23.9emu/cc and 38emu/cc, respectively and the magnetization under a magnetic field of 1T at 300K and 2K of the Si-doped GaAs:MnAs sample were 26.3emu/cc and 47.2emu/cc, respectively. From these results, it was found that the magnetization under a magnetic field of 1T at 300K and 2K of the Si-doped GaAs:MnAs sample was 1.1 and 1.28 times larger than that of the undoped GaAs:MnAs sample, respectively. The values of magnetization of these GaAs:MnAs samples measured at 2K under a magnetic field of 5T are 52 emu/cc and 40 emu/cc for the GaAs:MnAs samples with and without Si doping, respectively. From the measured magnetizations at 2K, the Mn mole fraction (x = 0.06) in these samples, and the reported saturation magnetization of bulk MnAs (880 emu/cc) [3.5], it was estimated that 99% and 77% of the total Mn ions contributed to the formation of MnAs nanoclusters in the GaAs matrix with and without Si doping, respectively. Furthermore, the Langevin fitting to the magnetization curves of these GaAs:MnAs samples, which show superparamagnetic properties at room temperature, revealed a slightly larger average MnAs cluster diameter (d = 7.5nm) in the Si-doped GaAs:MnAs than that (d = 6nm) in the undoped GaAs:MnAs sample. From these estimations, we concluded that the existence of Si in the GaAs matrix made the nucleation of MnAs easier during the annealing of (GaMn)As, and more

Mn ions contributed to form MnAs nanoclusters in the Si-doped GaAs:MnAs samples, although the Si concentration is much smaller (at most 1×10^{18}cm^{-3}) than the Mn concentration (>1×10^{21}cm^{-3}) in the GaAs matrix. The Si doping is one of the effective method for controlling the MnAs cluster size other than the methods by changing the annealing temperature, Mn concentration and so on.

3.4 Optical transmission and magneto-optical properties of GaAs:MnAs

3.4.1 GaAs:MnAs

Semiconductor / magnetic hybrid structures exhibit relatively large magneto-optical effects. Kuroiwa et al. reported that (GaMn)As showed Faraday rotation of 6deg./μm at 10K (ferromagnetic state) and 0.08deg./μm at room temperature (at 1T, paramagnetic state) at the wavelength of 800nm [3.6]. Also, Akinaga et al. reported that GaAs:MnAs showed Faraday rotation of 0.2deg./μm at the wavelength of 980nm at room temperature [3.3].

In order to explore the possibilities of magneto-optical device applications using GaAs:MnAs, optical transmission, Faraday rotation and ellipticity (or MCD) of GaAs:MnAs were measured. The magneto-optical measurements were carried out in the wavelength range of 800-1600nm using the circular polarization modulation technique under a magnetic field (maximum 1.2T) applied perpendicular to the sample surface at room temperature.

Fig. 3.4(a)-(c) show optical transmission, Faraday ellipticity (MCD), and Faraday rotation spectra of the 200nm-thick GaAs:MnAs with x_{Mn} = 0.047 in the wavelength range of 800-1100nm. The optical transmission measurement was done after removing the GaAs substrate selectively. The Faraday effect was measured under the magnetic field of 1T. It was found that the Faraday elliptcity and Faraday rotation were 0.5-0.8deg./μm and 0.4-1.0deg./μm, respectively, in this wavelength range. A clear absorption edge was not observed at 870nm, corresponding to the bandgap wavelength of GaAs, in the optical transmission spectrum (Fig. 3.4(a)). This is because MnAs nanoclusters break the translation symmetry of the host GaAs lattice. To investigate the origin of the magneto-optical effect, we measured MCD (Faraday ellipticity) spectra of $Al_yGa_{1-y}As$:MnAs (MnAs nanoclusters embedded in $Al_yGa_{1-y}As$) with the Al content y = 0.3 and 0.7, as shown in Fig. 3.5. The MCD spectral shape was found to be independent of the host semiconductor. Therefore, the origin of magneto-optical effect of GaAs:MnAs is from bulk MnAs, although the MnAs cluster size (~10nm) is much smaller than the measurement wavelength (800-1100nm).

Faraday rotation per unit magnetic layer thickness, of GaAs:MnAs is large

(0.4-1.0deg./μm), compared with that of commercially available II-VI based DMS, CdMnHgTe (0.03deg./ μm at 0.5T at the wavelength of 980 nm) [3.7]. However, a thick film (> 50μm) is necessary to obtain 45° Faraday rotation which is necessary for Faraday rotators in optical isolators. It is not realistic to grow such a thick film by epitaxial growth, therefore some thin-film-type devices with large Faraday rotation are required, as will be described in Chapter 4. Another problem to be solved is the optical absorption loss in GaAs:MnAs. In the following section 3.4.2 and 3.4.3, we describe two approaches to avoid the optical absorption loss of GaAs:MnAs.

3.4.2 Improvement of optical transmission in [GaAs:MnAs] / AlAs superlattices

For optical isolator application, high optical transmission as well as large magneto-optical effect is required. GaAs:MnAs is obtained by annealing (GaMn)As at 500-600℃, and the typical MnAs nanocluster size is around 10nm. However, both the size and density of the MnAs nanoclusters size are dependent on the Mn concentration, growth conditions of (GaMn)As, and annealing conditions (annealing temperature and time). Also, there is considerable fluctuation in the cluster size. Since the absorption and magneto-optical properties of GaAs:MnAs are strongly dependent on its cluster size, as will be described in section 3.6, it is important to control the MnAs nanocluster size and investigate its influence on the absorption and magneto-optical properties. For this purpose and towards higher magneto-optical performance, we have fabricated semiconductor-based magnetic superlattices (SLs) having MnAs nanoclusters, consisting of GaAs:MnAs and AlAs and measured their optical transmission and magneto-optical spectra. From the structural characterizations described in section 3.3, it can be said that we can suppress the formation of large MnAs clusters and reduce the fluctuation in the MnAs nanocluster size by introducing SL structures composed of a few nanometer-thick GaAs:MnAs and AlAs layers. This SL structure is one of the good candidate approaches for controlling the magneto-optical properties of GaAs:MnAs.

Here, we show the absorption and magneto-optical properties of [GaAs:MnAs] / AlAs SL structures, whose MnAs nanocluster size is controlled as described above. The magneto-optical spectra of such SLs were characterized by MCD, which is equal to the Faraday ellipticity. Fig. 3.6 shows optical transmission and MCD spectra of SL structures having 20 periods of GaAs:MnAs / AlAs (2.8nm), with different GaAs:MnAs thicknesses of 5 and 12nm. These SLs are obtained by annealing (GaMn)As / AlAs SLs with a Mn concentration x_{Mn} of 0.047 at 580℃ for 1 hour. Transmission and MCD spectra of a 200nm-thick GaAs:MnAs single layer are also shown by a dotted curve as a reference. From Fig. 3.6, it was found that the optical transmission of the SLs were improved by a

factor of 2 while keeping their magneto-optical intensities, compared with the single thick GaAs:MnAs film. A possible reason for this improvement is that formation of large MnAs nanoclusters, which lead to large absorption, was suppressed in the SL structures, and thus the transparency was improved.

3.4.3 Optical transmission and magneto-optical properties of GaAs:MnAs in a longer wavelength region of 1-1.6 μm and the effect of Si doping

Magneto-optical characterizations of GaAs:MnAs at the wavelength of 1.55μm are especially important for the application in the fiber-optic telecommunication system. In this section, we report on the magneto-optical properties of Si-doped GaAs:MnAs in a near infrared wavelength region of 0.9-1.6μm.

Fig. 3.7 (a)-(c) show optical transmission and magneto-optical spectra (Faraday ellipticity and Faraday rotation) of 200nm-thick GaAs:MnAs thin film samples. These GaAs:MnAs samples were fabricated by annealing $(Ga_{0.926}Mn_{0.074})As$ at 580℃ for 1 hour under the As pressure in our MBE chamber. Two of these samples were doped with Si with concentrations of $5\times10^{17}cm^{-3}$ (solid curves) and $1\times10^{18}cm^{-3}$ (gray curves) during the growth of (GaMn)As, and one sample was undoped (dashed curves). Here, Si donors were doped in order to compensate carriers (holes) supplied by remaining Mn ions in the GaAs matrix after the annealing, hence it is expected that the free carrier absorption in the mid-gap energy of GaAs, corresponding to the wavelength longer than 0.9μm, is suppressed. All the measurements were done at room temperature and the magneto-optical spectra were measured under a magnetic field of 1T applied perpendicular to the films. GaAs substrates below the GaAs:MnAs layers were removed by selective etching before the measurements.

It was found that Si doping during the growth of (GaMn)As enlarged the magneto-optical intensities, especially in Faraday ellipticity, although the optical transmission was almost unchanged, as shown in Fig. 3.7. The Faraday ellipticity of the Si-doped GaAs:MnAs sample with a Si concentration of $5\times10^{17}cm^{-3}$ (solid curve) is 1.3 times larger than that of the GaAs:MnAs sample without Si doping (dashed curve). To clarify this reason, we have done magnetization measurements on Si-doped and undoped GaAs:MnAs samples at 2-300K by SQUID, as described in section 3.3. The Mn concentration x was 0.06 and the Si doping concentration was $1\times10^{18}cm^{-3}$ in the GaAs:MnAs samples for the magnetization measurements. The magnetization under the magnetic field of 1T at 300K of the Si-doped GaAs:MnAs sample was 1.1 times larger than that of the undoped GaAs:MnAs sample. Also, the Faraday ellipticity measured at the wavelength of 1μm under the magnetic field of 1T at 300K of the Si-doped GaAs:MnAs sample of Fig. 3.7 was 1.28 times larger than that of the undoped

GaAs:MnAs sample of Fig. 3.7. Therefore, the increase of magneto-optical intensity mainly comes from the increase of magnetization. While the transmission was unchanged between the Si-doped and undoped GaAs:MnAs samples (Fig. 3.7 (a)), the resistivity of the Si-doped GaAs:MnAs samples was larger by a factor of 10 than that of the undoped GaAs:MnAs sample, indicating that the doped Si compensated carriers (holes) supplied by remaining Mn acceptors. Accordingly, it is suggested that the main origin of the optical transmission loss in GaAs:MnAs in the mid-gap energy region of GaAs is optical scattering and absorption loss by the MnAs nanoclusters, not the free carrier absorption by the remaining holes in the GaAs matrix.

Furthermore, the optical transmission of GaAs:MnAs is improved in the longer wavelength (>1.0μm), as shown in Fig. 3.7 (a). The optical transmission at 1.55μm was twice as large as that at 0.98μm. The Faraday rotation decreases monotonously with increasing wavelength and changes its sign at 1.48μm. The Faraday rotation of the Si-doped GaAs:MnAs (solid curve) is 0.17 deg./μm at 1.55μm, which is remarkably high and comparable to that of garnets [3.8]. From the investigations above, it can be said that magneto-optical properties of GaAs:MnAs are improved by Si doping and by using the longer operational wavelength.

3.5 The origin of the optical loss and magneto-optical effect in GaAs:MnAs

What is the mechanism of the optical absorption in GaAs:MnAs? We have to notice the fact that the MnAs cluster size is typically 5-10nm, which is much smaller than the wavelength of light (800~1600nm) discussed here. Therefore, the light wave probably propagates in a granular composite as if it were a continuous medium. In this section, we discuss the origin of the optical loss and magneto-optical effect in GaAs:MnAs.

The MnAs cluster size strongly depends on the annealing conditions (annealing temperature and time). Here, we describe the annealing condition dependence of the optical transmission and magneto-optical properties of GaAs:MnAs to clarify the origin of the optical loss in GaAs:MnAs. Fig. 3.8 (a)-(c) show optical absorption, Faraday ellipticity, Faraday rotation spectra of two GaAs:MnAs samples (sample (A) and sample (B)) with the same nominal Mn content $x_{Mn} = 0.06$. Measurements were done at room temperature and the magneto-optical Faraday effects were measured under a magnetic field of 1T applied perpendicular to the film plane. Annealing conditions of the two samples are as follows. Sample (A) was annealed at 580℃ for 1hr, and sample (B) was annealed at two step, annealed at 600℃ for 3min. and 650℃ for 30sec. Fig. 3.8 (d) shows the magnetic field dependence of Faraday ellipticity of these samples at the wavelength of

1μm. We can estimate the average MnAs cluster size from Fig. 3.8 (d) assuming that the magneto-optical intensity (Faraday ellipticity) is proportional to the magnetization of the sample and using the method described in section 3.3 (Langevin fitting). The average MnAs cluster sizes of the sample (A) and (B) were estimated to be 6nm and 8nm, respectively. From Fig. 3.8 (a)-(c), it was found that with increasing the MnAs cluster size, both the optical absorption and Faraday intensity increased. Based on these results, we propose a model in the formation of the MnAs clusters, as schematically shown in Fig. 3.9. Assuming that the Faraday intensity is proportional to the magnetization, there must be a difference in the proportion of the Mn ions which contributed to the formation of MnAs nanoclusters to the total Mn ions in the GaAs matrix, because magnetic *alloy* semiconductor (GaMn)As do not show sizable Faraday effect at room temperature, as will be described in section 3.6. In other words, there remain Mn ions in the GaAs matrix, which do not contributed to the formation of MnAs nanocluster and the magneto-optical intensity, in sample (A), as shown in Fig. 3.9. While the total number of Mn ions are the same between sample (A) and sample (B), more Mn ions contributed to the formation of MnAs clusters during the annealing in sample (B), resulting in the increase of optical absorption at the wavelength $\lambda > 900$nm, compared with sample (A).

Abe derived the dielectric-permeability tensor for magnetized granular composites [3.9]. In his theory, the effective tensor is derived for a composite containing an ensemble of oriented ellipsoidal particles embedded in a host medium, which is magnetized along an arbitrary direction. The effective tensor elements are given by the average of the tensor elements of particles and the host medium weighted by "virtual volume fractions". Since the dielectric-permeability of the metallic MnAs is negative, the dielectric-permeability of the GaAs:MnAs is probably smaller than that of the host matrix GaAs. The quantitative comparison of the dielectric-permeability tensor spectrum of GaAs:MnAs with the one derived by the theory is studied and will be reported in the near future.

3.6 Comparison of optical transmission and magneto-optical properties between (GaMn)As and GaAs:MnAs at room temperature

Which is more preferable as a magneto-optical material, (GaMn)As or GaAs:MnAs? Below we discuss the advantages and disadvantages of both materials *as a magneto-optical material at room temperature*. We measured the optical transmission and magneto-optical effect of these materials at room temperature. Fig. 3.10 shows (a) optical absorption, (b) Faraday ellipticity, and (c) Faraday rotation spectra of a 1μm-thick

(GaMn)As film and a 1μm-thick GaAs:MnAs film both with x_{Mn} = 0.06. Faraday effects were measured under the magnetic field of 1T applied perpendiculat to the film plane at room temperature. For reliable comparison, the GaAs:MnAs sample was obtained by annealing the same (GaMn)As wafer. The annealing was done in two steps, at 600℃ for 3min. and at 650℃ for 30sec. The absorption spectrum of a 1μm-thick GaAs is shown as a reference. Wavy structures in the spectra come from multiple interference of light within the films. Below we compare various properties between (GaMn)As and GaAs:MnAs.

(1) Optical absorption

The optical absorption of both materials was large even above the bandgap wavelength of GaAs (1.42eV = 870nm), 2.5×10^4cm^{-1} in (GaMn)As and 2.5-3.5×10^4cm^{-1} in GaAs:MnAs in the wavelength range of 0.9-1.6μm. Absorption edges were not so steep in both the (GaMn)As and GaAs:MnAs samples as in the GaAs film. This is because Mn ions and MnAs nanoclusters break the translation symmetry of the host GaAs lattice. In (GaMn)As, the free carrier absorption by Mn acceptors and alloy disorder are probably the main origin of this large absorption. In GaAs:MnAs, the absorption or light scattering by the metallic MnAs nanoclusters is the main origin as discussed in 3.4 and 3.5.

(2) Magneto-optical intensity

Next, we discuss the magneto-optical properties. As shown in Fig. 3.10 (b) and (c), the Faraday ellipticity and Faraday rotation of (GaMn)As were smaller than 0.1 deg./μm at room temperature, although it was reported that the Faraday rotation of (GaMn)As was 6 deg. / μm in the ferromagnetic state at 10K [3.6]. On the other hand, the Faraday ellipticity and Faraday rotation of GaAs:MnAs were large, compared with that of (GaMn)As, 1.14 deg. / μm and 0.6 deg. / μm, respectively, at room temperature.

(3) Magneto-optical figure of merits

To investigate the magneto-optical figure of merit of these materials, we calculated the Faraday ellipticity and Faraday rotation per optical absorption, as shown in Fig. 3.11. From Fig. 3.11, it is clear that the magneto-optical figure of merit of GaAs:MnAs is much larger than that of (GaMn)As by a factor of 20-30. Compared with other magnetic materials, the magneto-optical figure of merit of GaAs:MnAs (0.02-0.08) is lower than that (300-800) of II-VI based DMSs (CdMn)Te and (CdMnHg)Te, but slightly larger than that (0.03-0.06) of ferromagnetic metals Fe and Co [3.10]. GaAs:MnAs is not transparent enough to be directly applicable to optical isolators. Therefore, at the present stage, when we try to use GaAs:MnAs for optical isolator application, integration with

optically active materials having gain is needed, as will be described in Chapter 5.

(4) Operational magnetic field

Since (GaMn)As is paramagnetic at room temperature, high magnetic field is required to obtain large Faraday effects. On the other hand, low magnetic field operation is possible in GaAs:MnAs due to its superparamagnetic property. The saturation magnetic field of GaAs:MnAs is only 0.1-0.2T.

(5) Thermodynamic stability

Lastly, we comment on the thermodynamic stability of (GaMn)As and GaAs:MnAs. As mentioned above, (GaMn)As is a metastable material, which turns to GaAs:MnAs when it is heated at 500-700℃. This metastability limits the choice of device processes, for example, overgrowth of high quality GaAs / AlAs heterostructures and annealing after the deposition of metal electrodes will not be available. When we use (GaMn)As for electronic and optoelectronic devices, we have be careful about the thermodynamic metastability of (GaMn)As.

3.7 Summary

In chapter 3, we presented fabrication, structural characterization, magnetic, optical transmission, and magneto-optical properties of GaAs:MnAs (MnAs nanoclusters embedded in a GaAs matrix). We fabricated semiconductor-based magnetic superlattices (SLs) containing MnAs nanoclusters in GaAs, and have characterized their structure, transmission and magneto-optical properties. It was found that the superlattices have good crystalline quality and the MnAs nanocluster system shows excellent compatibility with GaAs / AlAs heterostructures. Also, it was found that the MnAs nanocluster size can be controlled to some extent by introducing [GaAs:MnAs] / AlAs superlattice structures and transmission properties were improved in the SLs with keeping their magneto-optical properties. The magneto-optical intensity of GaAs:MnAs became larger by a factor of 1.3 with Si doping. It was confirmed by magnetization measurements that Si doping enhanced the formation of bigger MnAs nanoclusters. We also found that the optical transmission was improved by a factor of 2 with increasing the wavelength from 0.9μm to 1.5-1.6μm. In addition, we investigate the origin of optical loss and magneto-optical effect in GaAs:MnAs, and discussed the superiority of GaAs:MnAs over (GaMn)As as a magneto-optical material at room temperature.

References

[3.1] J. De Boeck, R. Oesterholt, A. Van Esch, H. Bender, C. Bruynseraede, C. Van Hoof, and G. Borghs, Appl. Phys. Lett., **68**, 2744, (1996).

[3.2] H. Akinaga, J. De Boeck, G. Borghs, S. Miyanishi, A. Asamitsu, W. Van Roy, and Y. Tomioka, and L. H. Kuo, Appl. Phys. Lett. **72**, 3368 (1998).

[3.3] H. Akinaga, S. Miyanishi, K. Tanaka, W. Van Roy, and K. Onodera, Appl. Phys. Lett. **76**, 97 (2000).

[3.4] M. Tanaka, J. Mater. Sci. & Eng. **B31**, 117 (1995)., Physica **E2**, 372 (1998).

[3.5] S. Chikazumi, Physics of Ferromagnetism, vol. 1 magnetic properties of matters, (Shokabou, 1978), in Japanese.

[3.6] T. Kuroiwa, T. Yasuda, F. Matsukura, A. Shen, Y. Ohno, Y. Segawa, and H. Ohno, Electron Lett. **34**, 190 (1998).

[3.7] K. Onodera, T. Matsumoto, and M. Kimura, Electron. Lett. **25**, 1386 (1994).

[3.8] Modern Magneto Optics And Magneto Optical Materials, edited by A. K. Zvezdin and V. A. Kotov (Institute of Physics Publishing, 1997) Studies in Condensed Matter Physics.

[3.9] M. Abe, Phys. Rev. B**53**, 7065, (1996).

[3.10] K. Ando, J. Magn. Sci. Jpn.,**23**, 751, (1999).

(a)

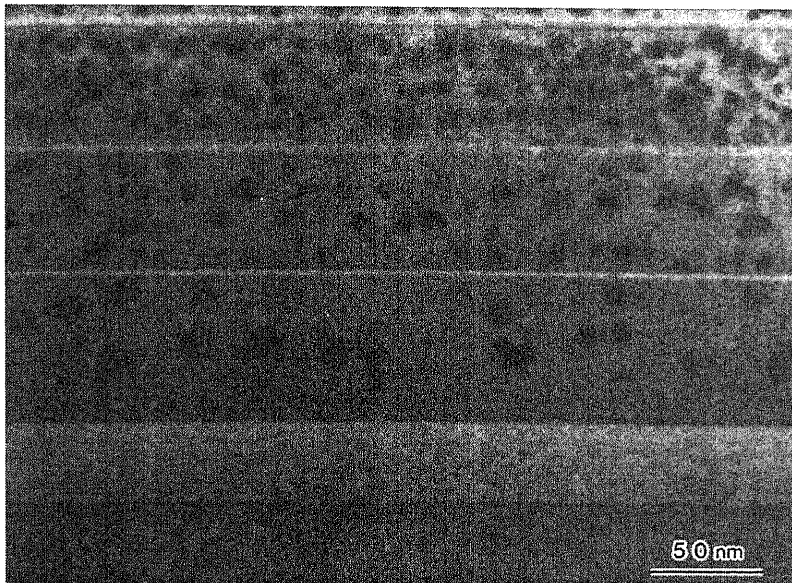

AlAs 3nm

x_{Mn}=0.048

AlAs 3nm

x_{Mn}=0.023

AlAs 3nm

x_{Mn}=0.011

(b)

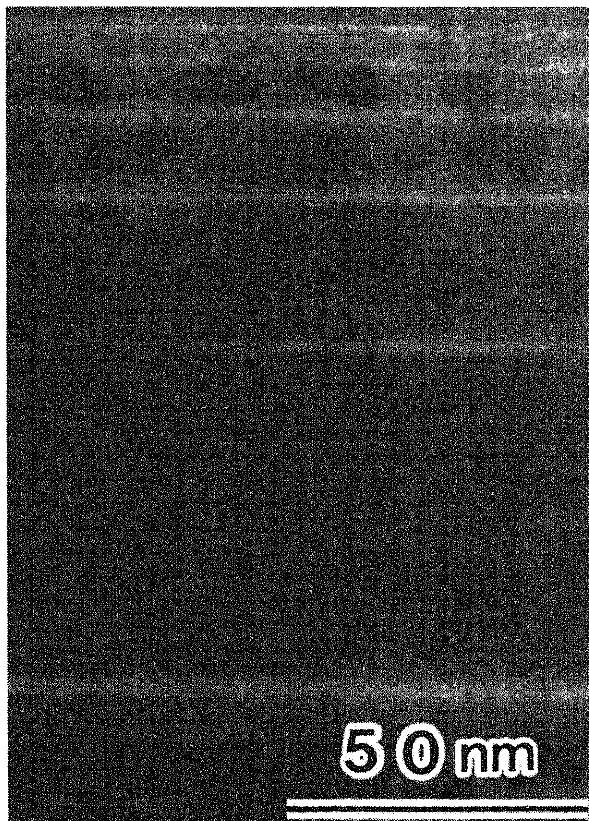

2nm

5nm

10nm

20nm

50nm

x_{Mn}=0.048

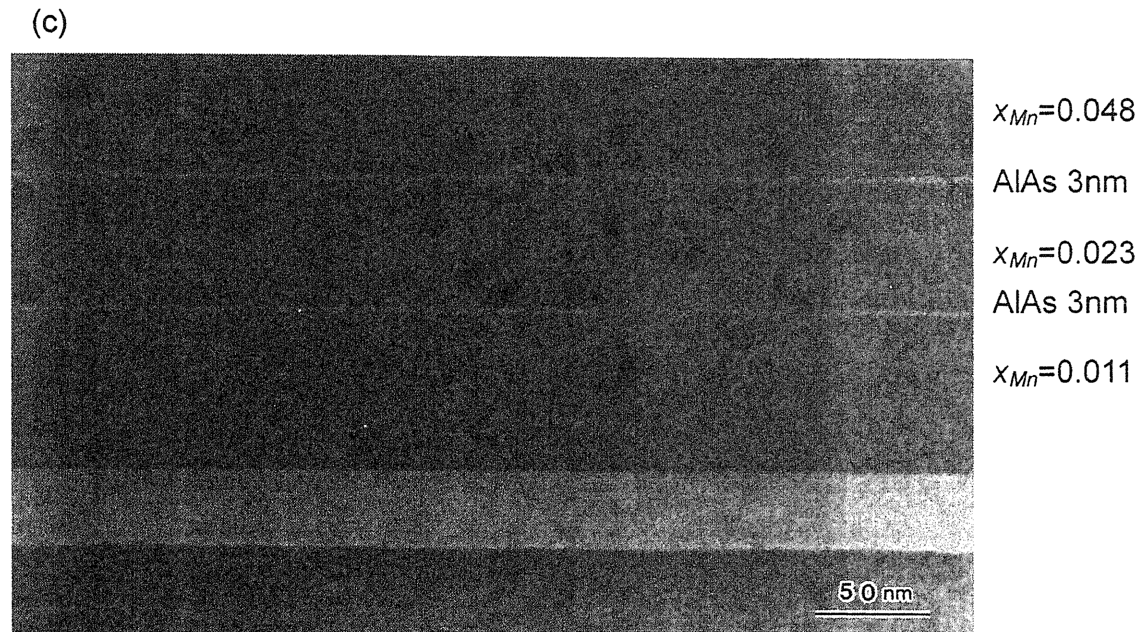

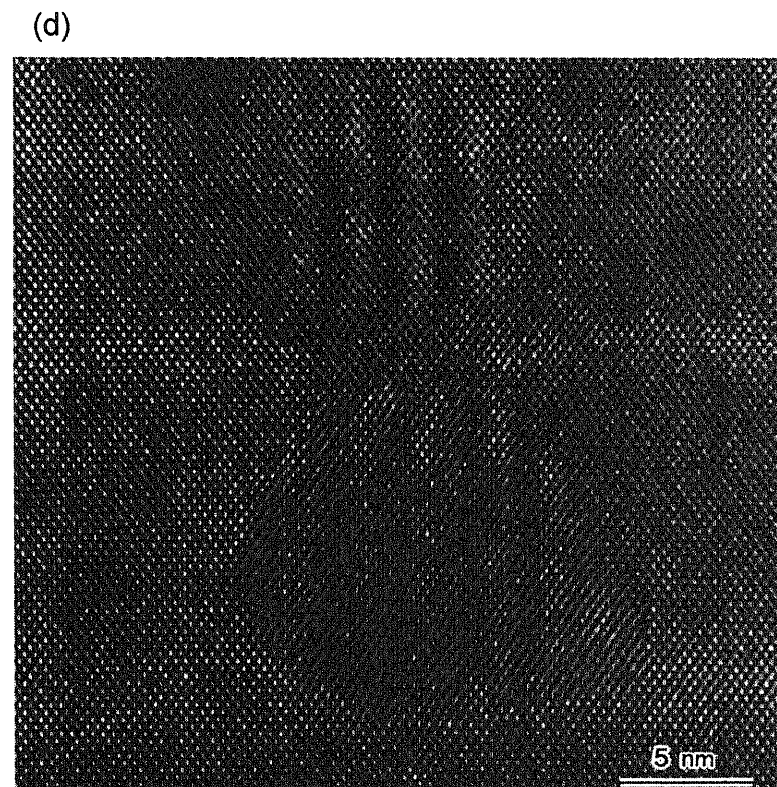

Fig. 3.1 Cross sectional images of MnAs nanoclusters embedded in a GaAs matrix taken by transmission electron microscopy (TEM). (a) Bright field image of 50nm-thick MnAs nanocluster layers with different Mn concentrations x_{Mn} = 0.011, 0.023 and 0.048. (b) Bright field image of MnAs nanocluster layers with different thicknesses of 50, 20, 10, 5, and 2nm at a fixed Mn concentration x_{Mn} of 0.048. (c) Bright field image of MnAs clusters, which is the same structure as that of (a), but annealed at different temperature of 650℃ for 1hour. (d) High resolution lattice image of MnAs nanoclusters taken from the same sample of (b). Bright regions are 3nm-thick AlAs layers.

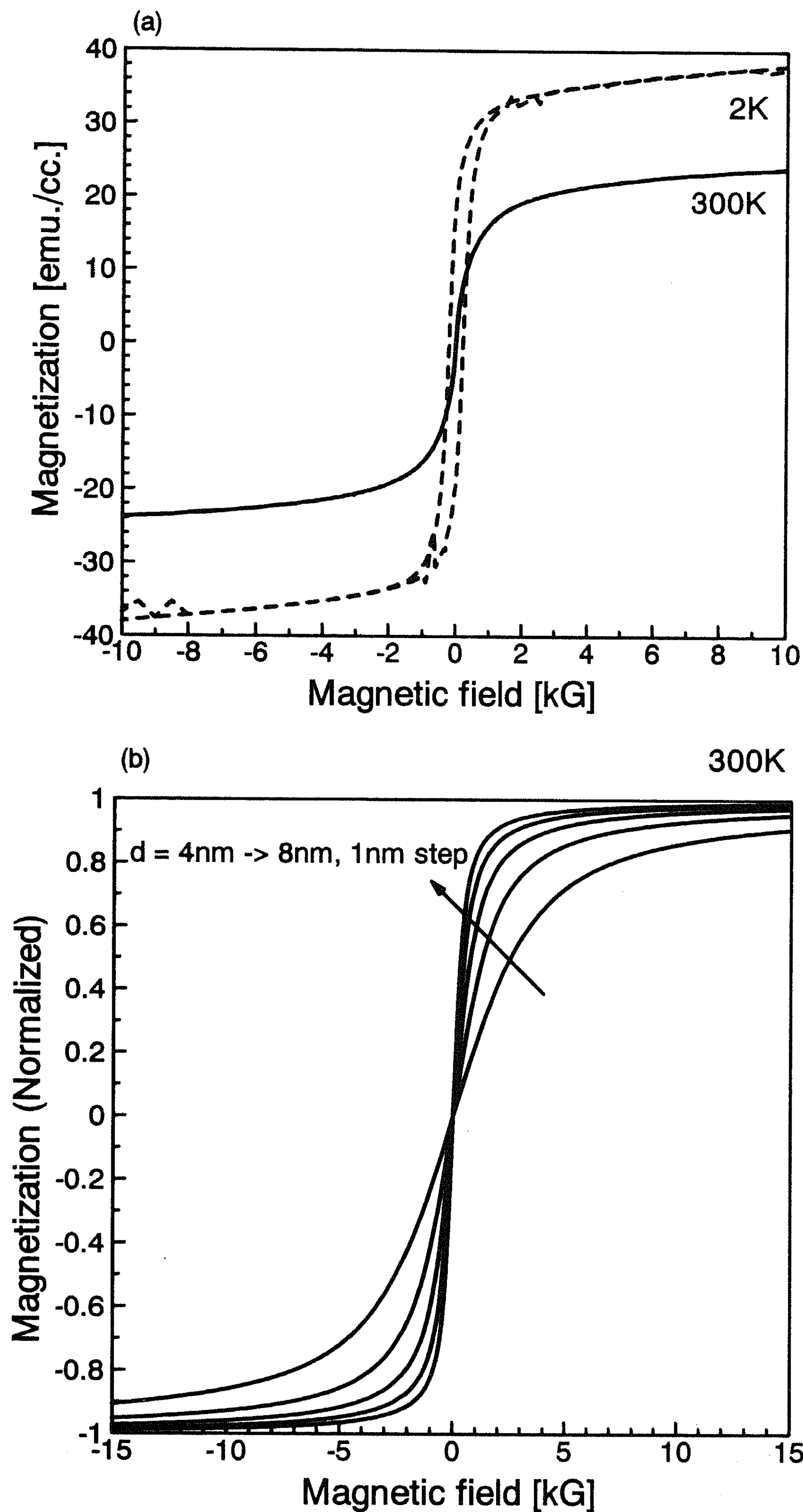

Fig. 3.2 (a) Magnetization of GaAs:MnAs samples measured by SQUID at 300K (solid line) and 2K (dashed line). The Mn concentration x is 0.06.

(b) Magnetization curves calculated by the Langevin function of equation (3-1). d denotes the diameter of the MnAs cluster.

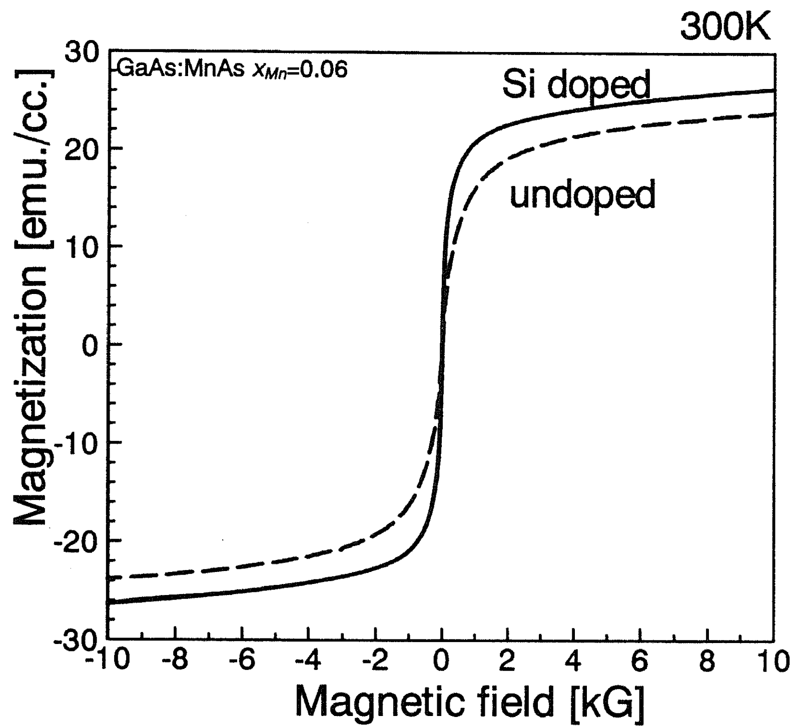

Fig. 3.3 Magnetization of GaAs:MnAs samples with (solid curve) and without (dashed curve) Si doping, measured by SQUID at 300K. The Mn concentration x is 0.06 and the Si doping concentration is $1 \times 10^{18}\text{cm}^{-3}$ in the GaAs:MnAs samples for these magnetization measurements.

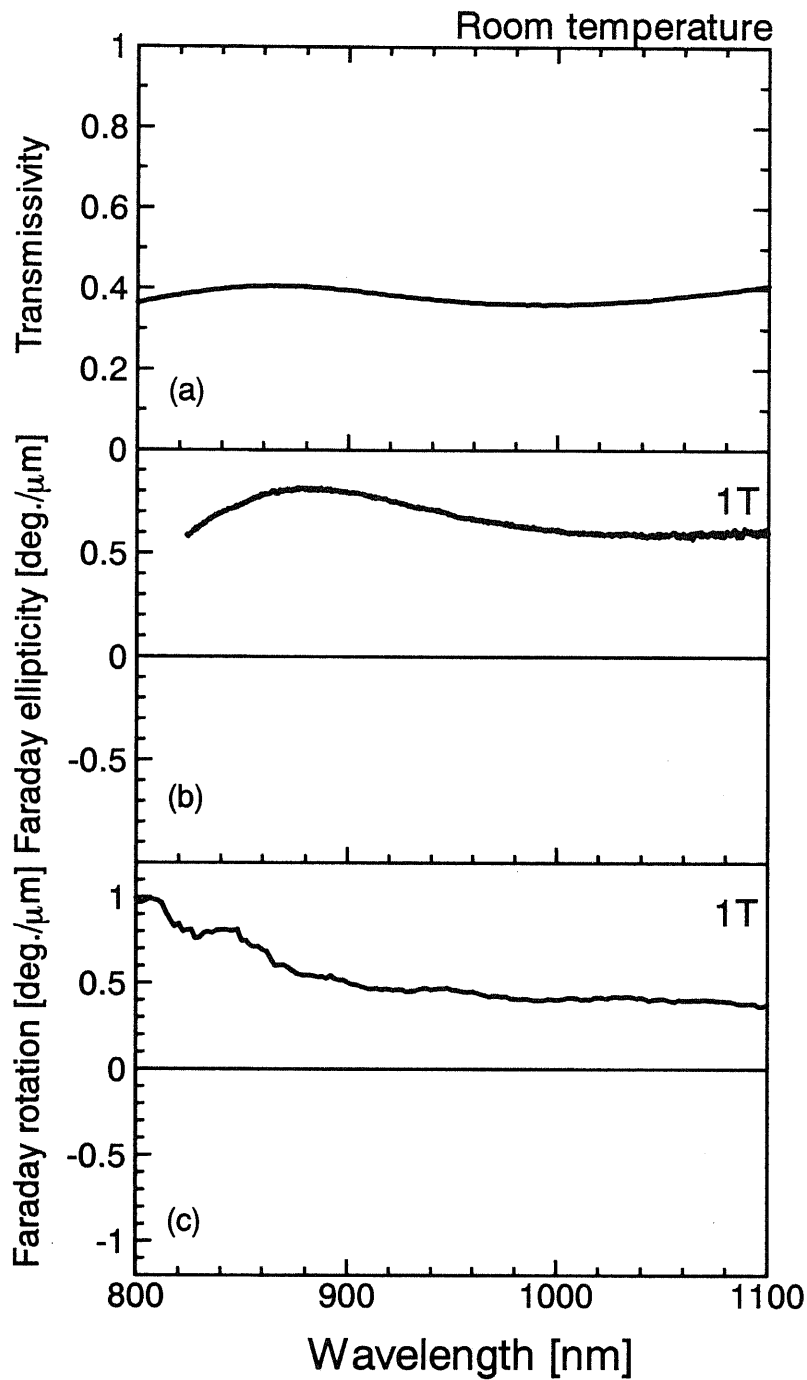

Fig. 3.4 (a) Optical transmission, (b) Faraday ellipticity (MCD), and (c) Faraday rotation spectra of a 200nm-thick GaAs:MnAs film with x_{Mn} = 0.047. Magneto-optical measurements were done under the magnetic field of 1T applied perpendicular to the film plane at room temperature.

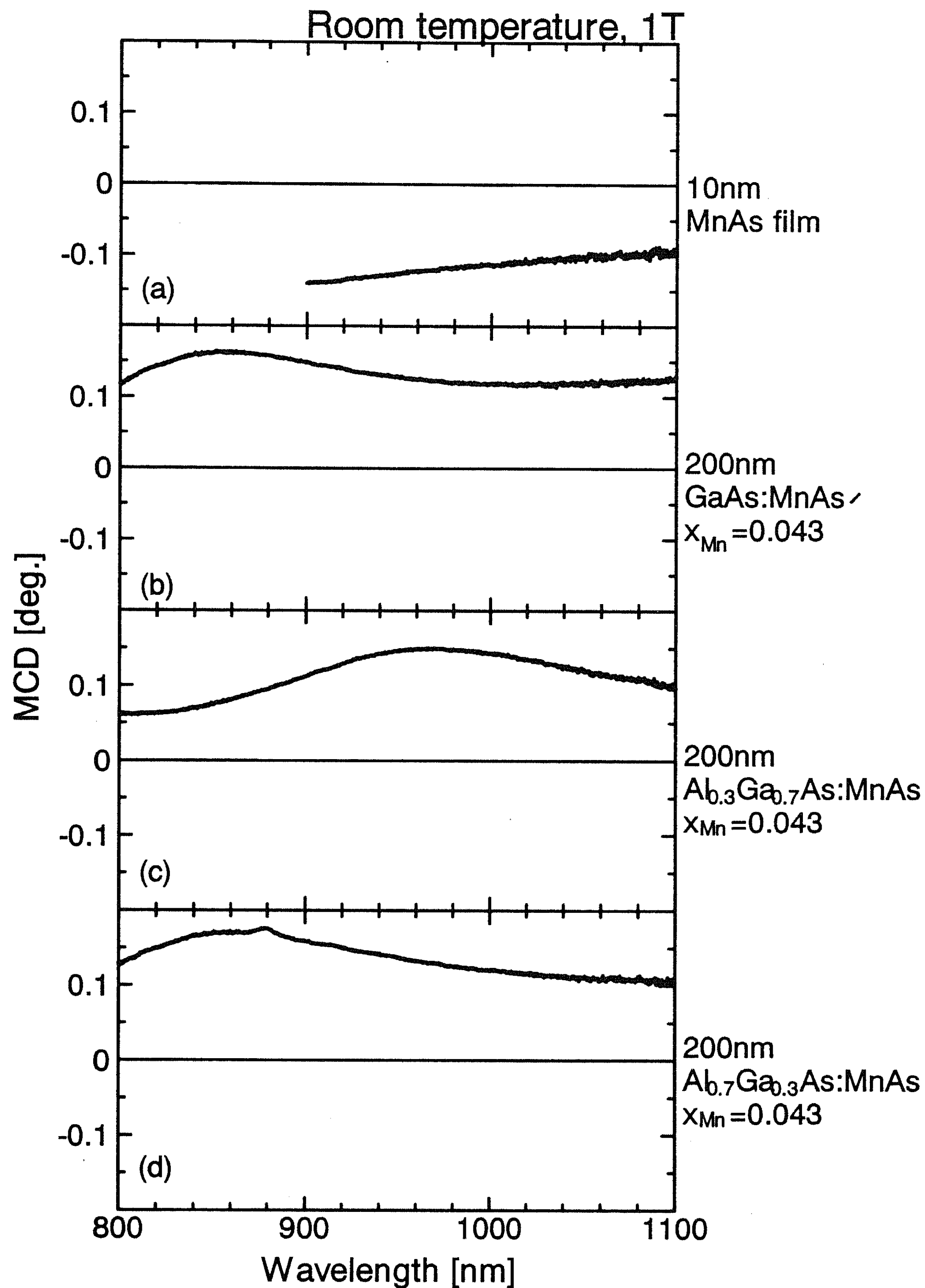

Fig. 3.5 Transmission MCD (Faraday ellipticity) spectra of GaAs:MnAs and $Al_yGa_{1-y}As$:MnAs nanoclusters with x_{Mn} = 0.043 and y = (b) 0, (c) 0.3, (d) 0.7, under the magnetic field of 1T perpendicular to the film plane at room temperature. MCD spectrum of a 10nm thick MnAs film is shown as a reference in (a).

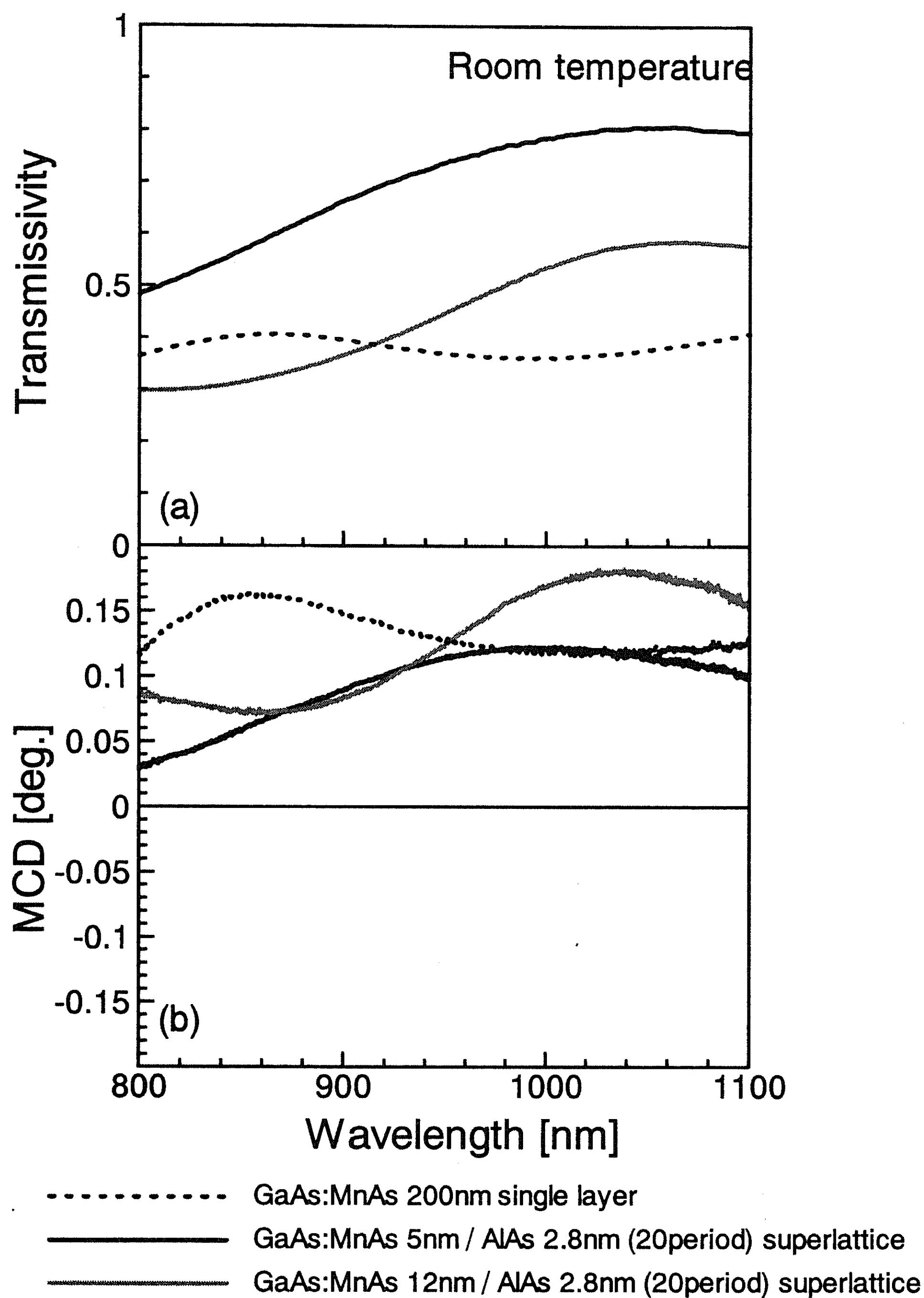

Fig. 3.6 (a) Transmission and (b) MCD (Faraday ellipticity) spectra of [GaAs:MnAs] / AlAs SL structures with GaAs:MnAs thicknesses of 5 and 12nm at a constant Mn concentration x_{Mn} = 0.047, measured at room temperature. MCD spectra were measured under the magnetic field of 1T applied perpendicular to film plane. Spectra of a GaAs:MnAs single thick layer (200nm), a [GaAs:MnAs] (5nm) / AlAs (2.8nm) SL, and a [GaAs:MnAs] (12nm) / AlAs (2.8nm) SL are indicated by dotted, solid, and gray curves, respectively.

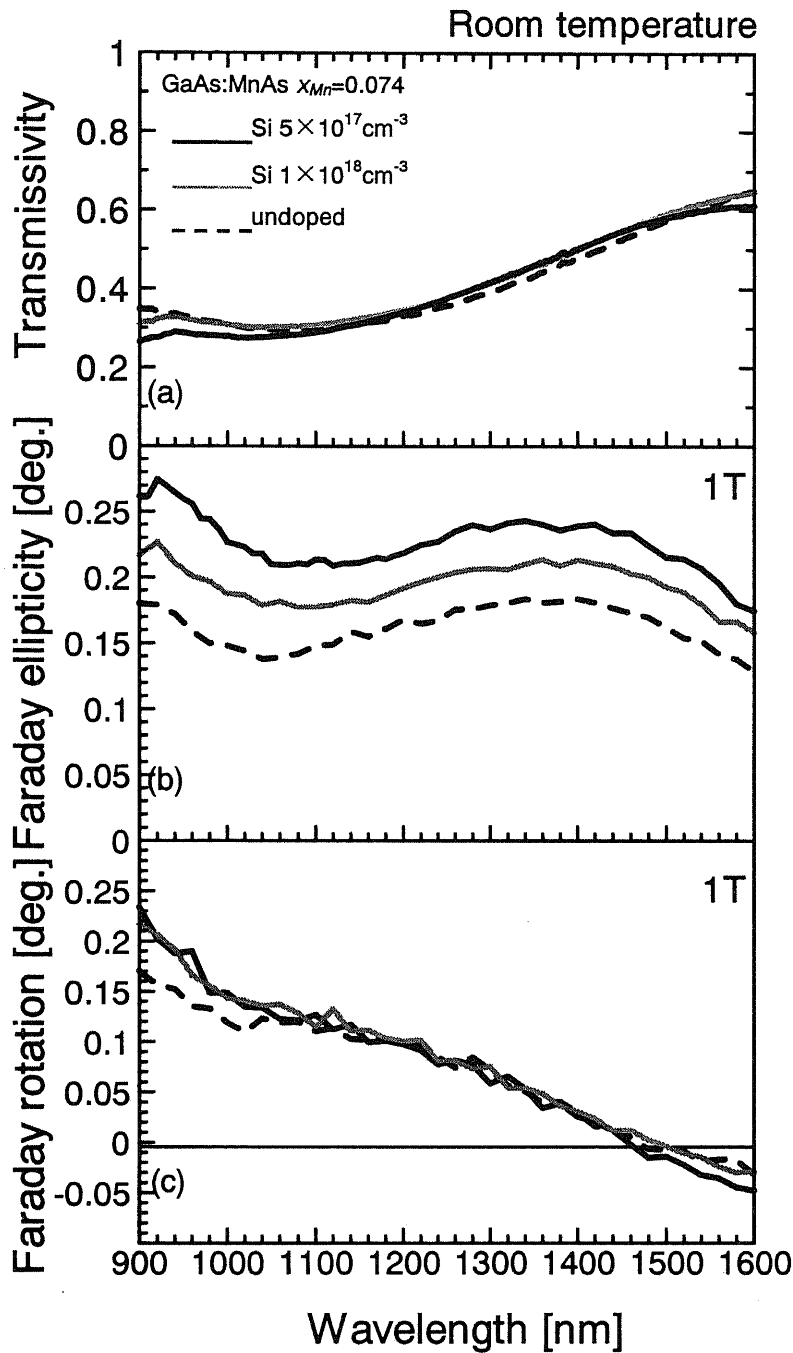

Fig. 3.7 (a) Optical transmission, (b) Faraday ellipticity, and (c) Faraday rotation spectra of 200nm-thick GaAs:MnAs films in wavelength region of 0.9-1.6μm at room temperature. Both Faraday effects ((b) and (c)) were measured under the magnetic field of 1T applied perpendicular to the films. Solid, gray, and dashed curves correspond to the spectra of the Si-doped GaAs:MnAs samples with Si with concentrations of $5\times10^{17}cm^{-3}$ and $1\times10^{18}cm^{-3}$, and the GaAs:MnAs sample without Si doping, respectively.

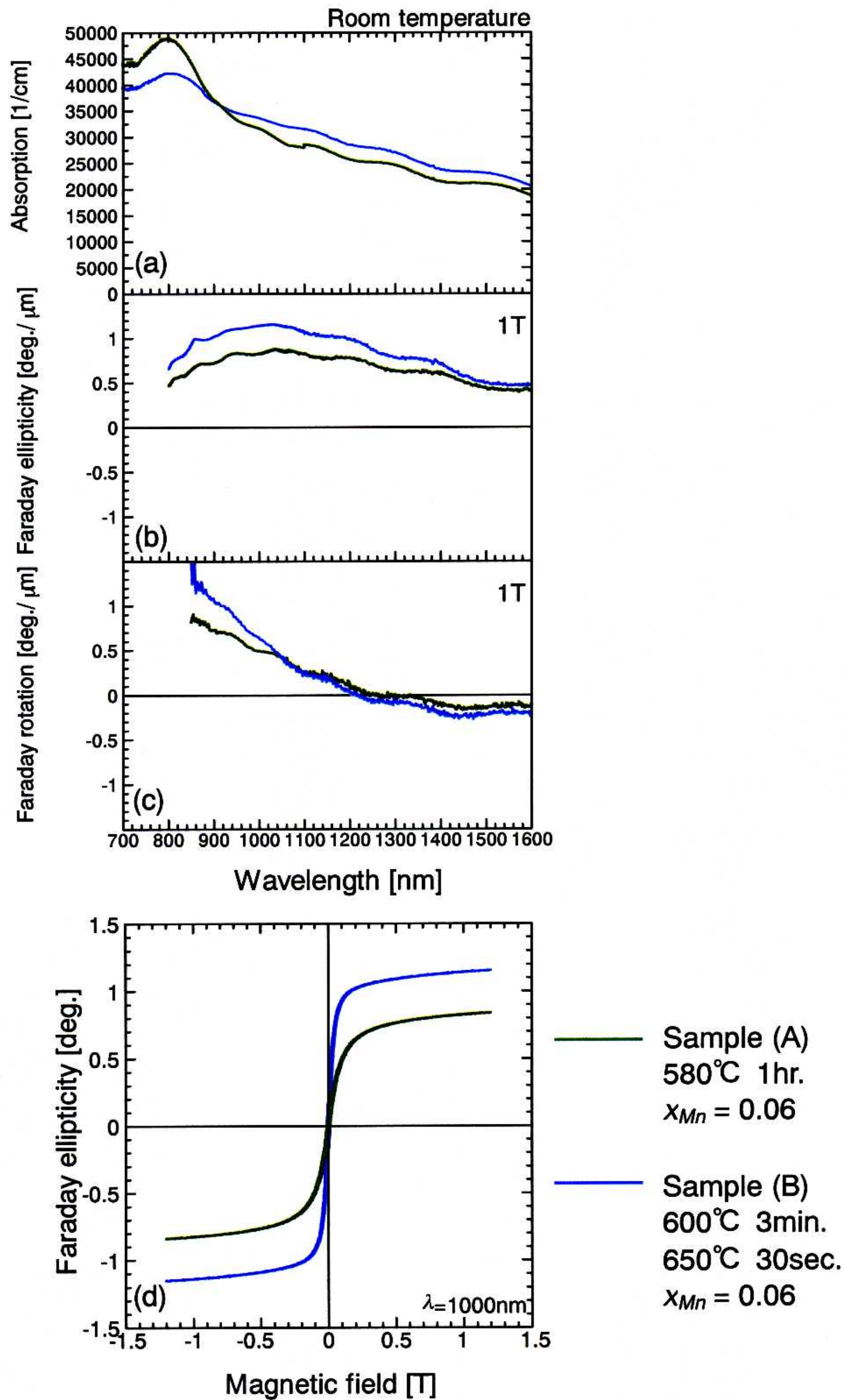

Fig. 3.8 (a) Optical absorption, (b) Faraday ellipticity, and (c) Faraday rotation spectra of 1μm-thick GaAs:MnAs films in a wavelength region of 0.9-1.6μm at room temperature. Both Faraday effects ((b) and (c)) were measured under the magnetic field of 1T applied perpendicular to the sample plane. The green and blue curves show the spectra of sample (A) (annealed at 580℃ for 1hr., green curves) and (B) (annealed at 600℃ for 3min. and 650℃ 30sec., blue curves) respectively. (d) Magnetic field dependence of Faraday ellipticity of these samples at the wavelength of 1μm.

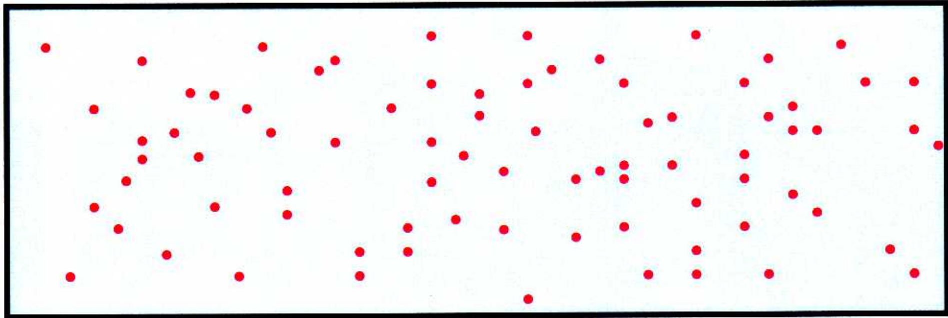

As grown
(GaMn)As

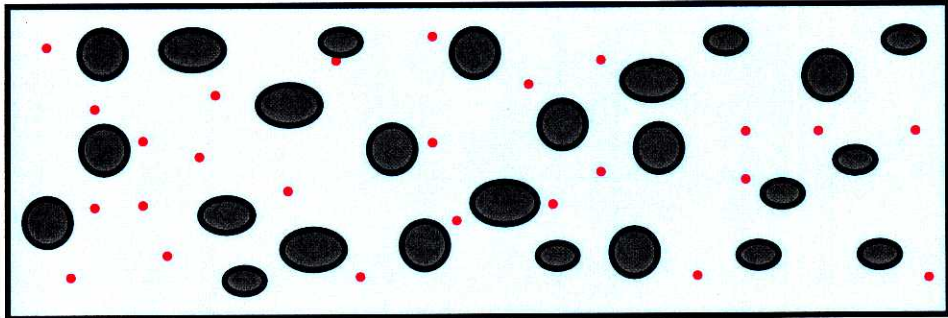

GaAs:MnAs
Sample (A)
Annealed at lower temperature,
580℃ for 1 hr.

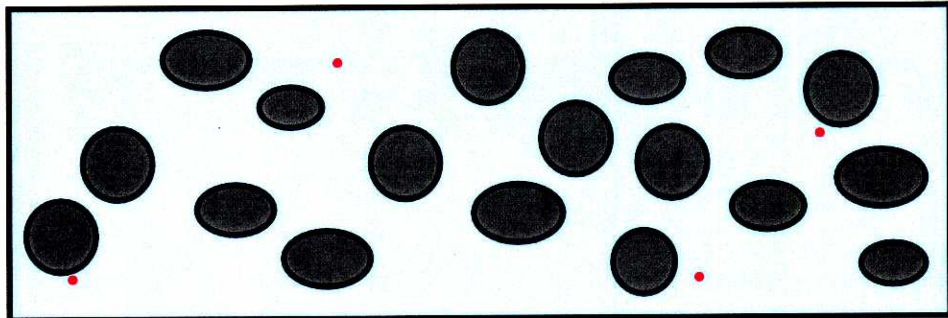

GaAs:MnAs
Sample (B)
Annealed at higher temperature,
600℃ for 3min. and
650℃ for 30sec.

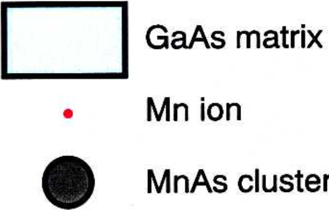

Fig. 3.9 Schematic images of (GaMn)As and MnAs clusters embedded in a GaAs matrix. (b) and (c) correspond to Sample (A) and (B) respectively.

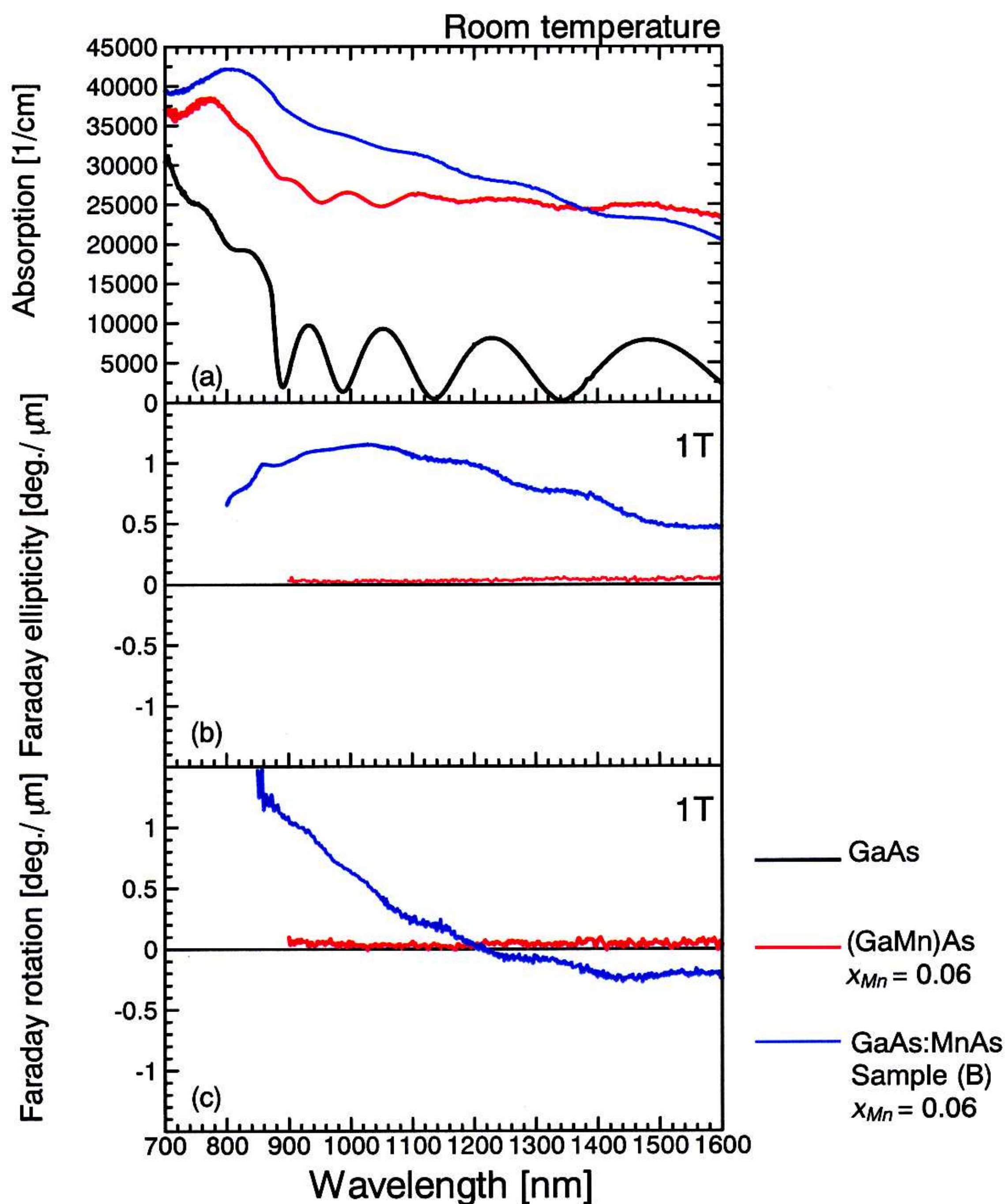

Fig. 3.10 (a) Optical absorption, (b) Faraday ellipticity, and (c) Faraday rotation spectra of 1μm-thick (GaMn)As (red curves) and GaAs:MnAs (blue curves) with x_{Mn} = 0.06. Magneto-optical measurements were done under the magnetic field of 1T applied perpendicular to the film plane at room temperature. An absorption spectrum of 1μm-thick GaAs film is shown as a reference by black curve.

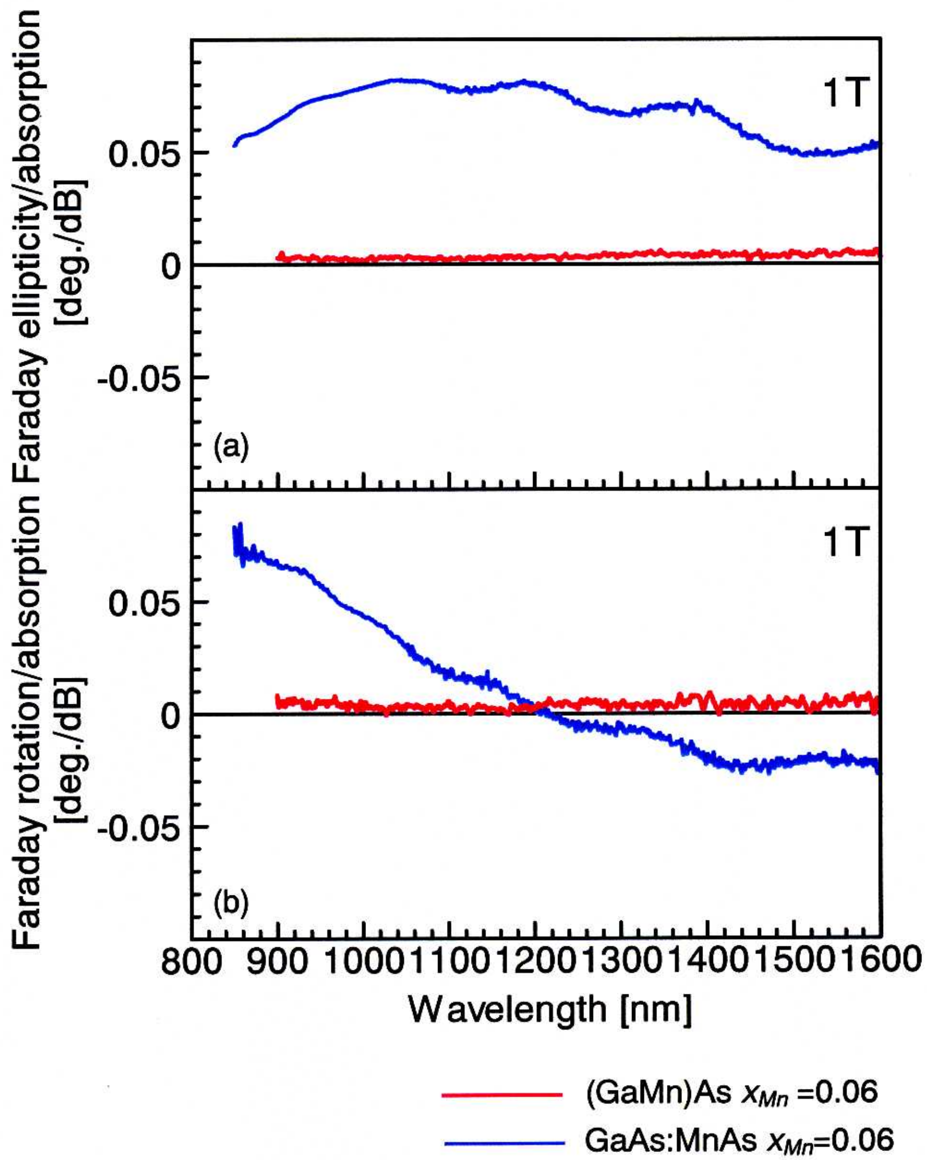

Fig. 3.11 Magneto-optical figure of merit, (a) Faraday ellipticity / absorption and (b) Faraday rotation / absorption of (GaMn)As (red curves) and GaAs:MnAs (blue curves) with x_{Mn} = 0.06 based on Fig. 3.10.

~Chapter 4~

Enhancement of magneto-optical effect in multilayer structures composed of the semiconductor / magnetic hybrid structure GaAs:MnAs and GaAs / AlAs DBR

The characteristic function of magneto-optical devices is the non-reciprocal property of light propagation in magnetic materials, which cannot be realized by nonmagnetic materials, and this property is applied to optical isolators and circulators. For such magneto-optical device applications, ferrimagnetic garnets such as Bi substituted rare-earth Fe garnet are widely used in the 1.3-1.55μm wavelength region in optical telecommunication systems [4.1]. On the other hand, II-VI based diluted magnetic semiconductors such as CdMnHgTe are used for optical isolators in the 0.98μm wavelength region for Er doped fiber amplifier (EDFA) systems [4.2]. However, both garnets and II-VI based materials are incompatible with III-V semiconductors, and their device sizes are much larger than that of laser diodes (LDs), because they are bulk crystals. Therefore it is difficult to integrate these materials with III-V optoelectronics. For integration of magneto-optical devices with III-V optoelectronic devices, it is required that large magneto-optical effect is obtained in III-V based thin films.

Although this requirement has been considered to be difficult, semiconductor / magnetic hybrid thin-film materials have been successfully grown by molecular-beam epitaxy (MBE). Representatives of such hybrid materials are, ferromagnetic metallic MnGa and MnAs thin films on GaAs and Si substrates [4.3, 4.4], ferromagnetic semiconductor (GaMn)As [4.5, 4.6], and ferromagnetic MnAs nanoclusters embedded in GaAs [4.7, 4.8]. These were shown to have good compatibility with existing III-V heterostructures [4.9], as well as large magneto-optical effect [4.8-4.11], therefore can be good candidate materials for magneto-optical devices integrated with III-V optoelectronics. It was reported that the Faraday rotation θ_F of (GaMn)As is 6 deg./μm at the wavelength of 0.8 μm at 10 K [4.10], and that of GaAs:MnAs is 0.2 deg./μm at the wavelength of 0.98 μm at room temperature [4.8]. However, the Curie temperature of (GaMn)As is at most 110 K, therefore room temperature operation is difficult. Also, the previously reported Verdet constant of GaAs:MnAs is not sufficient to obtain large enough magneto-optical effect in a thin film, and furthermore it is not realistic to fabricate bulky thick films exceeding 100μm by MBE. Since the magneto-optical effect is a non-reciprocal phenomenon, it is possible to enhance it by extending the effective optical path length through a magnetic layer by using multiple reflections [4.12, 4.13]. In this chapter, for

realizing a stronger magneto-optical effects in thin-film structures compatible with III-V optoelectronic devices, we have fabricated a multilayer structure composed of a GaAs:MnAs nanocluster material and GaAs / AlAs distributed Bragg reflectors (DBRs), as shown in Fig. 4.1, which is a magnetic microcavity or a one-dimensional semiconductor-based magneto-photonic crystal. It is shown that in such structures the magneto-optical Faraday effect is enhanced at room temperature at a controlled wavelength region and our experimental results are well explained by theoretical calculations. Also, possibility and potential solutions for optical isolator applications are described.

4.1 Fabrication of a one-dimensional semiconductor-based magneto-photonic crystal

The fabrication process consists of three steps in MBE growth. The operational wavelength λ was set at 980 nm for application to optical isolators which will be used for pumping laser diodes in EDFA systems. First, 10 periods of GaAs (70 nm) / AlAs (83 nm) DBR were grown at 550-580℃ on a 300nm-thick AlGaAs etch-stop layer on a (001) GaAs substrate at growth temperature of 550-580℃. The thickness of GaAs and AlAs was set at $\lambda/4n$, where n is the refractive index of each layer (n_{GaAs} = 3.52, and n_{AlAs} = 2.95). Secondly, the substrate temperature was lowered to 250℃, and a 139 nm-thick ($Ga_{1-x}Mn_x$)As was grown with a Mn concentration x = 0.047. Thirdly, the substrate temperature was raised again to 580-625℃, and then 10 periods of AlAs (83 nm) / GaAs (70 nm) DBR were grown at 550-580℃. During the third step where the substrate temperature was higher than 580℃, the homogenous (GaMn)As alloy turned to a inhomogeneous structure by phase separation, in which MnAs nanoclusters are embedded in GaAs (hereafter we call GaAs:MnAs), as described in Chapter 3. This GaAs:MnAs hybrid structure shows superparamagnetic properties at room temperature [4.7]. In this structural design, the refractive index of GaAs:MnAs layer was assumed to be the same as that of GaAs, so that the thickness of the central magnetic layer was set at $\lambda/2n$ (= 139 nm). Since this multilayer structure, which is a one-dimensional magneto-photonic crystal, works as a microcavity whose central layer is magnetic, the incident light of wavelength λ is confined to the central magnetic layer and the magneto-optical effect is enhanced due to multiple reflections. It is clearly seen from Fig. 4.1 that the overall structure is formed as intended with smooth interfaces, although the thickness of each layer is slightly smaller than designed.

4.2 *Magneto-optical properties of the multilayer structure*

Solid red curves in Fig. 4.2 show (a) transmissivity, (b) Faraday ellipticity (η_F) (equivalent to MCD), and (c) Faraday rotation (θ_F) spectra, measured at room temperature on the sample with DBR of Fig. 4.1. Faraday ellipticity and Faraday rotation spectra of a 200 nm-thick GaAs:MnAs single layer without DBR, were shown as a reference by green curves in Fig. 4.2(b) and (c). The Faraday ellipticity and Faraday rotation spectra were measured under a magnetic field of 1T applied perpendicular to the film plane. In the transmissivity spectrum, a local maximum was observed at 970 nm, which was slightly deviated from the designed wavelength of 980 nm, in the center of the optical stop band or the photonic band gap (900-1050 nm) where the transmissivity is low. It is clearly seen that both Faraday ellipticity and Faraday rotation are significantly enhanced at this wavelength (970-980nm) in the spectra of the sample with DBR, compared with those of the single GaAs:MnAs film. The enhancement factor of the Faraday ellipticity per unit magnetic layer thickness is estimated to be 7. Because the study of this material system is in the very early stage and its magneto-optical properties are not optimized, the intensity of the Faraday ellipticity and Faraday rotation is less than 1 deg., mainly due to the large absorption of the GaAs:MnAs magnetic layer. Theoretical understanding and future prospect will be discussed later. Fig. 4.3 shows a magnetic field dependence of Faraday ellipticity at 980nm measured at room temperature of the sample with DBR. The intensity of Faraday ellipticity was found to be saturated at relatively low field of 0.1-0.2T, which is smaller than the required field (0.3-0.5T) in the paramagnetic CdMnHgTe based optical isolators [4.2].

4.3 *Theoretical analysis of the magneto-optical effect of the multilayer structures*

In order to design and fabricate multilayer structures with higher magneto-optic figure of merits, it is important to theoretically calculate and predict their performance. For this purpose we simulated the magneto-optical spectra of our multilayer structure using the translation matrix approach [4.12]. Since the dielectric-permeability functions of GaAs:MnAs are unknown so far, the refractive index n of GaAs:MnAs is assumed to be the same as that of GaAs, and the off-diagonal elements related to the magneto-optical effect were obtained from the experimental Faraday ellipticity and Faraday rotation spectra of a GaAs:MnAs single layer. The extinction coefficient κ (the imaginary part of the complex refractive index $n^* = n - i\kappa$) of the GaAs:MnAs layer was determined to fit to the experimental transmissivity spectrum. Detail of the calculation is described in Appendix. Fig. 4.4 shows the derived dielectric-permeability function spectra of GaAs:MnAs. Calculated tansmissivity, Faraday ellipticity, and Faraday rotation spectra are shown by

dashed black curves in Fig. 4.2 (a)-(c). Experimental spectra were nicely reproduced by these calculations. Here, the extinction coefficient κ of the central magnetic layer (GaAs:MnAs) is fitted to 0.125, which corresponds to the absorption coefficient $\alpha = 1.6$ μm^{-1}, at 980 nm.

In order to understand the magneto-optical properties more deeply, we calculated distributions of the electric field intensity $|E|^2$ at the Bragg wavelength $\lambda = 980$ nm in the multilayers, as shown in Fig. 4.5. Fig. 4.5 (a) shows the present situation where κ is 0.125 as calculated in Fig. 4.2, and Fig. 4.5 (b) show a more ideal situation where κ is much lower, 0.00125. As shown in Fig. 4.5 (b), when the central magnetic layer has smaller absorption loss, the incident light is well confined to the central magnetic layer. In this case, with the increase of the number of the DBR period N, the light is more strongly localized in the magnetic layer and the Faraday rotation is rapidly increased, as shown in Fig. 4.5 (d). When $N = 19$, the Faraday rotation reaches as high as 44.2 deg, which is high enough for Faraday rotators. In contrast, in the present case as shown in Fig. 4.5 (a), the phase of the incident lightwave does not well match to the multilayer structure, resulting in the increase of reflection. Therefore, when the central magnetic layer has some amount of optical absorption loss, increase of N does not always contribute to the enhancement of the Faraday rotation, as shown in Fig. 4.5 (c).

4.4 Supression of the optical absorption loss in GaAs:MnAs

Since the research of the magneto-optical properties of the GaAs:MnAs nanocluster system is in the very early stage, the origin of the optical absorption and magneto-optical effect has not been theoretically clarified yet. Therefore, it is not clear at present whether the extinction coefficient of GaAs:MnAs can be reduced by a factor of 100. However, experimentally we have found that in order to reduce the optical loss, it is important to control and to make the MnAs cluster size uniform, because the absorption loss of GaAs:MnAs is sensitive to the cluster size. By introducing superlattice stuructures composed of nanometer-thick GaAs:MnAs and AlAs layers, the MnAs cluster size was found to be controlled more precisely, and the absorption coefficient decreased at least by a factor of 2 at 0.98μm, as described in section 3.4.2. It was also found that the transmission of GaAs:MnAs is improved in a longer wavelength of 1μm-1.6μm, and the reduction factor in the absorption coefficient is 3.7 at 1.55μm, as described in section 3.4,3. Furthermore, we predict that using good compatibility with III-V semiconductors, the introduction of active layers will help to solve this problem. The details of these attempts and results are described below.

4.4.1 Introduction of [GaAs:MnAs] / AlAs superlattice structures

As described in section 3.4.2, the optical transmission of [GaAs:MnAs] / AlAs superlattices was found to be improved by a factor of 2 while keeping their magneto-optical intensities, compared with the single thick GaAs:MnAs film. In our simulation of the Faraday effect in this multilayer structure, it is predicted that if the absorption loss of the central magnetic layer is half while keeping its magneto-optical properties, the Faraday rotation reaches 1.3 deg. (the enhancement factor of 18) at the same DBR period of 10.

Based on the improvement of the optical transmission in the SLs as shown in section 3.4.2, we have fabricated a multilayer structure with DBRs using a [GaAs:MnAs] / AlAs SL as the central magnetic layer in order to obtain higher magneto-optical performance. As shown in Fig. 4.6 (a), the multilayer structure has a magnetic SL in the center, sandwiched by 5.5 periods of GaAs / AlAs DBRs. The central SL consists of 5nm-thick GaAs:MnAs and 2.8nm-thick AlAs, with a Mn concentration $x_{Mn} = 0.047$. The operational wavelength was set at 980nm and the thickness of the SL was tuned to show a local maximum at 980nm in the center of the optical stop band in the transmission spectrum, taking into account the fact that the refractive index of the SLs is different from that of GaAs and the bulk GaAs:MnAs nanocluster material. The growth procedure of this multilayer was the same as described in the previous section. Fig. 4.6 shows (b) transmission, (c) Faraday ellipticity (η_F), and (d) Faraday rotation (θ_F) spectra of this multilayer with SL measured at room temperature. At 990nm, a local maximum was observed in the transmission spectrum and its transmissivity was 30%, greatly improved from 2% in the previous multilayer without SL. The extinction coefficient κ of the central magnetic layer, which is the [GaAs:MnAs] / AlAs SL, is estimated to be 0.06 by our theoretical analysis using the method described in the previous section. This value is half of that of the single thick GaAs:MnAs film. Assuming that the optical absorption loss of the central magnetic layer GaAs:MnAs is halved keeping its magneto-optical properties, theoretically the Faraday rotation will be 1 deg. at the DBR period number of 5.5, which is 24 times bigger than that of the same [GaAs:MnAs] / AlAs without DBR. However, the enhancement factor of the magneto-optical effect in our experiment was 3.3, in the Faraday rotation per unit magnetic layer thickness, compared with the [GaAs:MnAs] / AlAs SL structure without DBR. The reason for this smaller enhancement factor is probably due to the difficulty in obtaining good quality of the SL reproducibly. The transmission and magneto-optical effect of the [GaAs:MnAs] / AlAs SL in the DBR structure is probably not so good as those of Fig. 3.6, due to the complicated structures having many structural parameters such as layer thickness, Mn concentration and so on.

Still, by further optimization of the fabrication technology, this approach will be very effective to suppress the optical loss and enhance the magneto-optical figure of merits.

4.4.2 Longer wavelength operation and the effect of Si doping

As described in section 3.4.3, it was found that the magneto-optical intensity was enlarged by Si doping during the growth of (GaMn)As and the optical transmission is improved in a longer wavelength of 1.5-1.6μm. Based on the material characterizations described above, we have fabricated a semiconductor based magneto-photonic crystal with the operation wavelength λ set at 1.55μm. This wavelength region is obviously important for the optical fiber communication system. Fig. 4.7 (a) shows a cross sectional image by scanning electron microscopy (SEM) of this multilayer sample. The multilayer structure has top and bottom DBRs with 5 periods composed of GaAs (thickness: $\lambda/4n_{GaAs}$=115nm) and AlAs (thickness: $\lambda/4n_{AlAs}$=134nm). The magnetic layer in the center is GaAs:MnAs (thickness: $\lambda/2n_{GaAs:MnAs}$=230nm). Here, n_{GaAs}=3.37 and n_{AlAs}=2.89 are the refractive indices of GaAs and AlAs at 1.55μm, respectively. The refractive index of GaAs:MnAs $n_{GaAs:MnAs}$ is assumed to be the same as that of GaAs. The fabrication process consisted of three steps and the same as described in the previous section: First, the bottom DBR was grown at the substrate temperature (T_s) of 580℃ on a 200nm-thick AlGaAs etch-stop layer on a (001) GaAs substrate. Second, a 230nm-thick ($Ga_{1-x}Mn_x$)As layer was grown at T_s = 250℃, where the Mn concentration x was set at 0.065. During the growth of (GaMn)As, Si was doped with a concentration of $5\times10^{17}cm^{-3}$ to enhance the magneto-optical intensity, based on the investigation described in section 3.4.3. Third, the top DBR was grown at T_s = 580℃. During the third step, (GaMn)As turned to MnAs nanoclusters embedded in a GaAs matrix by phase separation.

Fig. 4.7 shows (b) optical transmission (T), (c) Faraday ellipticity (η_F) and (d) Faraday rotation (θ_F) spectra of this sample at room temperature. The Faraday ellipticity (η_F) and rotation (θ_F) spectra were measured under a magnetic field of 1T applied perpendicular to the film plane. A local maximum (T = 20%) was observed at 1.54μm at the center of the optical stop band in the optical transmission spectrum. Around this wavelength, the Faraday effect was successfully enhanced: η_F = 0.52deg. and θ_F = 0.21deg. were obtained. The Faraday effect per magnetic layer thickness was enhanced by a factor of 4.8 compared with a Si-doped GaAs:MnAs single layer without DBR at the wavelength of 1.54μm. The extinction coefficient κ of the central magnetic layer, which is the Si doped GaAs:MnAs, is estimated to be 0.08, which corresponds to the absorption coefficient α = 0.648 μm^{-1}, at 1.54 μm by our theoretical analysis using the method described in the previous section. The absorption coefficient of the Si doped GaAs:MnAs film at 1.54 μm is reduced by a factor of 2.47 compared with that of the undoped

GaAs:MnAs film at 0.98 μm. The figure of merit (FOM.) of η_F, which is defined by the ratio of Faraday ellipticity to optical loss, is 0.074deg./dB at the wavelength of 1.54μm, which is twice as large as the FOM. of 0.037deg./dB at 0.98μm obtained in previous section. This is because (1) the magneto-optical intensities of GaAs:MnAs is enlarged by Si doping and (2) the optical loss of GaAs:MnAs is lower at 1.54μm than that at 0.98μm and thus more effective enhancement of the Faraday effect was realized.

4.5 Advantages of these multilayer structures

Although there is a problem of the absorption loss and future work is needed for further optimization, our multilayer structures based on III-V semiconductors have a lot of advantages: (1) Monolithic integration of the present structure with III-V optoelectronic devices, such as laser diodes and waveguides, will be probably easier than any other materials. (2) Since the whole structure can be grown by MBE, we can fabricate high-quality multilayers with almost perfect interfaces and controlled thicknesses, leading to the excellent controllability of the operational wavelength. (3) Besides, it is possible to realize low magnetic field (0.1-0.2T) operation at room temperature, due to the superparamagnetic property of GaAs:MnAs, which will contribute to the realization of small scale devices.

Lastly, we summarize the comparison of Faraday rotation per magnetic layer thickness of GaAs:MnAs with that of other magneto-optical materials in table 4.1. The Faraday rotation of a GaAs:MnAs single film is comparable with that of conventional magneto-optical materials, CdMnHgTe and garnets. Furthermore, this Faraday rotation was 5-8 times amplified by combination with GaAs / AlAs DBR and is the largest among these magneto-optical materials.

Materials \ Wavelength	0.98μm	1.55μm	References
GaAs:MnAs Single film	0.2 deg. / μm 0.5 deg. / μm	 0.17 deg. / μm	Akinaga et al. APL, **76**, 97, (2000) **This work**
GaAs:MnAs with DBR	4 deg. / μm	0.87 deg. / μm	**This work**
CdMnHgTe At 0.5T	~0.03 deg. / μm		K. Onodera et al. Electron Lett. .30, p1954, 1994
((Gd,Bi)3(Fe,Al,Ga)5O12)		~0.15 deg. / μm	"Topics in Solid State and Quantum Electronics" 1972 John Wiley & Sons

Table 4.1 Comparison of Faraday rotation per unit magnetic layer thickness of GaAs:MnAs with other magneto-optical materials.

4.6 Summary

In summary, we have successfully demonstrated the enhancement of the magneto-optical effect in a GaAs:MnAs hybrid structure sandwiched by GaAs/AlAs DBRs, that is, one-dimensional semiconductor-based magneto-photonic crystal, at room temperature and under relatively low magnetic field. The enhancement factor of the magneto-optical effect is 7 at the wavelength of 980nm. We also discussed its advantages, possibilities and problems to be solved for the application to optical isolators to be monolithically integrated with III-V optoelectronics. To solve these problems, two approaches are examined. First, we have shown the magneto-optical properties of a semiconductor-based magnetic microcavity using a [GaAs:MnAs] / AlAs superlattice (SL) as the central magnetic layer, and its optical absorption was found to improved by a factor of 2 compared with that of the multilayers without SL. Secondly, we fabricated a semiconductor-based magneto photonic crystal whose operational wavelength was set at 1.55μm, and successfully improved its optical absorption by a factor of 2.47, as well as the magneto-optical effect. The magneto-optical FOM of our semiconductor based magneto-optical crystals was improved by a factor of 2 at the wavelength of 1.55μm compared with that at 0.98μm. This means that present structures could be used for semiconductor-based optical isolators and their integration with III-V optoelectronic devices for the optical telecommunication system.

References

[4.1] Modern Magneto Optics And Magneto Optical Materials, edited by A. K. Zvezdin and V. A. Kotov (Institute of Physics Publishing, 1997) Studies in Condensed Matter Physics.

[4.2] K. Onodera, T. Matsumoto, and M. Kimura, Electron. Lett. **25**, 1386 (1994).

[4.3] M. Tanaka, J. Mater. Sci. & Eng. **B31**, 117 (1995), Physica **E2**, 372 (1998).

[4.4] M. Tanaka, K. Saito, and T. Nishinaga, Appl. Phys. Lett. **74**, 64 (1999).

[4.5] H. Ohno, A. Shen, F. Matsukura, A. Oiwa, A. Endo, S. Katsumoto, and Y. Iye: Appl. Phys. Lett. **69**, 363 (1996).

[4.6] T. Hayashi, M. Tanaka, T. Nishinaga, H. Shimada, and Y. Otuka, J. Cryst. Growth **175/176**, 1063 (1997).

[4.7] J. De Boeck, R, Oesterholt, A. Van Esch, H. Bender, C. Bruynseraede, C. Van Hoof, and G. Borghs, Appl. Phys. Lett. **68**, 2744 (1996).

[4.8] H. Akinaga, S. Miyanishi, K. Tanaka, W. Van Roy, and K. Onodera, Appl. Phys. Lett.

76, 97 (2000).
[4.9] T. Hayashi, M. Tanaka, K. Seto, T. Nishinaga, and K. Ando, Appl. Phys. Lett. **71**, 1825, (1997).
[4.10] T. Kuroiwa, T. Yasuda, F. Matsukura, A. Shen, Y. Ohno, Y. Segawa, and H. Ohno, Electron Lett. **34**, 190 (1998).
[4.11] A. M. Ahsan, H. Shimizu, and M. Tanaka, J. Appl. Phys. **87**, 6791 (2000).
[4.12] M. Inoue and T. Fujii, J. Appl. Phys. **81**, 5659 (1997).
[4.13] M. Inoue, K. I. Arai, T. Fujii, and M. Abe, J. Appl. Phys., **85**, 5768, (1999).

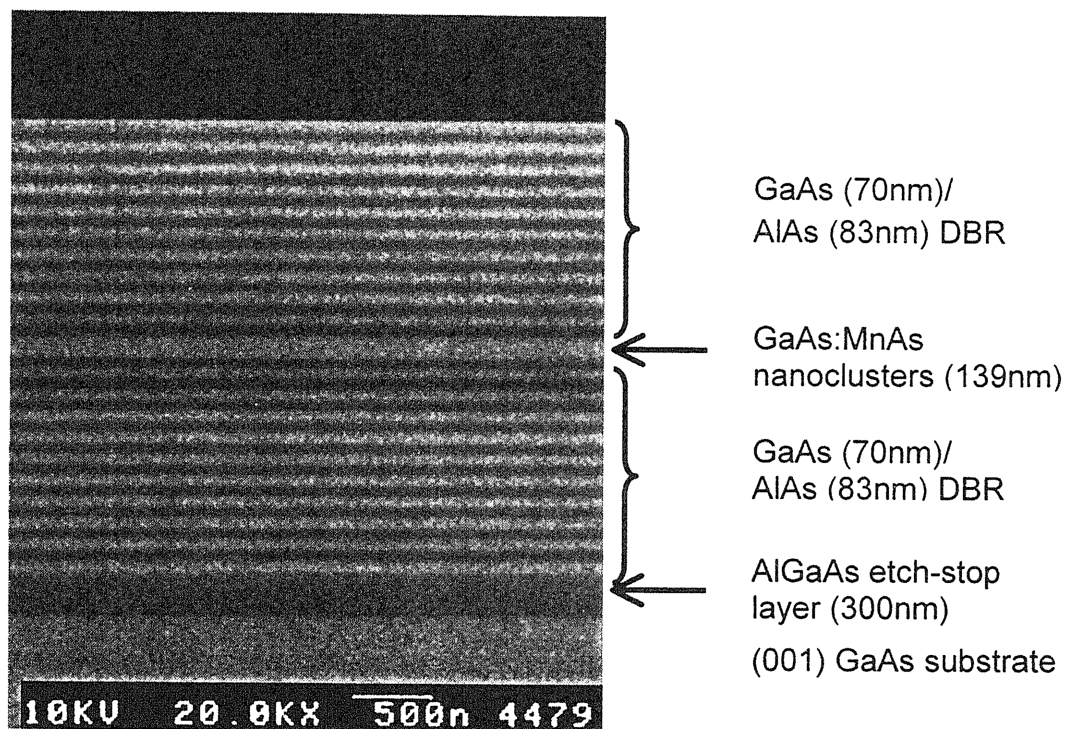

Fig. 4.1 Cross sectional scanning electron microscopy (SEM) image of the sample, a GaAs:MnAs nanoscale hybrid structure sandwiched by GaAs/AlAs DBRs grown on a (001) GaAs substrate.

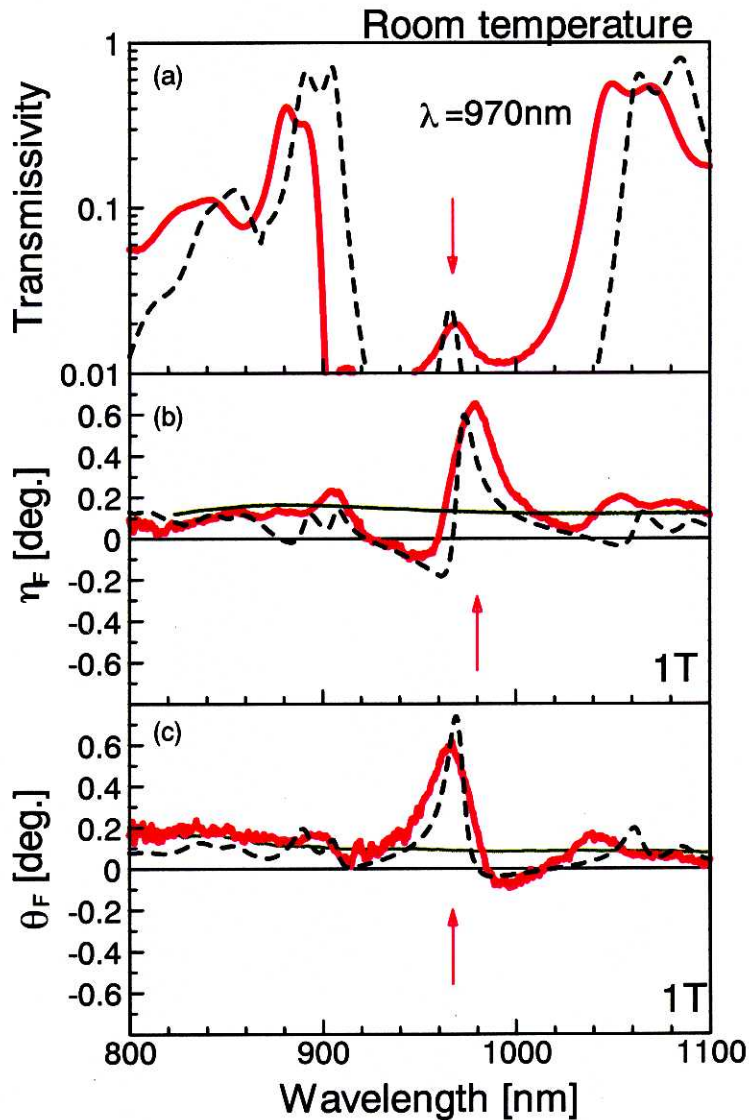

Fig. 4.2 (a) Transmissivity, (b) Faraday ellipticity (MCD) (η_F), and (c) Faraday rotation (θ_F) spectra of GaAs:MnAs sandwiched by 10 periods of DBRs (red curves). In (b) and (c), MCD and Faraday rotation spectra of a 200nm-thick GaAs:MnAs single layer are shown as references (green curves). All the measurements were done at room temperature. MCD and Faraday rotation spectra were measured under the magnetic field of 1T applied perpendicular to the film plane. Calculated magneto-optical spectra are also shown by dashed black curves, where κ is fitted to 0.125.

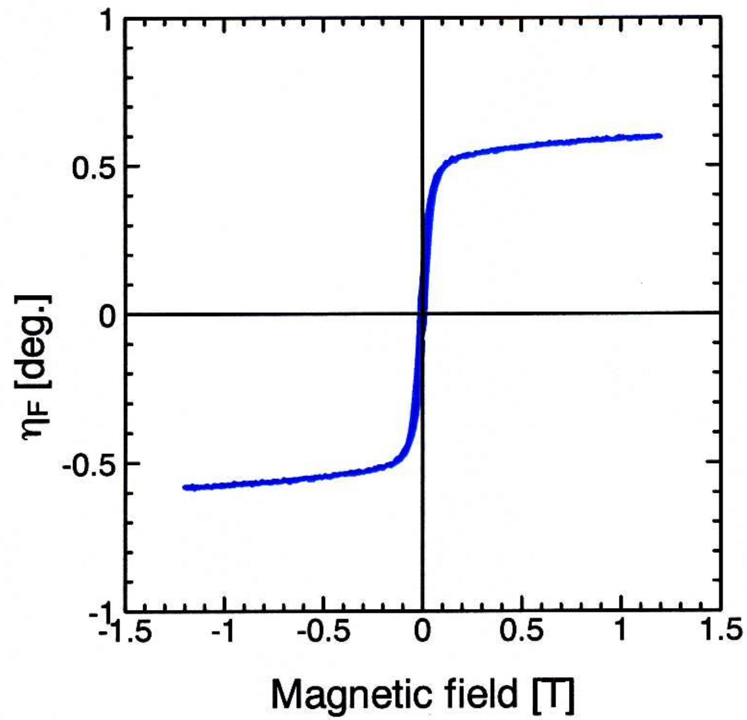

Fig. 4.3 Magnetic field dependence of Faraday ellipticity (MCD) (η_F) at 980nm of the multilayer structure of Fig. 4.1, measured at room temperature.

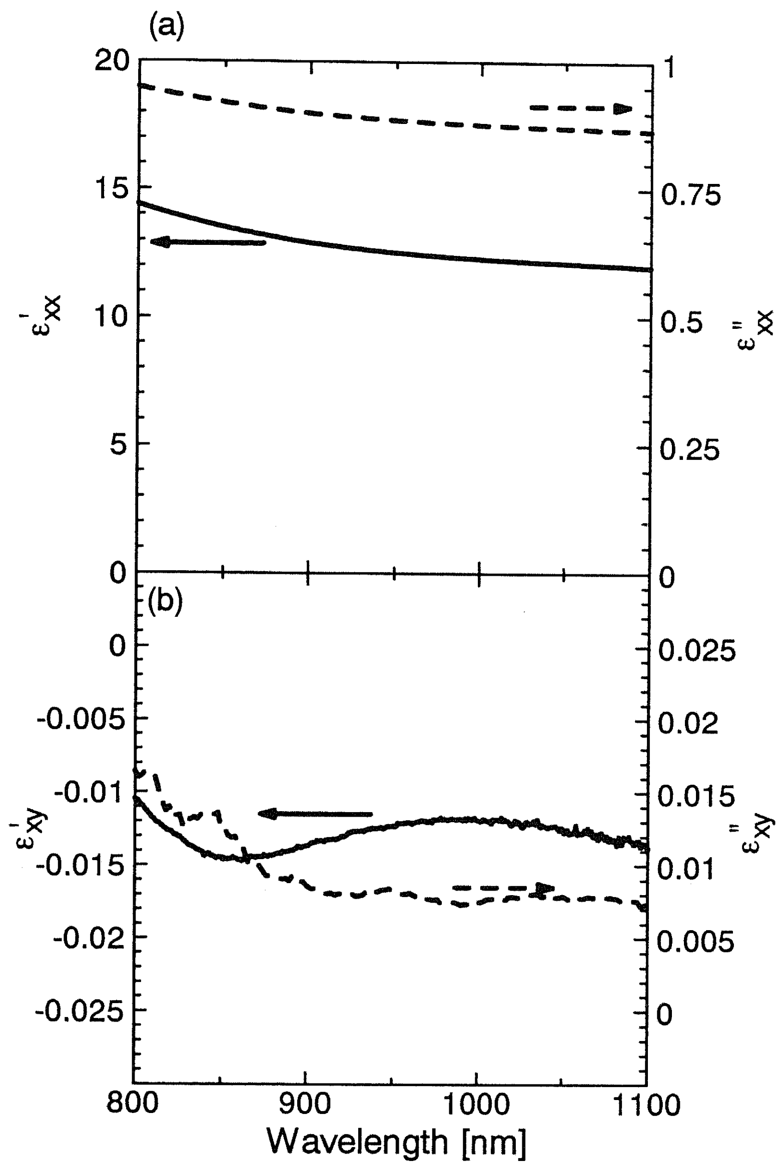

Fig. 4.4 Dielectric-permeability function spectra of GaAs:MnAs with x_{Mn} = 0.047 derived from the transmission, Faraday rotation and Faraday ellipticity spectra. (a) Diagonal elements $\varepsilon_{xx} = \varepsilon_{xx}' + i\varepsilon_{xx}''$. (b) Off-diagonal elements $\varepsilon_{xy} = \varepsilon_{xy}' + i\varepsilon_{xy}''$.

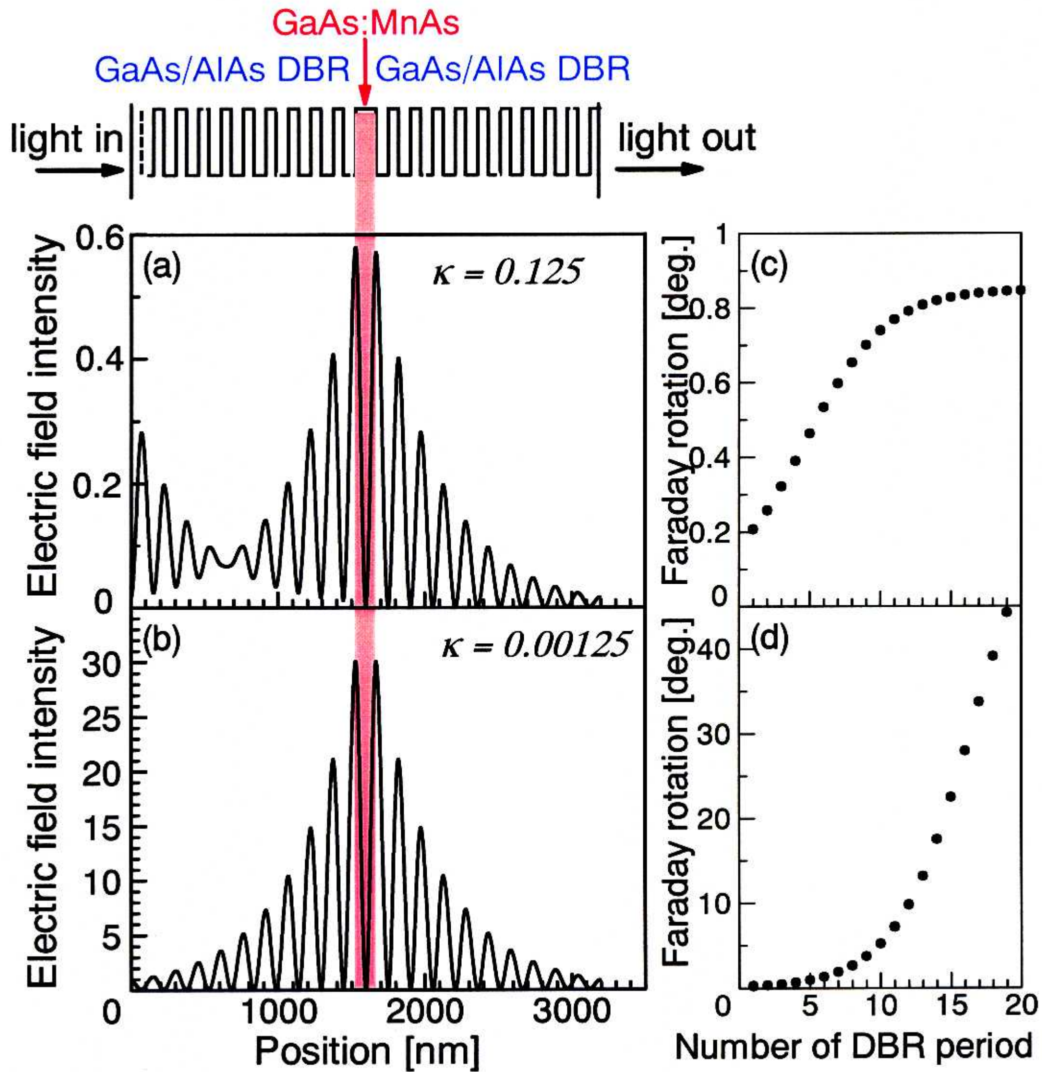

Fig. 4.5 Electric field intensity $|E|^2$ distributions of the light at the Bragg wavelength λ = 980 nm in the multilayer of 10 DBR / GaAs:MnAs / 10 DBR, (a) the present situation κ = 0.125, and (b) a more ideal situation where κ = 0.00125. Here we set the electric field intensity of the incident light to be unity. DBR period number dependences of the Faraday rotation angle are shown in (c) and (d) corresponding to the situations of (a) and (b), respectively.

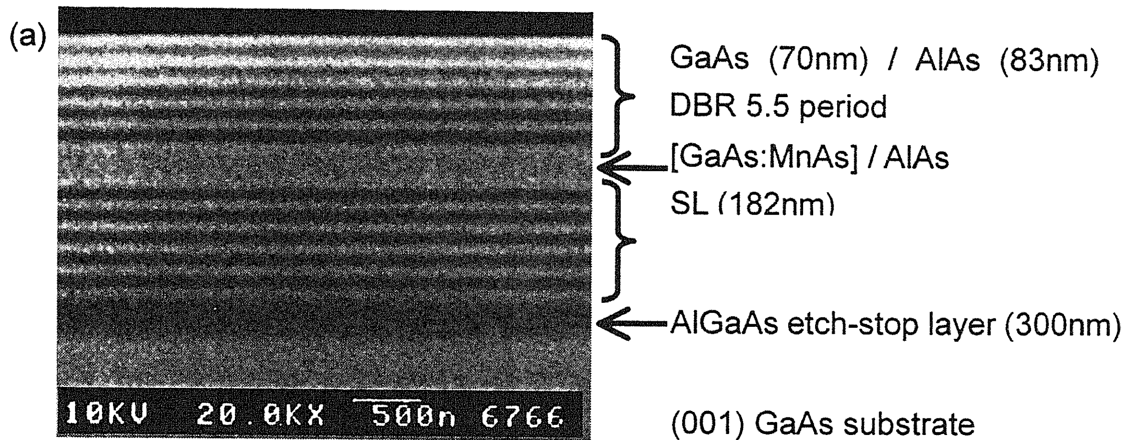

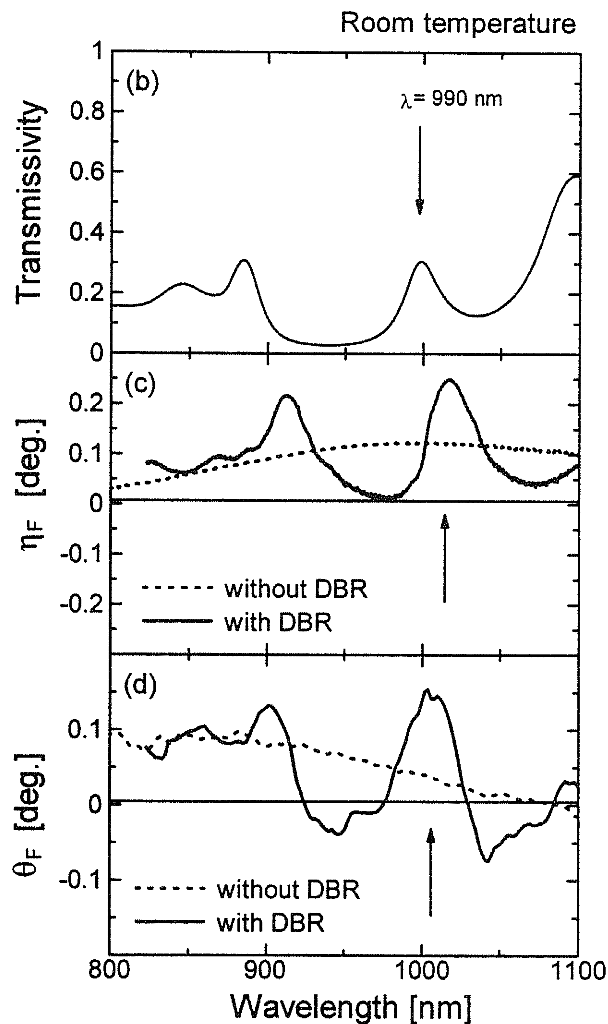

Fig. 4.6 (a) Cross-sectional scanning electron microscopy image of the multilayer structure with a magnetic SL sandwiched by DBRs. The SL consists of 5nm-thick GaAs:MnAs with a Mn concentration x_{Mn} = 0.047 and 2.8nm-thick AlAs, and its total thickness is 182nm. (b) Transmission, (c) Faraday ellipticity (MCD) (η_F), and (d) Faraday rotation (θ_F) spectra of the multilayer structure with DBR measured at room temperature are shown by solid curves. Magneto-optical spectra were measured under the magnetic field of 1T. Spectra of the same SL (total thickness: 156nm) without DBR are also shown by dotted curves as references.

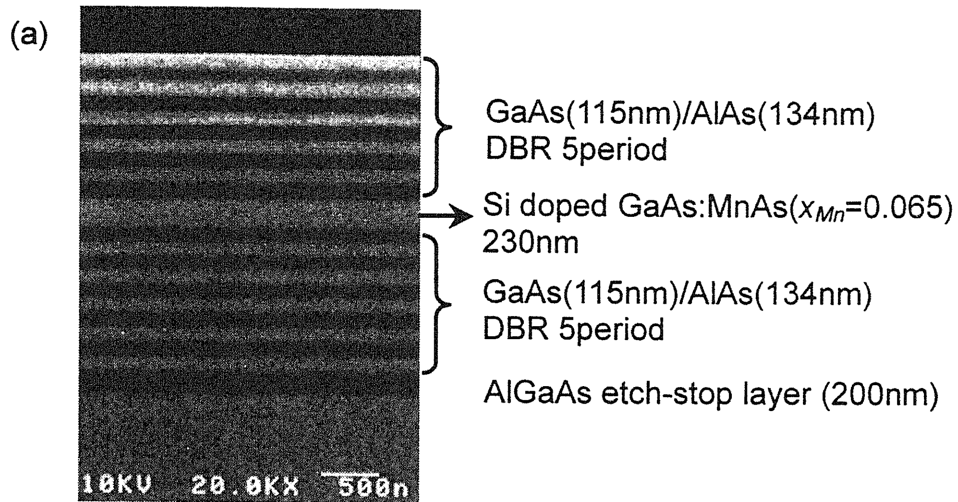

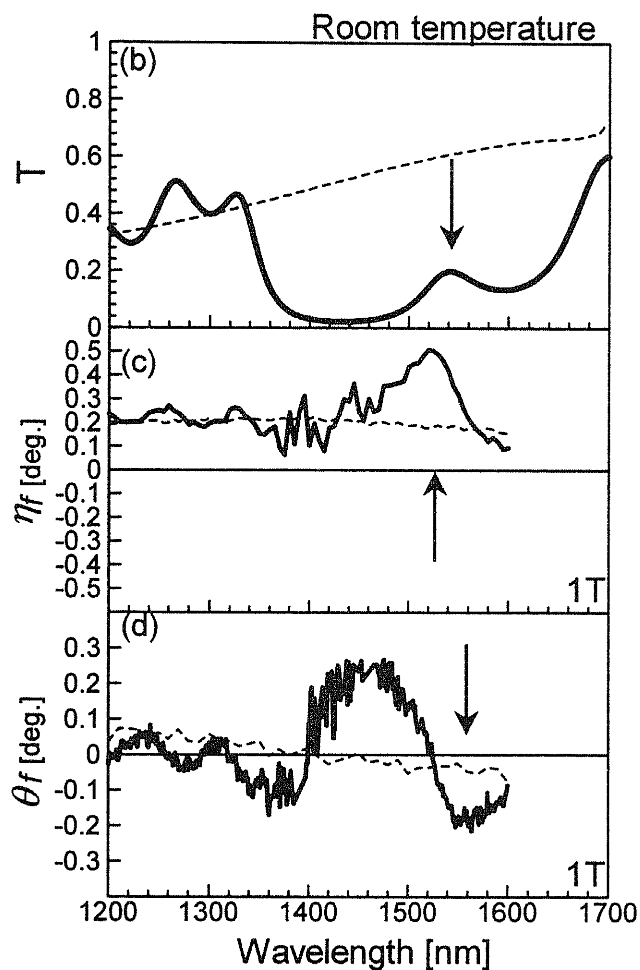

Fig.4.7 (a) Cross sectional image of semiconductor based magneto-photonic crystal composed of 5 DBR / Si-doped GaAs:MnAs / 5 DBR whose operational wavelength was set at 1.55μm, taken by scanning electron microscopy. (b) Optical transmission (T), (c) Faraday ellipticity (η_f), and (d) Faraday rotation (θ_f) spectra of the sample (solid curves) shown in (a). Spectra of a Si-doped GaAs:MnAs single layer (200nm) of the same Mn and Si concentration without DBR, were also plotted as references (dotted curves). All the measurements were done at room temperature, and the Faraday effect (η_f and θ_f) spectra were measured under the magnetic field of 1T applied perpendicular to the samples.

~Chapter 5~

Design of semiconductor-waveguide-type optical isolators using the non-reciprocal refractive index change in the magneto-optical waveguides having MnAs clusters

Optical isolators are the optical devices which block unwanted reflected light, and are dispensable for stable operation of semiconductor lasers. A commercially available optical isolator is composed of a Faraday rotator with Faraday rotation of 45 deg. and two linear polarizers. The multilayer structures discussed in Chapter 4 can be used for this kind of optical isolators. Although conventional optical isolators are easy to be aligned with optical fibers, they are not compatible with edge-emitting semiconductor lasers and optical waveguides, because of the difference in size, materials, and device shape, between semiconductor lasers and optical isolators. Waveguide-type optical isolators, which are compatible with edge-emitting semiconductor lasers, are needed for smaller device modules and integration with III-V optoeletronic devices. At present, ferrimagnetic garnet bulk crystals, such as $Y_3Fe_5O_{12}$ (YIG) and $(GdBi)_3Fe_5O_{12}$, are used for discrete optical isolators. Waveguide-type optical isolators using garnet crystals have also been reported [5.1-5.6]. Since it is impossible to grow garnet crystals on semiconductor substrates, monolithic integration of the optical isolators with III-V optoelectronic devices has been considered very difficult. To date, several approaches are attempted for III-V semiconductor-based waveguide-type optical isolators. Mizumoto et al. [5.7] and Levy et al. [5.8] demonstrated direct bonding of the garnet waveguide structures onto semiconductor GaAs and InP substrates. Zaets et al. fabricated II-VI based diluted magnetic semiconductor CdMnTe based waveguide on a GaAs substrate and demonstrated magneto-optical TE-TM mode conversion [5.9].

Unlike the conventional optical isolators using a Faraday rotator, here, we focus on semiconductor based optical isolators based on nonreciprocal refractive index change. The nonreciprocal refractive index change occurs in TM modes that travel in magneto-optical planar waveguides where the magnetization of the film is aligned transverse to the light propagation direction in the film plane [5.10-5.12], as shown in Fig. 5.1. This phenomenon is based on the transverse magneto-optical Kerr effect within the magneto-optical planar waveguide. Yokoi et al. fabricated a Mach-Zehnder interferometric waveguide optical isolator composed of garnet / InGaAsP / InP using the nonreciprocal phase shift (real part of the nonreciprocal refractive index change), and achieved 4.9 dB isolation [5.10]. Zaets et al. [5.11] and Takenaka et al. [5.12] proposed

GaAs or InGaAsP based optical waveguide isolators using the nonreciprocal loss/gain shift (imaginary part of the nonreciprocal refractive index change) of an amplifier covered by ferromagnetic metal (Co or Fe), which is a called ferromagnetic-metal-layer (FML) optical isolator, as shown in Fig. 5.2. The latter one can be operated by compensating the propagation loss of the forward traveling light by a semiconductor optical amplifier (SOA), as shown in Fig. 5.3. However, the ferromagnetic-metal-layer optical isolator [5.11,5.12] has not been realized experimentally as yet.

The GaAs:MnAs nanocluster material system we studied in Chapter 3 and Chapter 4 is fully compatible with GaAs / AlGaAs heterostructures and exhibits the large magneto-optical effect, although it has optical absorption loss. The magneto-optical figure of merit of GaAs:MnAs is larger than that of ferromagnetic metals such as Fe and Co, as described in Chapter 3. Therefore, the MnAs nanocluster system is a suitable for realizing the ferromagnetic-metal-layer optical isolator. In this chapter, we propose waveguide-type optical isolators based on the non-reciprocal loss/gain shift in the magneto-optical waveguides having the MnAs nanocluster system, and theoretically predict their device performance.

5.1 Design of a waveguide-type optical isolator using the non-reciprocal loss/gain shift in the magneto-optical waveguide having MnAs clusters ~TM mode operation~

5.1.1 Device structure

Here we propose a waveguide-type optical isolator using MnAs clusters, to be integrated on an InP substrate, as shown in Fig. 5.4. The waveguide-type optical isolator is composed of a bottom electrode, a n^+-InP substrate, a n-InP cladding layer, an InGaAsP active layer whose bandgap wavelength is 1.55μm, a magnetic layer of InAlAs:MnAs (MnAs nanoclusters embedded in InAlAs), a p-InAlAs cladding layer, a p^+-InGaAs contact layer, and a top electrode. As a magneto-optical layer, we adopted MnAs clusters embedded in an InAlAs matrix (InAlAs:MnAs) which is lattice-matched to the InP substrate. Table 5.1 shows the refractive index of the each layer. The target operational wavelength is set at 1.55μm. Since it is expected that the optical loss of InAlAs:MnAs is smaller than that of ferromagnetic metals and it is possible to overgrow high quality semiconductor heterostructures on top of the InAlAs:MnAs cluster layer, we can set the InAlAs:MnAs magneto-optical layer near the InGaAsP core layer of the waveguide, thus a strong magneto-optical effect is expected to be obtained. The magneto-optical effect (Faraday rotation and Faraday ellipticity) of the MnAs cluster system is independent of the host semiconductor matrix, as discussed in Chapter 3. We estimated the off-diagonal

element of the dielectric-permeability tensor, ε_{xz} to be 0.027986 - 0.00576 i, using the Faraday rotation θ_F and ellipticity η_F (θ_F = -0.034° and η_F = 0.186°) of a 200nm-thick GaAs:MnAs film at the wavelength of 1.55μm.

The operation principle is as follows. In the TM mode, a non-reciprocal loss shift is brought about by the reflection of light at the interface between the InAlAs:MnAs layer and InGaAsP active layer. The propagation loss for the forward traveling light is compensated by the InGaAsP active layer, whereas the propagation loss for the backward propagating light still remains, as shown in Fig. 5.3. Therefore the optical isolator operation is realized.

Fabrication of the waveguide-type optical isolator which is depicted in Fig. 5.4, can be carried out by two steps of epitaxial growth. First, a n-InP lower cladding layer and an InGaAsP active layer are grown by molecular-beam epitaxy (MBE), or metal-organic vapor-phase epitaxy (MOVPE) on a n^+ InP substrate. On top of the InGaAsP active layer, (InAlMn)As is grown at 250℃ by MBE, and then InAlAs:MnAs is formed by the subsequent annealing. After the annealing, a p-InAlAs layer and a p^+-InGaAs contact layer are grown at 500℃, thus the waveguide-type optical isolator, as depicted in Fig. 5.4, can be fabricated.

5.1.2 Calculation procedure

The nonreciprocal loss / gain shift was calculated by solving Maxwell's equations of the planar waveguide, as shown in Fig. 5.5. Below, the calculation procedure is described briefly.

Let us solve Maxwell's equations (5-1, 5-2),

$$\begin{cases} \nabla \times E = -\mu_0 \dfrac{\partial H}{\partial t} & (5-1) \\ \nabla \times H = \varepsilon_0 \tilde{\varepsilon} \dfrac{\partial E}{\partial t} & (5-2) \end{cases}$$

where

$$\tilde{\varepsilon} = \begin{pmatrix} \varepsilon_x & 0 & \varepsilon_{xz} \\ 0 & \varepsilon_x & 0 \\ -\varepsilon_{xz} & 0 & \varepsilon_x \end{pmatrix} \qquad (5-3)$$

Here, we assume that the propagation light is the TM mode propagating along the z direction, and $\boldsymbol{E}$ and $\boldsymbol{H}$ have a harmonic dependence on the time and the coordinates as follows,

$$\begin{cases} E = (E_x, 0, E_z)\exp(i(\omega t - \beta z)) & (5-4) \\ H = (0, H_y, 0)\exp(i(\omega t - \beta z)) & (5-5) \end{cases}$$

where ω is the angle frequency and β is the propagation constant.
Assuming that $\boldsymbol{E}$ and $\boldsymbol{H}$ are constant in the y direction ($d/dy = 0$) and substituting (5-4) and (5-5) into (5-1) and (5-2), we get the differential equation (5-6),

$$\frac{d^2}{dx}H_y + \left\{k_0^2\frac{\varepsilon_x^2 + \varepsilon_{xz}^2}{\varepsilon_x} - \beta^2\right\}H_y = 0 \qquad (5-6)$$

where k_0 is wavenumber in vacuum.

E_z is expressed as

$$E_z = \frac{1}{\omega\varepsilon_0(\varepsilon_x^2 + \varepsilon_{xz}^2)}\left(\beta\varepsilon_{xz}H_y - i\varepsilon_x\frac{d}{dx}H_y\right) \qquad (5-7)$$

One can obtain an eigenvalue equation by satisfying the boundary conditions of the H_y and E_z. By solving the eigenvalue equation, we obtain effective refractive index $n_{eff,TM}$ of the waveguide. The nonreciprocal loss / gain shift $\Delta\kappa_{eff,TM}$ was derived as follows.

$$\Delta\kappa_{eff,TM} = \mathrm{Im}\left[n_{eff,forward}\right] - \mathrm{Im}\left[n_{eff,backward}\right] \qquad (5-8)$$

$n_{eff,backward}$ can be calculated by reversing the sign of the off-diagonal term ε_{xz}.
The extinction coefficient of the optical isolator can be expressed as

$$Extinction\ \ coefficient = \exp(-2k_0\Delta\kappa l) \qquad (5-9)$$

,where l is the propagation length.

5.1.3 Calculation results

Fig. 5.6 shows the calculated waveguide loss / gain as a function of the internal gain of the InGaAsP active layer, when the core layer thickness a = 250nm, and the InGaAsP guiding layer thickness d = 300nm. In this case, the extinction ratio and the required internal gain for compensating the forward propagating light were calculated to be 119dB/cm and 1300cm^{-1}, respectively. The extinction ratio of 119dB/cm corresponds to the device length of 2.52mm to obtain the isolation of 30dB. This device size is small enough for practical application. The required internal gain of 1300cm^{-1} is within the achievable range by InGaAsP active layer. Here, we have to note that the propagation loss for the TM mode is larger than that for the TE mode. Therefore, for optical isolator operation, we have to adopt tensile-strained quantum wells as a active layer, which amplifys the TM mode, as discussed in ref. [5.11, 5-12]

We also changed the InGaAsP guiding layer thickness d, and investigate the internal gain dependence of the isolation characteristics, as shown in Fig. 5.7. It was

found that with increasing the guiding layer thickness, the isolation and the required internal gain of InGaAsP active layer decrease. This is because the overlap of the electromagnetic field on the magnetic layer is decreased with increasing the InGaAsP guiding layer thickness. Furthremore, to investigate the optimum structure for our waveguide-type optical isolator, we calculated the figure of merit, which is a parameter defined as the isolation divided by the required internal gain based on Fig. 5.7. This figure of merit is proportional to the product of the gain and the device length. Fig. 5.8 shows the InGaAsP guiding layer thickness d dependence of the figure of merit as defined above. The figure of merit showed peak at d = 150nm. Therefore, we can conclude that this InGaAsP guiding layer thickness, 150nm, brings the optimum performance of our waveguide-type optical isolator, under the condition that the InGaAsP active layer thickness a is 250nm.

5.2 *Design of a waveguide-type optical isolator using the non-reciprocal loss/gain shift in the magneto-optical waveguide having MnAs clusters ~TE mode operation~*

The waveguide-type optical isolator based on the magneto-optical planar waveguide operates in the TM mode, as discussed in 5.1. However, many semiconductor laser diodes usually operate in the TE mode. Therefore, waveguide-type optical isolators which can be operated in the TE mode, are needed. In this section, we propose a waveguide-type optical isolator for the TE mode.

5.2.1 *Device structure*

For realizing the TE mode operation in a waveguide-type optical isolator, the magnetic field vector (H_x) of the TE mode light (E_y, H_x, H_z) has to be aligned parallel to the magnetization vector of the magneto-optical material [5.13]. To realize this alignment, the magento-optical layer has to be put at the one side of the waveguide (region 1 in Fig. 5.9) and the magnetic field has to be applied perpendicular to the waveguide along the x direction, in Fig. 5.9. We propose a device structure of the TE mode waveguide-type optical isolator, as shown in Fig. 5.9. By putting the InAlAs:MnAs layer on top of the waveguide (region 2 in Fig. 5.9), TM mode operation can also be realized. By combining the TE and TM mode operation, we can realize a polarization-independent waveguide-type optical isolator.

5.2.2 *Calculation procedure*

The nonreciprocal loss / gain shift for the TE mode was calculated by the

procedure explained as follows.

It is difficult to solve the Maxwell's equations in the 3-dimensional waveguide as shown in Fig. 5.9, so that we adopted the perturbation theory [5.14] and the effective refractive index method [5.15]. Here, "TE mode" discussed here is "TE-like mode" whose dominant components are E_y and H_x, and "TM mode is "TM-like mode" whose dominant components are E_x and H_y in the three-dimensional waveguide.

In the perturbation theory, the change in the effective refractive index Δn_{eff} was expressed as follows.

$$\Delta n_{eff} = -c\varepsilon_0 \frac{\iint E^* \Delta\tilde{\varepsilon} E dxdy}{\iint [E \times H^* + E^* \times H]_z dxdy} \qquad (5-10)$$

In the present case, the perturbation $\Delta\varepsilon$ for the TE and TM mode can be expressed as follows.

$$\Delta\tilde{\varepsilon} = \begin{pmatrix} 0 & 0 & 0 \\ 0 & 0 & \varepsilon_{yz} \\ 0 & -\varepsilon_{yz} & 0 \end{pmatrix} \quad for \quad TE\ \mathrm{mode} \qquad (5-11)$$

$$\Delta\tilde{\varepsilon} = \begin{pmatrix} 0 & 0 & \varepsilon_{xz} \\ 0 & 0 & 0 \\ -\varepsilon_{xz} & 0 & 0 \end{pmatrix} \quad for \quad TM\ \mathrm{mode} \qquad (5-12)$$

By substituting (5,11) and (5,12) into (5-10), the nonreciprocal refractive index change $\Delta n_{eff,TE}$, for TE mode, and $\Delta n_{eff,TM}$, for the TM mode, are derived as follows.

$$\Delta n_{eff,TE} = -\frac{i}{2k_0} \frac{\iint \frac{\varepsilon_{yz}}{\varepsilon} H_x^* \frac{\partial H_x}{\partial y} dxdy}{\iint |H_x|^2 dxdy} \qquad (5-13)$$

$$\Delta n_{eff,TM} = -\frac{i}{2k_0} \frac{\iint \frac{\varepsilon_{xz}}{\varepsilon} H_y^* \frac{\partial H_y}{\partial x} dxdy}{\iint |H_y|^2 dxdy} \qquad (5-14)$$

To calculate (5-13) and (5-14), we have to calculate the electromagnetic field distribution inside the waveguide. To obtain the electromagnetic field distribution inside the waveguide of Fig. 5.9, we adopted the effective refractive index method [5.15].

5.2.3 *Calculation results*

Fig. 5.10 show the electromagnetic field intensity $|E|^2$ distribution inside the waveguide, when the core layer thickness a = 0.2μm, the ridge height h = 0.3μm, the ridge width d = 1.1μm, the width and height of the MnAs cluster layer $d_{Mag} = h_{Mag}$ = 1μm. In this case, the isolation and the required internal gain for the TE mode were calculated to be 36dB/cm and 730 cm^{-1}, respectively. The extinction ratio of 36dB/cm corresponds to the device length of 8.3mm to obtain the isolation of 30dB. This device size is a littile larger than that of the optical isolator described in 5.1.3, but within the reacheable range for practical application. The required internal gain of 730cm^{-1} is much smaller than the value which is realized by InGaAsP active layer, thus these parameters are achievable. For the TM mode, the isolation and the required internal gain for TE mode were calculated to be 69dB/cm and 2200 cm^{-1}, respectively. The extinction ratio of 69dB/cm corresponds to the device length of 4.3mm to obtain the isolation of 30dB. This device size is small enough for practical application. The required internal gain of 2200cm^{-1} is a littile large but within the achievable range by InGaAsP active layer. From the calculation described above, it was found that with decreasing the ridge width d of the waveguide, the non-reciprocal refractive index change $\Delta n_{eff,TE}$, for the TE mode, increased, and with decreasing the ridge height h of the waveguide, non-reciprocal refractive index change for TM mode, $\Delta n_{eff,TM}$, increased. This is because the overlap of the electromagnetic field of the TE mode on the magnetic layer of the sidewall (regioin 1 of Fig. 5.9) is increased with decreasing the ridge width d of the waveguide and the overlap of the electromagnetic field of the TM mode on the magnetic layer on top the InGaAsP guiding layer (regioin 2 of Fig. 5.9) is increased with decreasing the ridge height h of the waveguide. Fig. 5.11 (a) shows ridge width d dependence of the extinction ratio for TE mode when a = 0.2μm, h = 0.3μm, $d_{Mag} = h_{Mag}$ = 1μm. Fig. 5.11 (b) shows ridge height h dependence of the extinction ratio for TE mode when a = 0.2μm, d = 1.1μm, $d_{Mag} = h_{Mag}$ = 1μm. Optimum device structure for the TE mode waveguide-type optical isolator can be obtained by the decrease of ridge width d under the condition that single mode operation is realized.

5.3 *Summary*

In chapter 5, we proposed and simulated the waveguide-type optical isolator using MnAs clusters. For TM mode, 119dB/cm of isolation was estimated and the optimum structure for our waveguide-type optical isolator was discussed. Furthermore, we proposed TE mode waveguide-type optical isolator for the first time, and 36dB/cm of isolation was estimated. Furthermore, we discussed the optimum design for our

waveguide-type optical isolators. The estimated isolation ratio is large enough for practical isolation and the required internal gain is within the achievable range.

Advantages of our waveguide-type optical isolator compared with conventional waveguide-type optical isolators are follows. (1) Since the optical absorption loss and the magneto-optical figure of merit of the MnAs cluster system are smaller and a little larger respectively than those of the ferromagnetic metals such as Fe and Co, it is possible to put the MnAs cluster magnetic layer near the core (active) layer of the waveguide, thus a strong magneto-optical effect can be obtained. (2) Due to the excellent compatibility of the MnAs cluster system with nonmagnetic semiconductor heterostructures, flexible design of device structure can be considered as shown in Fig. 5.9.

References

[5.1] K. Ando, T. Okoshi, and N. Koshizuka, Appl. Phys. Lett., **53**, 4, (1988)

[5.2] N. Sugimoto, T. Shintaku, A. Tate, H. Terui, M. Shimokozono, E. Kubota, M. Ishii, and Y. Inoue, IEEE., Photon. Tech. Lett., **11**, 355, (1999).

[5.3] T. Shintaku, Appl. Phys. Lett., **73**, 1946, (1998)

[5.4] M. Levy, R. M. Osgood, Jr., H. Hegde, F. J. Cadieu, and V. J. Fratello, IEEE., Photon. Tech. Lett., **8**, 903, (1996).

[5.5] H. Yokoi, T. Mizumoto, T. Takano, and N. Shinjo, Appl. Opt., **38**, 7409 (1999)

[5.6] J. Fujita, M. Levy, R. M. Osgood, Jr., L. Wilkens, and H. Dotsch, Appl. Phys. Lett., **76**, 2158, (2000)

[5.7] H. Yokoi and T. Mizumoto, Electron. Lett., **33**, 1787, (1998).

[5.8] M. Levy, R. M. Osgood, Jr., A. Kumar, and H. Bakhru, Appl. Phys. Lett., **71**, 2617, (1997)

[5.9] W. Zaets, and K. Ando, Appl. Phys. Lett., **77**, 1593, (2000)

[5.10] H. Yokoi, T. Mizumoto, N. Shinjo, N. Futakuchi, and Y. Nakano, Appl. Opt., **39**, 6158 (2000)

[5.11] W. Zaets, and K. Ando, IEEE., Photon. Tech. Lett., **11**, 1012, (1999)

[5.12] M. Takenaka, Master thesis (2000), The Univ. of Tokyo

[5.13] J. Fujita, and M. Levy, R. M. Osgood, Jr., L. Wilkens, and H. Dotsch, IEEE., Photon. Tech. Lett., **12**, 1510, (2000)

[5.14] P. M. Morse and H. Feshbach: Method of Theoretical Physics, McGraw-Hill (1953)

[5.15] W. Streifer and E. Kapon, Appl. Opt., **18**, 3724 (1979)

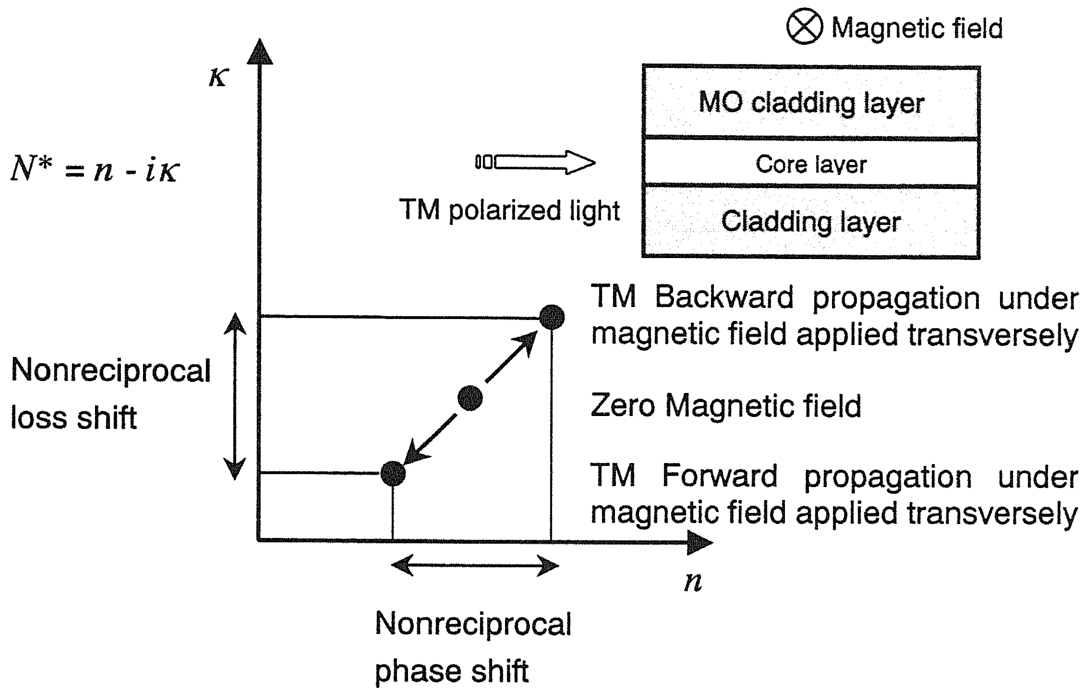

Fig. 5.1 Nonreciprocal refractive index change of the TM mode in a magneto-optical planar waveguide. Upper cladding layer is a magneto-optical layer, as shown in the inset. Real and imaginary parts correspond to the nonreciprocal phase shift and loss shift, respectively.

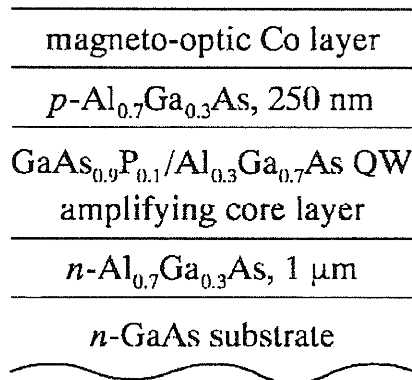

Fig. 2. Schematic diagram of the optical ampli er covered by ferromagnetic metal. The 156-nm-thick amplifying layer includes three 16 nm GaAs P tensile-strained QW's with 27-nm Al Ga As barriers. The absorption by the Co layer is compensated by an optical gain in the amplifying core layer.

Fig. 5.2 Waveguide-type optical isolator based on the nonreciprocal loss / gain of the amplifier covered by a ferromagnetic layer, proposed by Zaets et al. [5.11]

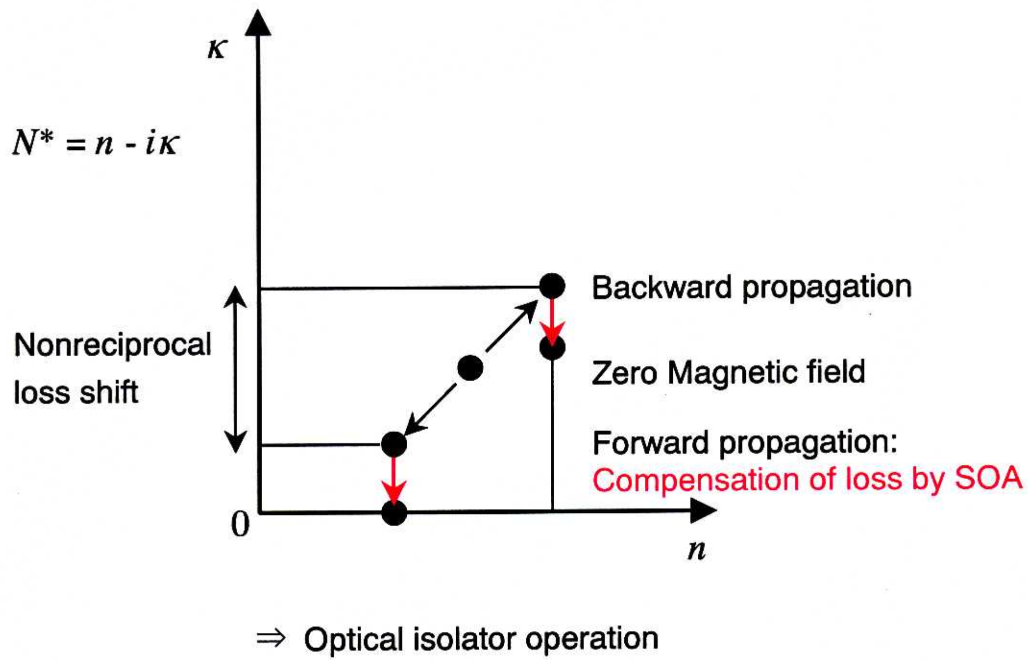

Fig. 5.3 Principle of waveguide-type optical isolator operation based on the nonreciprocal loss / gain shift.

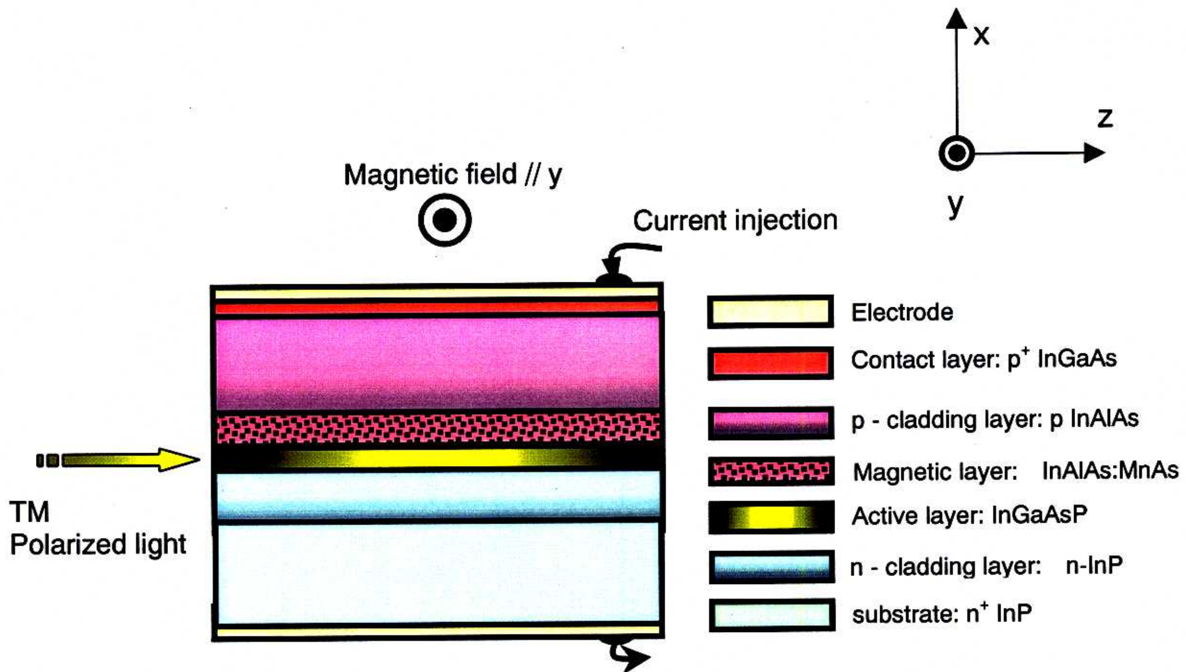

Fig. 5.4 Waveguide-type optical isolator structure proposed in this study.

Materials	n	κ	ε_{xz}
InP	3.16	0	0
InGaAsP (E_g = 1.55μm)	3.53	Gain: variable	0
InGaAsP (E_g = 1.25μm)	3.37	0	0
InAlAs:MnAs	3.24	0.08	0.027986-0.00576 i

Table 5.1 Material parameters of each layer. Refractive index n, extinction coefficient κ, of each layer and off-diagonal element ε_{xz} of the dielectric-permeability tensor of InAlAs:MnAs.

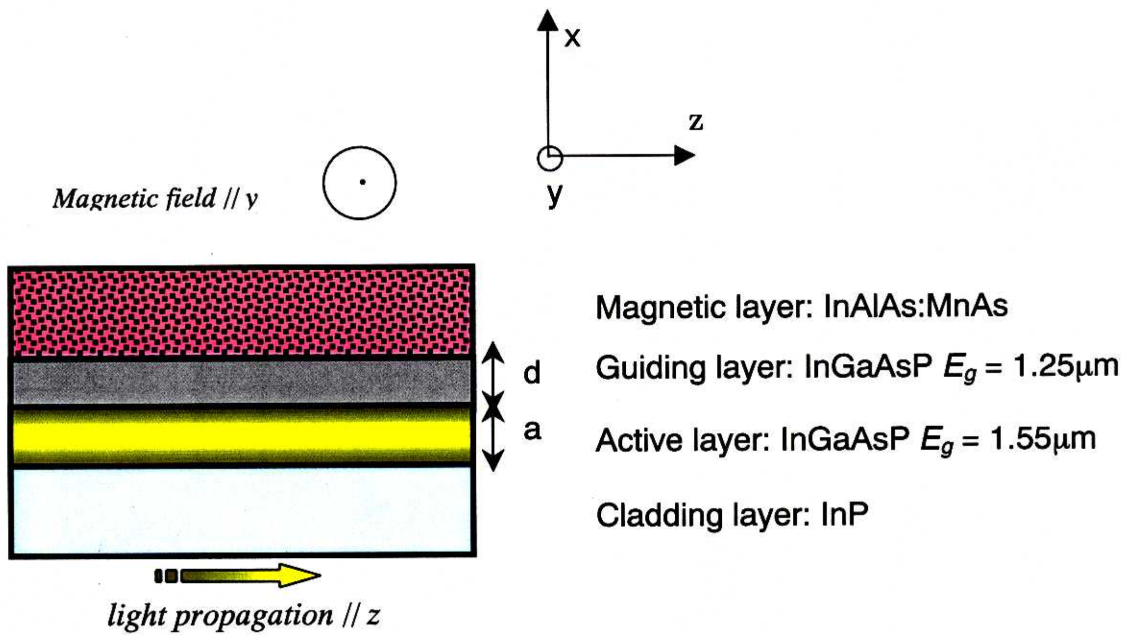

Fig. 5.5 Planar waveguide structure for solving Maxwell's equation

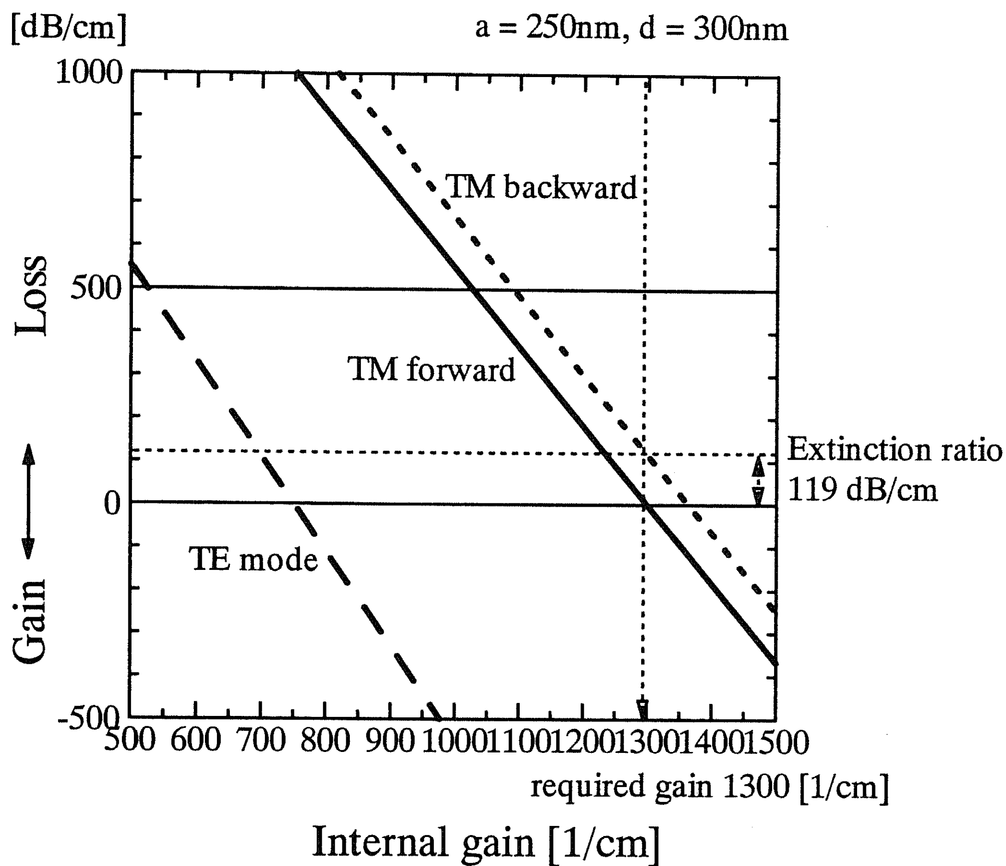

Fig. 5.6 Waveguide loss / gain as a function of the internal gain of the InGaAsP active layer, when the core layer thickness a = 250nm, and the InGaAsP guiding layer thickness d = 300nm. The wavelength λ was set at 1.55μm.

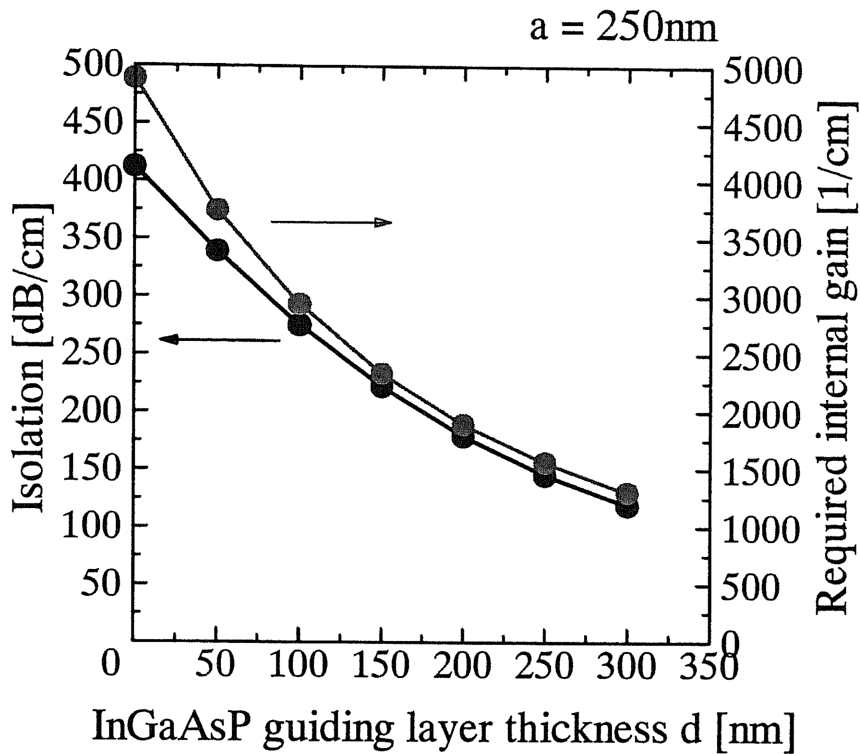

Fig. 5.7 InGaAsP guiding layer thickness d dependence of the isolation ratio and the required internal gain of InGaAsP active layer. The wavelength λ was set at 1.55μm.

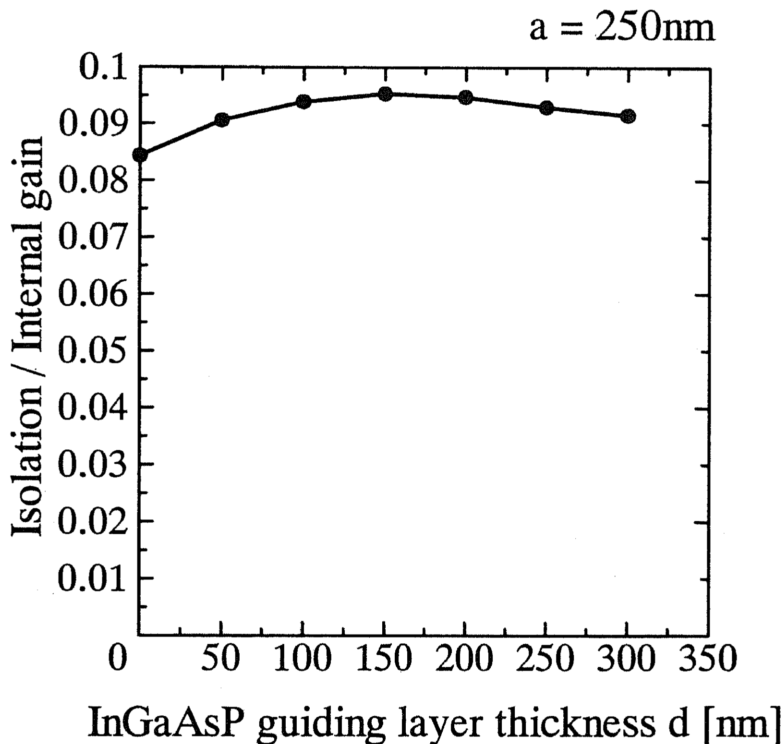

Fig. 5.8 InGaAsP guiding layer thickness d dependence of the figure of merit which is defined as the isolation divided by the required internal gain based on Fig. 5.7.

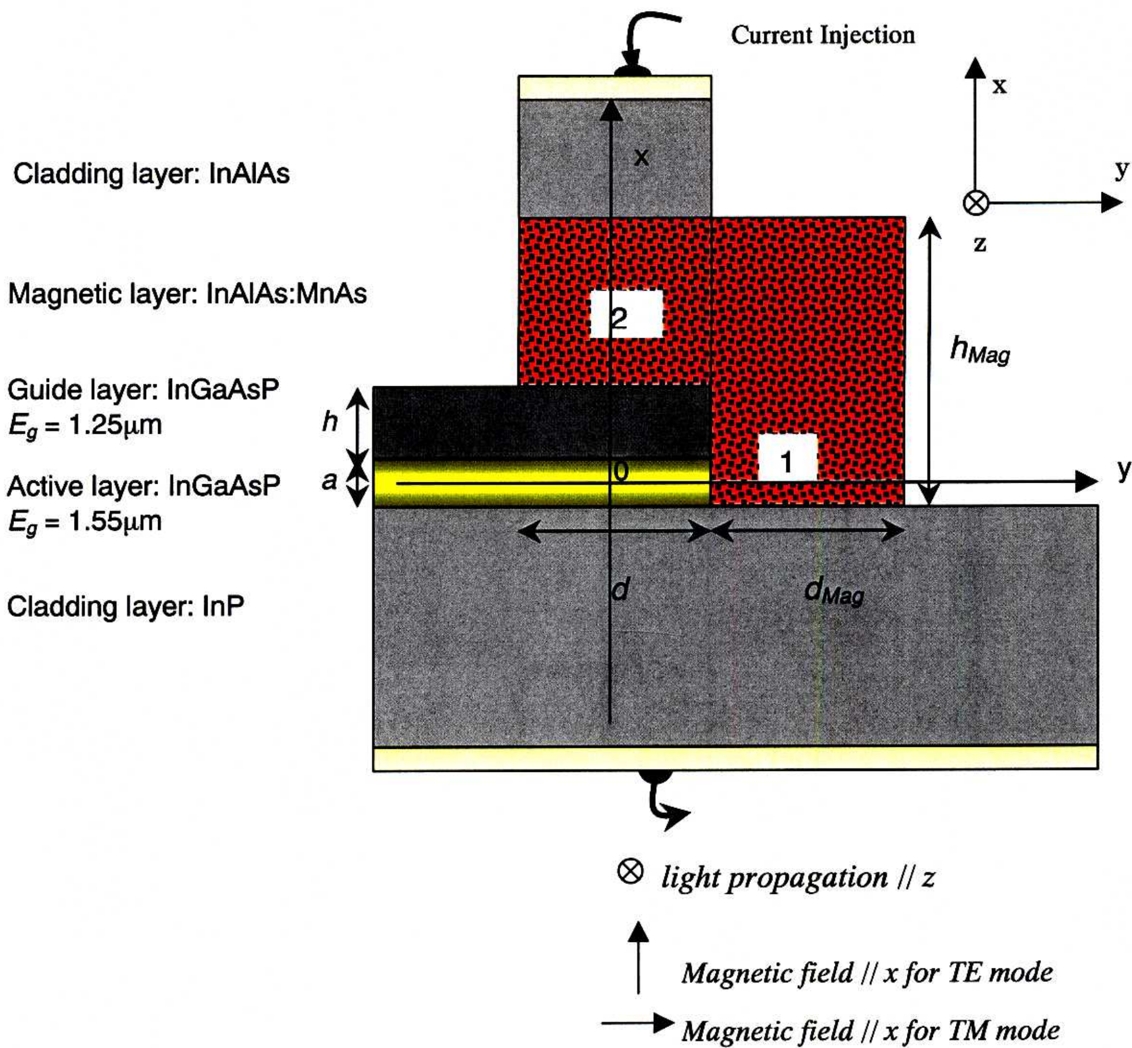

InP layer	n = 3.16,
InGaAsP active layer	n = 3.53, gain: variable
InAlAs:MnAs magnetic layer	n = 3.23, κ = 0.08, ε_{yz} = 0.02492+0.0052i

Fig. 5.9 TE mode optical waveguide type isolator structure proposed in this study.

(a)

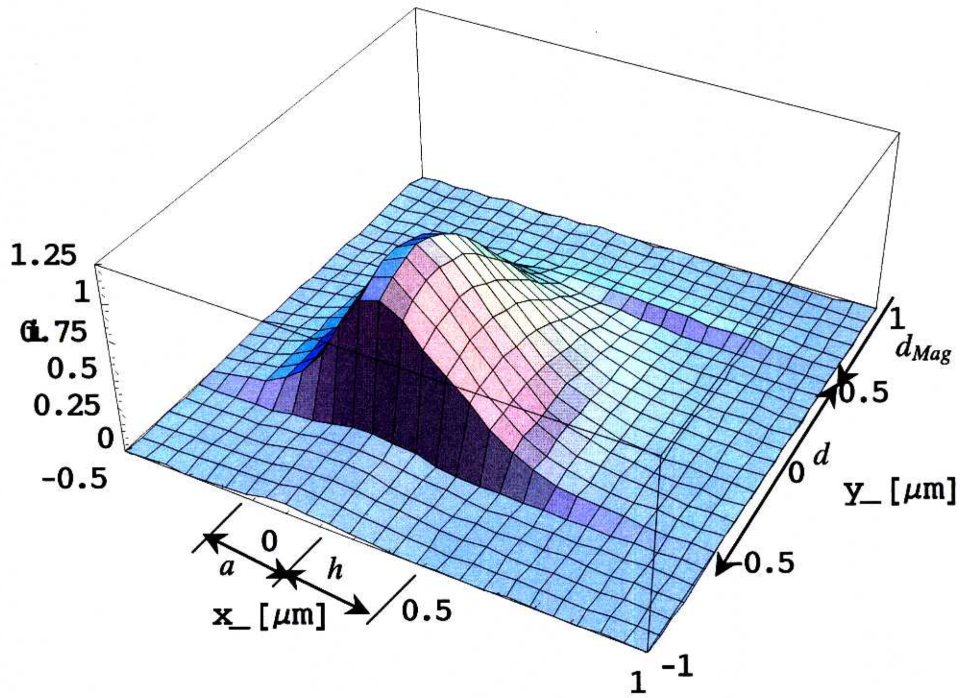

(b)

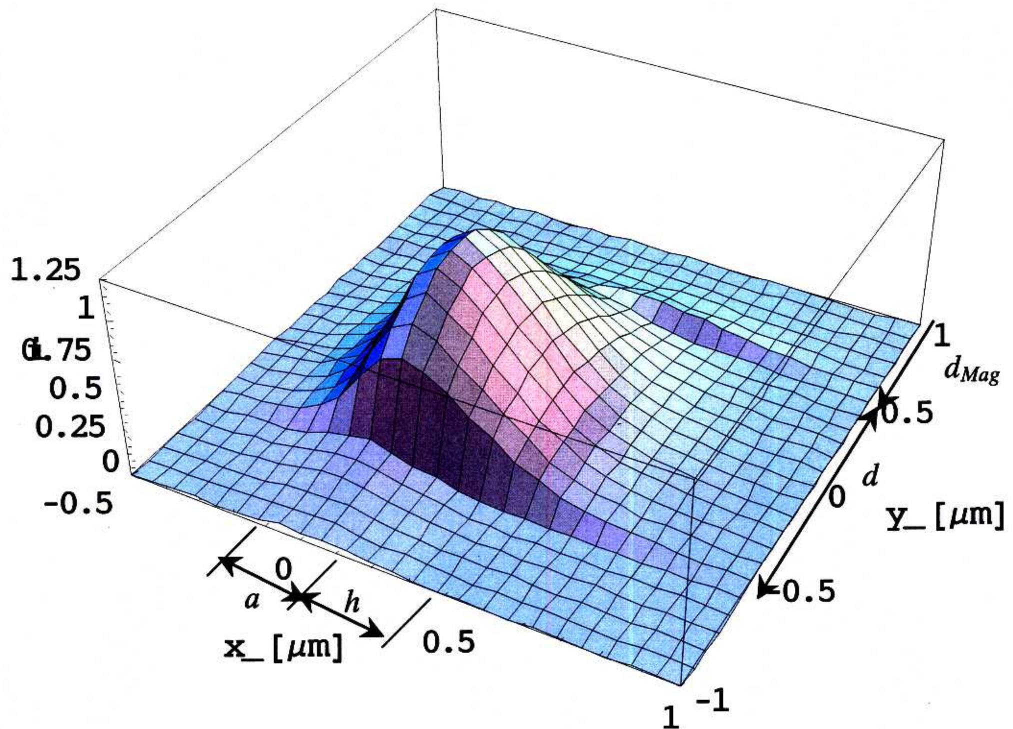

Fig. 5.10 Electromagnetic field intensity $|\boldsymbol{E}|^2$ distribution of the (a) "TE-like" mode, and (b) "TM-like" mode when a = 0.2μm, h = 0.3μm, d = 1.1μm, $d_{Mag} = h_{Mag}$ = 1μm.

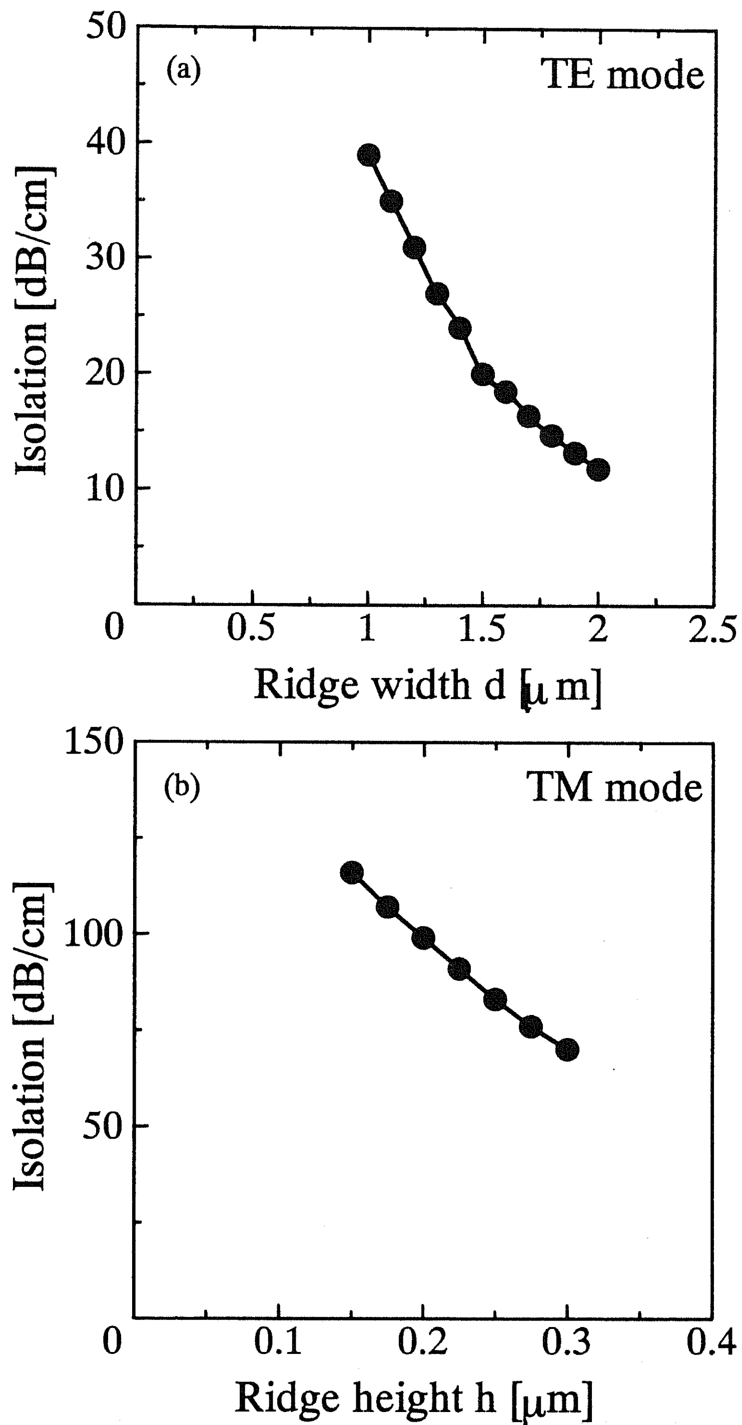

Fig. 5.11 (a) Ridge width d dependence of the isolation for TE mode when a = 0.2μm, h = 0.3μm, $d_{Mag} = h_{Mag}$ = 1μm. (b) Ridge height h dependence of the isolation for TE mode when a = 0.2μm, d = 1.1μm, $d_{Mag} = h_{Mag}$ = 1μm.

~Chapter 6~
Concluding remarks

This thesis is devoted to the research on semiconductor (GaAs) / magnetic (Mn) hybrid structures, focusing on their magneto-optical properties. In the first half (Chapter 2 and Chapter 3), we described fabrication and fundamental properties (magnetic, optical, and magneto-optical properties) of III-V based ferromagnetic semiconductor (GaMn)As and related quantum heterostructures, and the MnAs-GaAs granular material, that is, MnAs nanoclusters embedded in a GaAs matrix (GaAs:MnAs). In the latter half (Chapter 4 and Chapter 5), we described the proposal and demonstration of optical isolators using GaAs:MnAs, which is one of the attractive applications of semiconductor / magnetic hybrid structures. Below, we summarize the thesis and describe concluding remarks.

In Chapter 1, we briefly outline the state of the art of the semiconductor spin electronics, focusing on GaAs based materials, and discussed the research directions in this field. We stressed the importance of taking advantage of the unique properties of semiconductor / magnetic hybrid structures, which can not be realized solely by semiconductors or solely by magnetic materials.

In Chapter 2, we described the epitaxial growth and magneto-optical characterizations of the III-V ferromagnetic semiconductor (GaMn)As and its quantum heterostructures. We observed clear blue shift in the MCD spectra of (GaMn)As / AlAs ultrathin heterostructures and found that the quantum well states were formed in (GaMn)As / AlAs heterostructures when the (GaMn)As layer was thinner than 5nm. We also discovered ferromagnetic ordering when the (GaMn)As layer thickness as thin as 2nm. The finding of ferromagnetic quantum well states in the (GaMn)As / AlAs heterostructures are promising for (GaMn)As based quantum electronic devices, such as a (GaMn)As based magnetic tunnel junction with a resonant tunneling structure.

In Chapter 3, we described the fabrication, and structural, magnetic, optical and magneto-optical properties of GaAs:MnAs. We fabricated semiconductor-based magnetic superlattices containing GaAs:MnAs, and have characterized their structural, optical transmission and magneto-optical properties. It was found that the superlattices have good crystalline quality and the MnAs nanocluster system shows excellent compatibility with GaAs / AlAs heterostructures from cross sectional TEM characterizations. We also found that the MnAs cluster size can be controlled and the optical loss can be reduced by introducing [GaAs:MnAs] / AlAs superlattice structures. It was also found that the magnetization and magneto-optical effect were enhanced by additional Si doping during the growth of (GaMn)As. We investigated the origin of the optical loss and the

magneto-optical effect of GaAs:MnAs, from the MnAs cluster size dependence of the properties. Based on our experimental results, we also discussed the advantages and disadvantages of (GaMn)As and GaAs:MnAs, as magneto-optical materials which will be used at room temperature, and concluded that the MnAs cluster system is more promising, at present stage, for magneto-optical device applications at room temperature.

In Chapter 4, we fabricated one-dimensional semiconductor-based magneto-photonic crystals (1D-SMPC), which are multilayer structures composed of GaAs:MnAs and GaAs / AlAs distributed Bragg reflectors (DBRs). In SMPC of 10 periods DBR / GaAs:MnAs / 10 periods DBR, we realized 7 times enhancement of the magneto-optical effect and 4 deg./μm of Faraday rotation at the wavelength of 0.98μm. We also theoretically predict the required conditions for optical isolator application, and proposed and demonstrated two approaches for solving the problems. Since it is not realistic to fabricate thick (>100μm) GaAs:MnAs films, the SMPC approach is one of the promising methods for optical isolators using semiconductor / magnetic hybrid materials which can be obtained only by epitaxial growth.

In Chapter 5, we proposed a waveguide-type optical isolator using the non-reciprocal loss/gain shift in the magneto-optical waveguide having the MnAs nanocluster system. For the TM mode, 120dB/cm of isolation was predicted. Furthermore, we proposed a TE mode waveguide-type optical isolator for the first time, and 36dB/cm of isolation was predicted. Furthermore we discussed the optimum design for our waveguide-type optical isolators. The MnAs nanocluster system is fully compatible with nonmagnetic semiconductor heterostructures and it is possible to overgrow high quality semiconductor heterostructures, so that it can allow more flexible design of waveguide-type optical isolators, compared with the previously proposed isolator devices using ferromagnetic metals.

Since semiconductor spin electronics is still in the early stage, no practical application has been proposed in the field of GaAs based semiconductor / magnetic hybrid structures. One of the promising and attractive applications is the field of magneto-optical devices. Semiconductor based magneto-photonic crystals and the waveguide-type optical isolators studied in this thesis are surely the promising approaches that takes advantages of the unique properties of the semiconductor / magnetic hybrid structures, and these results will lead to real magneto-optical device applications.

Acknowledgements

First of all, I would like to sincerely thank Prof. M. Tanaka, my supervisor of doctoral research, for his constant encouragement, guidance, and thorough discussion about my doctoral work.

This work was partially supported by the CREST project of Japan Science Technology Cooperation (Function Evolution of Materials and Devices based on Electron / Photon Related Phenomena, Prof. Nakano team: "Innovative Photon-Controlling Devices Based on Artificial Optical Properties of Semiconductors"). I could have discussion with and receive fruitful advice from the members of the CREST project team and would like to thank Prof. Y. Nakano, Prof. Y. Shimogaki, Prof. M. Tsuchiya, and Prof. S. Yamashita.

I received the fellowship from the Japan Society for the Promotion of Science (JSPS) for Young Scientists and I acknowledge the financial support from the JSPS.

I have worked under the powerful support of Prof. T. Nishinaga, and Prof. S. Naritsuka (Meijo Univ.) I would like to greatly thank Prof. T. Nishinaga and Prof. S. Naritsuka.

About magneto-optical experiments, I could receive technical guidance and valuable discussion from Dr. K. Ando (Advanced Industrial Science and Technology). I would like to greatly thank Dr. K. Ando

I could receive a lot of technical guidance of my growth and transport experiments from and have discussion with Dr. T. Hayashi (NTT) during my master and doctoral works. I would like to greatly thank Dr. T. Hayashi.

Thanks are also due to Dr. S. Sugahara for his collaboration and advice.

Part of my work was done with coworkers. I would like to thank M. Miyamura and M. Onouchi.

Lastly I would like to thank all the members of M. Tanaka Laboratory for their guidance, discussion, and collaborations.

We derive the magneto-optical effect in a multilayer structure discussed in Chapter 4. The calculation is based on the random matrix approach [A.1]. We modified the treatment of the magneto-optical layer in our simulation. Let us consider a multilayer structure composed of n periods of GaAs / AlAs DBRs and GaAs:MnAs, as shown in Fig. A.1. The multilayer does not have boundary in the X-Y plane. The eigen modes in magneto-optical materials are left and right circular polarized light as was described in 2.4.1. These eigen modes which propagate in $+z$ direction can be expressed as (A.1),

$$\begin{cases} E_{\pm} = E_0(x \pm iy)\exp(-i\omega(t - \frac{N_{\pm}}{c}z)) \\ \xi_0 H_{\pm} = E_0 N_{\pm}(\mp ix + y)\exp(-i\omega(t - \frac{N_{\pm}}{c}z)) \\ N_{\pm} = \varepsilon_{xx} \pm i\varepsilon_{xy} \end{cases} \tag{A.1}$$

where $N_{\pm}$ are refractive index for right and left circular polarized light, and $\xi_0 = c\mu_0$ is the characteristic impedance in the vaccum.

The eigen modes which propagate in $-z$ direction can be expressed as (A.2)

$$\begin{cases} E_{\pm} = E_0'(x \pm iy)\exp(-i\omega(t + \frac{N_{\pm}}{c}z)) \\ \xi_0 H_{\pm} = E_0' N_{\pm}(\mp ix + y)\exp(-i\omega(t + \frac{N_{\pm}}{c}z)) \end{cases} \tag{A.2}$$

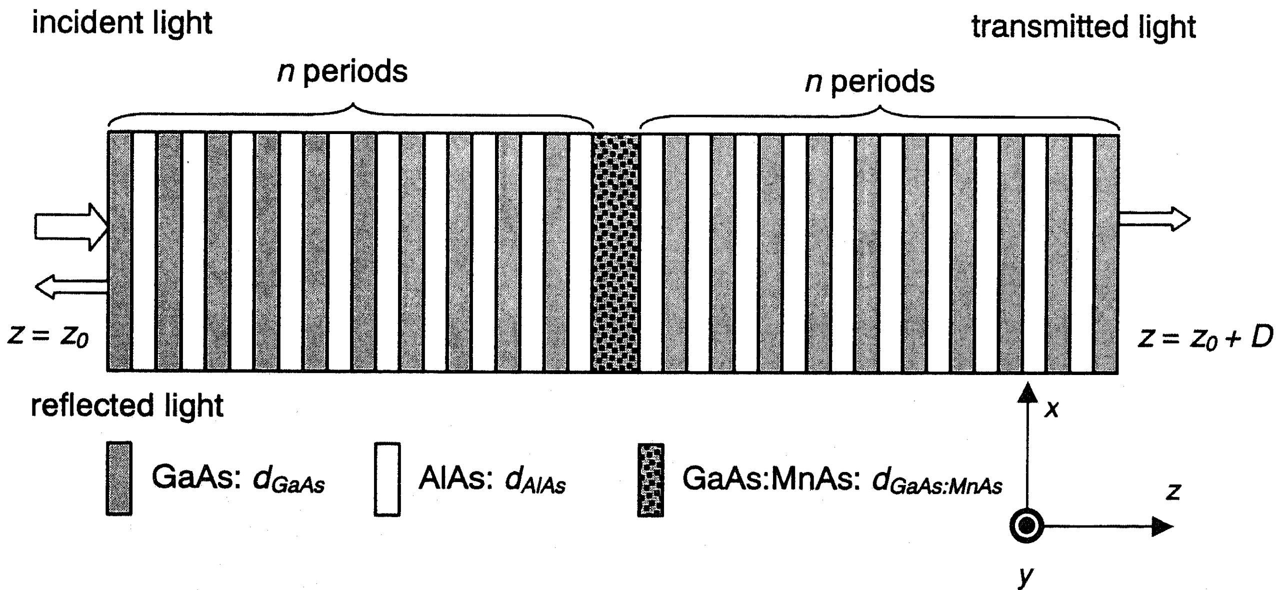

Fig. A.1 The multilayer structure composed of GaAs / AlAs DBRs and GaAs:MnAs.

The state vector $\tau(z)$ of the standing wave in the multilayer can be expressed in (1 ×4) column vector (A.3),

$$\tau(z)=\begin{pmatrix}E_x\\E_y\\\xi_0H_x\\\xi_0H_y\end{pmatrix}=\begin{pmatrix}1\\-i\\iN_+\\N_+\end{pmatrix}E_1e^{ik_+z}+\begin{pmatrix}1\\-i\\-iN_+\\-N_+\end{pmatrix}E_2e^{-ik_+z}+\begin{pmatrix}1\\i\\-iN_-\\N_-\end{pmatrix}E_3e^{ik_-z}+\begin{pmatrix}1\\i\\iN_-\\-N_-\end{pmatrix}E_4e^{-ik_-z}$$

$$=\begin{pmatrix}1&1&1&1\\-i&-i&i&i\\iN_+&-iN_+&-iN_-&iN_-\\N_+&-N_+&N_-&-N_-\end{pmatrix}\begin{pmatrix}E_1e^{ik_+z}\\E_2e^{-ik_+z}\\E_3e^{ik_-z}\\E_4e^{-ik_-z}\end{pmatrix}$$

(A.3)

$$k_\pm=\frac{\omega}{c}N_\pm \quad (A.4)$$

where $k_\pm$ are wave vector for right and left circular polarized light.

The evolution of the state vector after passing through a layer of thickness d is expressed as follows,

$$\tau(z+d)=\Phi\cdot\tau(z) \quad (A.5)$$

where Φ is translation matrix.

By substituting (A.3) into (A.5), we get following relation.

$$P\cdot\begin{pmatrix}E_1e^{ik_+(z+d)}\\E_2e^{-ik_+(z+d)}\\E_3e^{ik_-(z+d)}\\E_4e^{-ik_-(z+d)}\end{pmatrix}=\Phi\cdot P\cdot\begin{pmatrix}E_1e^{ik_+z}\\E_2e^{-ik_+z}\\E_3e^{ik_-z}\\E_4e^{-ik_-z}\end{pmatrix}\qquad P\equiv\begin{pmatrix}1&1&1&1\\-i&-i&i&i\\iN_+&-iN_+&-iN_-&iN_-\\N_+&-N_+&N_-&-N_-\end{pmatrix} \quad (A.6)$$

$$P\cdot\begin{pmatrix}e^{ik_+d}&0&0&0\\0&e^{-ik_+d}&0&0\\0&0&e^{ik_-d}&0\\0&0&0&e^{-ik_-d}\end{pmatrix}\cdot\begin{pmatrix}E_1e^{ik_+z}\\E_2e^{-ik_+z}\\E_3e^{ik_-z}\\E_4e^{-ik_-z}\end{pmatrix}=\Phi\cdot P\cdot\begin{pmatrix}E_1e^{ik_+z}\\E_2e^{-ik_+z}\\E_3e^{ik_-z}\\E_4e^{-ik_-z}\end{pmatrix} \quad (A.7)$$

From (A.7), we can express translation matrix Φ by using $k_{\pm}$ and $N_{\pm}$ as follows.

$$\Phi = P \cdot \begin{pmatrix} e^{ik_+d} & 0 & 0 & 0 \\ 0 & e^{-ik_+d} & 0 & 0 \\ 0 & 0 & e^{ik_-d} & 0 \\ 0 & 0 & 0 & e^{-ik_-d} \end{pmatrix} \cdot P^{-1} \tag{A.8}$$

Since the dielectric-permeability functions of GaAs:MnAs are unknown so far, the refractive index n of GaAs:MnAs is assumed to be the same as that of GaAs, and the off-diagonal elements ε_{xy} (= $\varepsilon_{xy}'+ i\varepsilon_{xy}''$) related to the magneto-optical effect were obtained from the experimental Faraday ellipticity and Faraday rotation spectra of a GaAs:MnAs single layer as follows,

$$\begin{cases} \varepsilon_{xy}' = -\dfrac{2c}{\omega d}(n\eta_F + \kappa\theta_F) \\ \varepsilon_{xy}'' = -\dfrac{2c}{\omega d}(\kappa\eta_F - n\theta_F) \end{cases} \tag{A.9}$$

The extinction coefficient κ (the imaginary part of the complex refractive index n^* $= n - i\kappa$) of the GaAs:MnAs layer was determined to fit to the experimental transmissivity spectrum [A.2].

Translation matrix Φ_{multi} of the multilayer can be expressed as,

$$\Phi_{multi} = (\Phi_{GaAs} \cdot \Phi_{AlAs})^n \cdot \Phi_{GaAs:MnAs} \cdot (\Phi_{AlAs} \cdot \Phi_{GaAs})^n \tag{A.10}$$

The state vector at the incident plane τ_{in} ($z = z_0$) is given by the sum of the incident linear polarized light and the reflected light as,

$$\tau_{in} = \begin{pmatrix} 1 \\ 0 \\ 0 \\ 1 \end{pmatrix} e^{ik(z-z_0)} + \left(\begin{pmatrix} C_1 \\ 0 \\ 0 \\ -C_1 \end{pmatrix} + \begin{pmatrix} 0 \\ C_2 \\ C_2 \\ 0 \end{pmatrix} \right) e^{-ik(z-z_0)} = \begin{pmatrix} 1 & C_1 & 0 & 0 \\ 0 & 0 & 0 & C_2 \\ 0 & 0 & 0 & C_2 \\ 1 & -C_1 & 0 & 0 \end{pmatrix} \tag{A.11}$$

The state vector at the output plane τ_{out} ($z = z_0 + D$)can be expressed as,

$$\tau_{out} = \left(\begin{pmatrix} C_3 \\ 0 \\ 0 \\ C_3 \end{pmatrix} + \begin{pmatrix} 0 \\ C_4 \\ -C_4 \\ 0 \end{pmatrix} \right) e^{ik(z-z_0-D)} = \begin{pmatrix} C_3 & 0 & 0 & 0 \\ 0 & 0 & C_4 & 0 \\ 0 & 0 & -C_4 & 0 \\ C_3 & 0 & 0 & 0 \end{pmatrix} \quad \text{(A.12)}$$

where C_1-C_4 are coupling constants.

C_1-C_4 can be calculated by solving following equation.

$$\tau_{out}(z) = \Phi_{multi} \cdot \tau_{in}(z) \quad \text{(A.13)}$$

Faraday rotation and ellipticity of the multilayer can be expressed by using C_3 and C_4 as follows,

$$\begin{cases} \textit{Faraday} \quad \textit{rotation}[\text{deg.}] = -\dfrac{180}{2\pi} \arctan\left(\dfrac{2\,\text{Re}(\chi)}{1-|\chi|^2} \right) \\ \textit{Faraday} \quad \textit{ellipticity}[\text{deg.}] = \dfrac{180}{\pi} \tan\left(\dfrac{1}{2} \arcsin\left(\dfrac{-2\,\text{Im}(\chi)}{1+|\chi|^2} \right) \right) \end{cases} \quad \text{(A.14)}$$

where $\chi = C_3/C_4$.

Transmissivity T can be expressed as,

$$T = |C_3|^2 + |C_4|^2 \quad \text{(A.15)}$$

Reference

[A.1] M. Inoue and T. Fujii, J. Appl. Phys. **81**, 5659 (1997).
[A.2] H. Shimizu, M. Miyamura, and M. Tanaka, Appl. Phys. Lett. **78**, 1523, (2001)

Publications and presentations

Papers

1. H. Shimizu, T. Hayashi, T. Nishinaga, M. Tanaka, "Magnetic and transport properties of III-V based magnetic semiconductor (GaMn)As: Growth condition dependence", Appl. Phys. Lett., **74** 398 (1999).
2. M. Tanaka, H. Shimizu, T. Hayashi, H. Shimada, and K. Ando, "Ferromagnetic Semiconductor Heterostructures Based on (GaMn)As", J. Vac. Sci. Tech. **A18**, 1247, (2000).
3. H. Shimizu, M. Miyamura, and M. Tanaka, "Enhanced Magneto-Optical Effect in a GaAs/MnAs Nanoscale Hybrid Structure Sandwiched by GaAs/AlAs Distributed Bragg Reflectors", J. Vac. Sci. Tech. **B18**, 2063, (2000).
4. H. Shimizu, M. Miyamura, and M. Tanaka, "Magneto-optical properties of a GaAs:MnAs hybrid structure sandwiched by GaAs/AlAs distributed Bragg reflectors: Enhanced magneto-optical effect and theoretical analysis", Appl. Phys. Lett. **78**, 1523, (2001)
5. M. Tanaka, M. Miyamura, and H. Shimizu, "Enhancement of magneto-optical effect in a GaAs:MnAs hybrid structure sandwiched by GaAs/AlAs distributed Bragg reflectors", invited paper, J. Cryst. Growth, **227-228**, 839, (2001).
6. H. Shimizu and M. Tanaka, "Magneto-optical properties of semiconductor-based superlattices having GaAs with MnAs nanoclusters", J. Appl. Phys., **89**, 7281, (2001).
7. H. Shimizu and M. Tanaka, "Magneto-optical properties of a Si-doped GaAs:MnAs based magneto-photonic crystal operating at 1.55μm", to be published in Physica E.
8. H. Shimizu and M. Tanaka, "Blue shift of magneto-optical spectra and ferromagnetic ordering in (GaMn)As / AlAs ultrathin ($\leq$5nm) heterostructures" to be published in J. Appl. Phys.

(in Japanese)

1. 清水大雅、宮村信、田中雅明、「GaAs / AlAs DBR を用いた半導体/強磁性体金属複合構造 GaAs:MnAs 及び磁性半導体(GaMn)As の磁気光学効果の増大」、電気学会マグネティックス研究会資料、MAG-00-14、(2000).
2. 清水大雅、宮村信、田中雅明、「MnAs ナノクラスターと GaAs / AlAs 半導体 DBR からなる多層膜における磁気光学効果の増大」 日本応用磁気学会誌 Vol. 25, 655-658, (2001)

Presentations in International Conferences and Symposia

1. H. Shimizu, T. Hayashi, M. Tanaka, T. Nishinaga, "Control of Magnetic Properties of III-V Based Ferromagnetic Semiconductor $(Ga_{1-x}Mn_x)As$", 4th International Symposium on Physics of Magnetic Materials, Sendai, Japan, August, 1998.
2. H. Shimizu, T. Hayashi, T. Nishinaga, M. Tanaka, "Control of Electronic, Magnetic and Optical Properties of Ferromagnetic Semiconductor (GaMn)As", 43rd Conference on Magnetism & Magnetic Materials, Miami, USA, November, 1998.
3. H. Shimizu, T. Hayashi, M. Tanaka and K. Ando, "Magneto-optic properties of (GaMn)As thin films and its heterostructure", 1999 spring meeting of the Material Research Socity, San Francisco.
4. H. Shimizu, M. Miyamura, and M. Tanaka, "Enhanced Magneto-Optical Effect in a GaAs/MnAs Nanoscale Hybrid Structure Sandwiched by GaAs/AlAs Distributed Bragg Reflectors", 27th Conferences on the Physics and Chemistry of Semiconductor Interfaces, Salt Lake City, January, 2000.
5. H. Shimizu, M. Miyamura, and M. Tanaka, "Engineered Magneto-optical Effect in a Semiconductor-Based Magneto-Photonic Crystal", Symposium on Spin-Electronics, Halle, Germany, July, 2000.
6. M. Tanaka, M. Miyamura, and H. Shimizu, "Enhancement of magneto-optical effect in a GaAs:MnAs hybrid structure sandwiched by GaAs/AlAs distributed Bragg reflectors", invited talk, 11th International Conference on Molecular Beam Epitaxy, Bejing, September, 2000.
7. H. Shimizu, M. Miyamura, and M. Tanaka, "Engineered Magneto-Optical Effect in Semiconductor-Magnetic Hybrid Structures: Theoretical Design and Improvement of Magneto-Optical Properties", International Conference on the Physics and Application of the Spin-Related Phenomena in Semiconductors, 2000, Sendai, September, 2000.
8. H. Shimizu, M. Miyamura, and M. Tanaka, "Engineered Magneto-Optical Effect due to Localization of Light in Semiconductor-Magnetic Hybrid Structures", 25th International Conference on Physics of Semiconductors, Osaka, September, 2000.; Proceedings of the 25th International Conference on the Physics of Semiconductors, pp1711-1712, (Eds. N. Miura and T. Ando) 87 Springer Proceedings in Physics.
9. H. Shimizu and M. Tanaka," Enhancement and control of magneto-optical properties in III-V semiconductor / ferromagnet (MnAs) hybrid structures: Semiconductor-based magneto-photonic crystal approach", 8th Joint MMM-Intermag Conference, San Antonio, January, 2001.
10. H.Shimizu and M.Tanaka, "Enhanced magneto-optical effect in III-V semiconductor-based magneto-photonic crystals", 6th International Symposium on Advanced Physical Fields, Tsukuba, March, 2001

11. H. Shimizu and M. Tanaka, "Magneto - Optical Properties of GaAs Based Semiconductor Magneto Photonic Crystals", 10th International Conference on Modulated Semiconductor Structures, Linz, Austria, July, 2001.
12. M. Tanaka and H. Shimizu, "Engineered Magneto-Optical Effect in Semiconductor-Based Magneto-Photonic Crystals", 13th International Conference on Crystal Growth / 11th International Conference on Vapor Growth and Epitaxy, Kyoto, Japan, August, 2001.
13. H. Shimizu and M. Tanaka, "Quantum size effect and ferromagnetic ordering in ultrathin (GaMn)As/AlAs heterostructures", 46th Conference on Magnetism & Magnetic Materials, Seattle, USA, November, 2001.

Presentations in Domestic Conferences (in Japanese)

1. 清水大雅、林稔晶、田中雅明、西永頌　「磁性半導体(GaMn)Asの成長条件依存性」　平成10年度春季第45回応用物理学会関係連合講演会　29pR-1　東京工科大学　1998年3月
2. 清水大雅、林稔晶、田中雅明、西永頌　「磁性半導体(GaMn)Asの電気的磁気的特性の成長条件依存性」　第23回日本応用磁気学会学術講演会　北海道大学　1998年9月
3. 清水大雅、林稔晶、西永頌、田中雅明、安藤功兒　「(GaMn)Asの透過磁気円二色性」　平成11年春季第46回応用物理学会関係連合講演会　29pY-1 東京理科大学　1999年3月
4. 清水大雅、宮村信、田中雅明、「GaAs/AlAs DBRを用いた半導体/強磁性体金属複合構造 GaAs:MnAs及び磁性半導体(GaMn)Asの磁気光学効果の増大」、電気学会マグネティックス研究会、豊橋技術科学大学、2000年2月
5. 清水大雅、宮村信、西永頌、田中雅明、安藤功兒、「GaAs/AlAs DBRを用いたGaAs:MnAsハイブリッド構造の磁気光学効果の増大」、第47回応用物理学関係連合講演会、29aYC-9、青山学院大学、2000年3月
6. 宮村信、清水大雅、西永頌、田中雅明、「GaAs/AlAs DBRを用いたGaAs:MnAsハイブリッド構造の磁気光学効果の増大」、第47回応用物理学関係連合講演会、29aYC-10、青山学院大学、2000年3月
7. 清水大雅、田中雅明、安藤功兒、「半導体ベース一次元磁性フォトニック結晶の磁気光学特性の改善」、第61回応用物理学会学術講演会、4pZN-10、北海道工業大学: 講演奨励賞受賞、2000年9月
8. 清水大雅、宮村信、田中雅明、「半導体ベース磁性フォトニック結晶」第24回日本応用磁気学会シンポジウム、早稲田大学、2000年9月
9. 清水大雅、田中雅明 「半導体ベース一次元磁性フォトニック結晶の磁気光学特

性の改善 II」、第 48 回応用物理学関係連合講演会、31pY-1、明治大学、2001 年 3 月

10. 清水大雅、田中雅明 「(GaMn)As 超薄膜の磁気光学効果測定による量子化準位の検討」、第 61 回応用物理学会学術講演会、11pYA-5、愛知工業大学、2001 年 9 月
11. 清水大雅、田中雅明 「MnAs ナノクラスターを用いた半導体導波路型光アイソレータの提案」、第 49 回応用物理学関係連合講演会、2002 年 3 月、東海大学 にて発表予定
12. 清水大雅、田中雅明 「III-V 族半導体中に形成された MnAs ナノクラスター構造の磁気光学効果と半導体導波路型光アイソレータへの応用」、電気学会マグネティックス研究会、2002 年 3 月、東北大学電気通信研究所、にて発表予定

Presentations in Domestic Symposia

1. H. Shimizu, T. Hayashi, M. Tanaka, T. Nishinaga, "Metallic and Nonmetallic Properties of (GaMn)As: Growth Parameter Dependence", 17th Electronic Materials Symposium, Izu-nagaoka, July, 1998.
2. H. Shimizu, T. Hayashi, M. Takenaka, Y. Nakano, M. Tanaka, and K. Ando, "Transmission Magnetic Circular Dichroism of (GaMn)As Thin Films and a (GaMn)As/AlAs Superlattice", The 4th Symposium on the Physics and Application of Spin-Related Phenomena in Semiconductors, Sendai, Japan, December, 1998.
3. H. Shimizu, T. Hayashi, M. Tanaka, and K. Ando, "Magneto-Optical Spectra of Ferromagnetic Semiconductor (GaMn)As and related heterostructures", the 5th Symposium on the Physics and Applications of Spin-Related Phenomena in Semiconductors, Sendai, December, 1999.
4. H. Shimizu, M. Miyamura, and M. Tanaka, "Enhanced Magneto-Optical Effect of GaAs:MnAs Magnetic Nanoclusters with GaAs/AlAs Distributed Bragg Reflectors : A Semiconductor-Based Magneto-Photonic Crystal", the 5th Symposium on the Physics and Applications of Spin-Related Phenomena in Semiconductors, Sendai, December, 1999.
5. M. Tanaka, H. Shimizu, and M. Miyamura, "Enhancement of Magneto-optical Effect in a GaAs:MnAs Hybrid Structure Sandwiched by GaAs/AlAs Distributed Bragg Reflectors", the 19th Electronic Material Symosium, Izu-nagaoka, June, 2000.
6. M. Tanaka and H. Shimizu, "Enhancement of Magneto-optical Effect in a GaAs:MnAs Hybrid Structure Sandwiched by GaAs/AlAs Distributed Bragg Reflectors: Epitaxial Semiconductor-based Magneto-Photonic Crystal", The 5th Symposium on Atomic-Scale Surface and Interface Dynamics, Tokyo, March, 2001.
7. M. Tanaka and H. Shimizu, "Magneto-optical properties of semiconductor-based

magneto-photonic crystals having GaAs with MnAs nanoclusters", to be presented at the 6th Symposium on Atomic-Scale Surface and Interface Dynamics, Tokyo, March, 2002.

Awards

- 第 9 回（2000 年秋季）応用物理学会講演奨励賞、2001 年 3 月 28 日受賞
  受賞講演名「半導体ベース一次元磁性フォトニック結晶の磁気光学特性の改善」、清水大雅、田中雅明
- 平成 13 年度日本応用磁気学会学術奨励賞(武井賞)、2001 年 9 月 26 日受賞
  受賞論文名「MnAs ナノクラスターと GaAs / AlAs 半導体 DBR からなる多層膜における磁気光学効果の増大」、清水大雅、宮村信、田中雅明